

Generation of highly reactive species by plasma-liquid interaction

I N A U G U R A L D I S S E R T A T I O N

zur

Erlangung des akademischen Grades eines

Doktors der Naturwissenschaften (Dr. rer. nat.)

der

Mathematisch-Naturwissenschaftlichen Fakultät

der

Ernst-Moritz-Arndt-Universität Greifswald

vorgelegt von

Helena Martha Jabłonowski (geb. Tresp)

geboren am 04.06.1985

in Berlin

Greifswald, den 29.01.2016

Dekan: Prof. Dr. Werner Weitschies

1. Gutachter: Dr. Stephan Reuter

2. Gutachter: Prof. Dr. Antoine Rousseau

Tag der Promotion: 11.07.2016

Contents

List of abbreviations	V
1 Introduction and motivation	1
1.1 State of the art of plasma-liquid interaction in plasma medicine	3
2 Fundamentals	7
2.1 Liquid chemistry relevant for plasma-liquid interaction	7
2.1.1 Role of the pH value	7
2.1.2 Reactive species in plasma treated liquids	8
2.2 Electron paramagnetic resonance spectroscopy	19
2.2.1 Basic principles of EPR	19
2.2.2 Spin trapping technique	32
3 Materials and methods	35
3.1 Plasma jet and treatment of liquids	35
3.2 Colorimetric assays	37
3.2.1 Nitrate and nitrite	37
3.2.2 Hydrogen peroxide	39
3.2.3 Ozone	41
3.3 Chemicals and devices	43
3.4 pH measurement	47
3.5 EPR	48
4 Results and discussion	51
4.1 Radicals in plasma treated liquids	51
4.1.1 Spin trapping in plasma-liquid interaction analysis	53
4.1.2 Choice of spin trap	56
4.2 Controlled conditions	63
4.2.1 Influence of ambient conditions	63
4.2.2 Impact of molecular gas admixture into the feed gas on liquid chemistry	73
4.2.3 Impact of liquid ingredients	77
4.3 Origin of selected reactive species in the liquid	80
4.3.1 Hydrogen peroxide	80
4.3.2 Singlet oxygen	86
4.3.3 Plasma jet VUV radiation	91
4.3.4 Ion transport from the gas phase	100
4.4 Impact on biological targets	101
4.4.1 Curtain gas impact - eukaryotes versus prokaryotes	101
4.4.2 Impact of plasma jet VUV radiation on cell suspension	104
5 Summary	107
Bibliography	115

Contents

Appendix	137
List of publications and conference contributions	147
Eigenständigkeitserklärung	153

List of abbreviations

$^1\text{O}_2, \text{O}_2^1\Delta_{\text{g}}$	singlet oxygen
A	hyperfine structure constant
A_{control}	absorption of the control
a_H	hyperfine splitting value for hydrogen
a_{H^+}	activity of hydrogen ion
a_N	hyperfine splitting value for nitrogen
APF	aminophenyl fluorescein
Ar_2^*	argon excimer
A_{sample}	absorption of the sample
ΔB	magnetic field difference
\vec{B}	magnetic field
b	path length of the well
B_{int}	inner magnetic field
BMPO	5-tert-butoxycarbonyl-5-methyl-1-pyrroline-N-oxide
C_{radical}	radical concentration
Caboxy-PTIO, CPTIO	2-(4-Carboxyphenyl)-4,4,5,5-tetramethylimidazoline-1-oxyl-3-oxide
$c\text{O}_3$	concentration of ozone
CPH-HCl	1-hydroxy-3-carboxy-2,2,5,5-tetramethylpyrrolidine
CW-EPR	continuous wave electron paramagnetic resonance
CYPMPO	5-(2,2-dimethyl-1,3-propoxy-5-methyl-1-pyrroline N-oxide
D	bond dissociation energy
DEPMPO	5-(diethoxyphosphoryl)-5-methyl-1-pyrroline-N-oxide
DETC	N,N-diethyldithiocarbamate
DIPMPO	5-(diisopropoxyphosphoryl)-5-methyl-1-pyrroline-N-oxide
DMEM	Dulbecco's modified Egel Medium

List of abbreviations

DMPO	5,5-dimethyl-1-pyrroline-N-oxide
DMPO●/OH	DMPO adduct with the hydroxyl radical
DMPO●/OOH	DMPO adduct with the superoxide anion / hydroperoxyl radical
DNA	deoxyribonucleic acid
DTC	dithiocarbamate complexes
ΔE	energy difference
E_{Ij}	energy of the inner magnetic field
E_{lost}	lost energy per microwave period
EMPO	2-ethoxycarbonyl-2-methyl-3,4-dihydro-2H-pyrrole-1-oxide
EMR	electron magnetic resonance
EPR	electron paramagnetic resonance
ESR	electron spin resonance
E_{stored}	stored energy
F	total atomic angular momentum
f	sensitivity coefficient
Fe ²⁺	iron (II) salt
FTIR	Fourier transform infrared radiation
g_e	free electron g-factor
g_J	Landé g-factor
g_L	orbital g value
g_S	spin g value
γ	gyromagnetic ratio
γ_L	orbital gyromagnetic ratio
γ_S	spin gyromagnetic ratio
H [•]	hydrogen radical
H ⁺	hydrogen cation
H ₂ O	water
H ₂ O ₂	hydrogen peroxide
H ₃ O ⁺	hydronium cation
H ₃ PO ₄	phosphoric acid

\hbar	reduced Planck's constant
HBSS	Hank's balanced salt solution
HCl	hydrochloric acid
h	height
HNO	nitroxyl
HNO ₂	nitrous acid
HNO ₃	nitric acid
HO ₂ [•]	hydroperoxyl radical
HO ₂ ⁻	hydroperoxide
HOCl	hypochlorous acid
HPF	hydroxyphenyl fluorescein
HRP	horseradish peroxidase
\vec{I}	nuclear spin angular momentum
I	intensity
IMDM	Iscove's modified Dulbecco's medium
\vec{j}	total angular momentum
j	total angular quanten number
k_B	Boltzmann constant
K_a	acid dissociation constant
KCl	potassium chloride
KH ₂ PO ₄	potassium dihydrogen phosphate
λ	wavelength
\vec{l}	orbital angular momentum
l	orbital quanten number
LS-coupling	spin-orbit coupling
m_e	electron mass
m_j	projection of the total angular momentum
m_l	total angular momentum
m_s	projection of the spin magnetic moment
MgF ₂	magnesium fluoride

List of abbreviations

MGN	N-methyl-D-glutamine dithiocarbamate
m_{H^+}	molarity of hydrogen ion
MRSA	methicilin-resistant <i>Staphylococcus aureus</i>
$\vec{\mu}$	magnetic momentum
μ_B	Bohr's magneton
$\vec{\mu}_I$	nuclear magnetic moment
$\vec{\mu}_J$	total angular momentum
$\vec{\mu}_L$	orbital magnetic momentum
μ_N	nuclear magneton
$\vec{\mu}_S$	magnetic moment of the electron
η	factor
N_2	molecular nitrogen
N_2^*	metastable molecular nitrogen
N_2O_5	dinitrogen pentoxide
Na_2HPO_4	disodium hydrogen phosphate
$NaCl$	sodium chloride
NaH_2PO_4	sodium dihydrogen phosphate
$NaHCO_3$	sodium bicarbonate
N	atomic nitrogen
$\bullet NO$	nitric oxide radical
NO^+	nitrosonium cation
NO^-	nitroxyl anion
$NO_2\bullet$	nitrogen dioxide
NO_2^-	nitrite
$NO_3\bullet$	nitrate radical
NO_3^-	nitrate
$O(^1D)$	excited atomic oxygen
O_2	molecular oxygen, dioxygen
$O_2\bullet^-$	superoxide anion radical
O_2^{2-}	peroxide anion

O_3	ozone
OCI^-	hypochlorite anion
OCI^-	hypochlorite
$\bullet OH$	hydroxyl radical
OH^-	hydroxide anion
$ONOO^-$	peroxynitrite
$ONOOH$	peroxynitrous acid
PBN	phenyl tert-butyl nitron
pK_a	negative logarithm of the acid dissociation constant K_a
PPH-HCl	1-hydroxy-4-phosphono-oxy-2,2,6,6-tetramethylpiperidine
PTFE	polytetrafluoroethylene
Q	quality factor
q	charge
$R-NO$	nitroso
R_{net}	net production rate
RNS	reactive nitrogen species
$RO\bullet$	alkoxyl radical
$RO_2\bullet$	peroxyl radical
ROS	reactive oxygen species
RPMI 1640	Rosewell Park Memorial Institute cell culture medium 1640
r	radius
\vec{s}	spin angular moment
S	spin quantum number
S_z	z-component of the spin magnetic moment
$\bullet SG$	glutathione thiyl radical
slm	standard liters per minute
SOD	superoxide dismutase
SPB	Sørensen's phosphate buffer
syn. air	synthetic air
T	temperature

List of abbreviations

$t_{1/2}$	half-life
$t_{treatment}$	treatment time
τ_1	spin-lattice-relaxation time
τ_2	spin-spin-relaxation time
TEMPD-HCl	2,2,6,6-tetramethyl-4-piperidone hydrochloride
UPW	ultrapure water (HPLC grade)
UV	ultraviolet radiation
V_{sample}	sample volume
V_{total}	total volume
VUV	vacuum ultraviolet radiation
V	volume
ω	Larmor frequency
x	distance

1 Introduction and motivation

Plasma medicine, the therapeutic application of physical plasmas, can reach the final step of application in hospitals only through the development of plasma sources operating at atmospheric pressure and at tissue-tolerable temperatures. The composition and reactive components of these plasma sources interact with a mammalian system such as the human body. For new therapies and new possibilities to tailor these reactive components, the plasmas and their effect on biological cells need to be investigated including their benefits and potential risks.

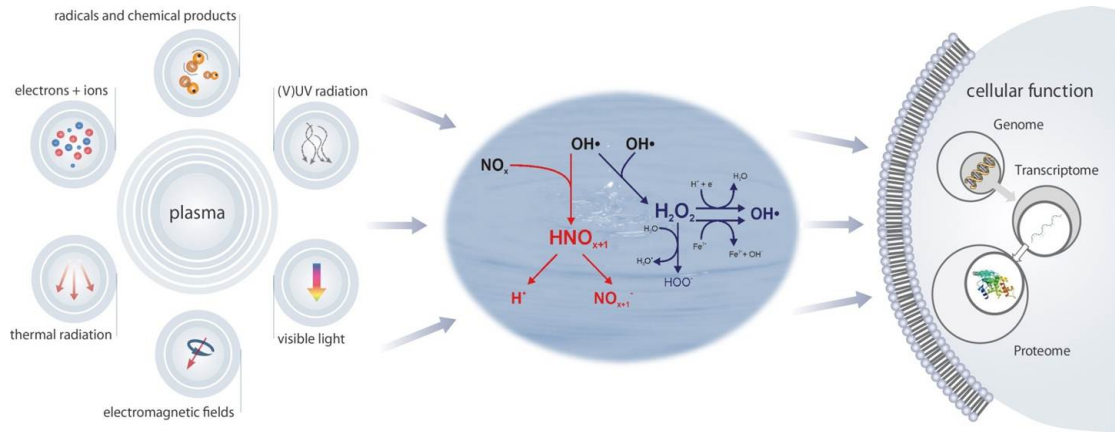


Figure 1.1: Plasma effect mediated by the liquid to the biological target (translated and reprinted with permission from [1]. ©2014, John Wiley and Sons).

The ignition of the plasma takes place in the gas phase, so that the first interaction of the plasma in most cases will be with the surrounding gaseous environment. The components generated by the plasma are for example different kinds of radiation (thermal, visible, and also ultraviolet radiation) as well as electromagnetic fields, charged particles, and other chemically active species (see left hand side in figure 1.1). These reactive components in the gas phase have been intensively investigated by many groups [2–19]. However, the interaction of the plasma with biological tissue involves in most cases plasma-liquid interactions (see figure 1.1). In particular, open wounds are covered with a liquid layer or at least are situated in a moist environment. Representing an interface in medical applications, the liquid layer between the plasma and the biological target has a double function: on the one hand it is protecting the subjacent cells against radiation and on the other hand it is also an origin of plasma generated reactive species, which can yield a beneficial effect for instance for wound healing.

The kINPen® MED (neoplas tools GmbH, Greifswald, Germany) is the first certified argon plasma jet for plasma medical application. Therefore, this thesis is focused on the plasma-liquid chemistry generated by a similar argon atmospheric plasma jet, the kinpen09 (neoplas GmbH, Greifswald, Germany). This plasma jet has the great advantage over other

plasma medical devices such as for instance surface or volume dielectric barrier discharges by being independent of the surface topology and less dependent of the surrounding humidity. Movement of the jet allows the treatment adjusted to specific topology. Additionally, due to the electrode geometry and the gas flux, the gas phase and the liquid below the plasma plume is well stirred, enabling a distribution of the effect in the liquid. In combination with the movement of the plasma jet, the treatment of the liquid can be assumed to be homogeneous. Although this work is focused on the plasma-liquid interaction, studies were also performed in close collaboration with researchers working on plasma and gas phase diagnostics, as the plasma is ignited in the gas phase and reactive species generated there are also able to interact with the liquid. With respect to the subsequent application of this plasma jet in medicine also studies are performed together with researchers dealing with the intracellular effects of the plasma [20–23].

Because of the vital role of the liquid as interface in plasma medicine, this work is focused on the elucidation of the interaction of plasmas with biologically relevant liquids. In contrast to many other studies, in this work liquids of different complexities are implemented. These liquids, namely ultrapure water, sodium saline solution, buffered saline solutions as well as different cell culture media are investigated and compared with one another to allow conclusions of the underlying mechanisms. The results of this thesis are an important step in the direction of the applications to real biological liquids such as blood and wound secretion *ex vivo* as well as *in vivo*. In this thesis the following questions are investigated and answered with the special focus on the free radicals as highly reactive and, therefore, hard to detect relevant group of chemical species:

- What is the impact of the atmospheric-pressure argon plasma jet on biologically relevant solutions?
 - ▷ Which species are generated due to the plasma treatment of liquids?
 - ▷ What is an appropriate detection procedure for the qualification and and quantification of the short-lived species?
- Does the surrounding conditions influence the formation of liquid-phase reactive species and can this influence be used to tailor a desired liquid composition?
 - ▷ What is the influence of the plasma surroundings?
 - ▷ What is the influence of feed gas manipulation regarding the reactive species generation?
 - ▷ Can these impacts be used for a selected reactive species composition generation?
 - ▷ Does the treated liquid medium affect the plasma-generated reactive species output and in what way?
- Which are the underlying mechanisms and origins of the plasma-caused chemical changes in the solutions?
 - ▷ Do reactive species exist, which origin is located in the gaseous phase?
 - ▷ What is the impact of the plasma jet radiation?

1.1 State of the art of plasma-liquid interaction in plasma medicine

Due to its increased relevance, in the past five years several groups in the plasma medicine community have focused on the investigation of plasma-liquid interaction. The here presented work yields an important contribution to reveal the mechanisms in plasma medicine relevant plasma-liquid interaction for argon fed plasmas. This can be seen in table 1.1 [24], where an overview of plasma-liquid interaction literature in the field of plasma medicine of the past five years is given. The relevant contributions of the present work in this context is highlighted in the table.

In table 1.1, the publications are sorted by the detected species for the most common working gases: helium, argon, and air. These categories are subdivided regarding the investigated liquid - water, saline solution, buffered saline solution, or cell culture medium. By comparison of these studies, the set of generated active compounds, independent of all working gases, are more or less the same: in general, reactive oxygen species (ROS) and reactive nitrogen species (RNS). The role of ROS and RNS, as they are also formed in solution during plasma treatment, has been known for a while in biology and medicine [25, 26]. They are involved in many biochemical processes in mammalian systems; some can cause illnesses but they are also essential for the human body [27, 28].

One of the most highly reactive species group which can be formed in solution due to plasma treatment is for instance the group of oxygen radicals [29]. However, also nitrogen free radicals [30] and non-radical oxygen and nitrogen species can be highly reactive and relevant [26, 31–33]. The first measurements of the plasma generated free radicals in the solution were performed via colorimetric assays in combination with scavengers [34]. As known from literature [25], the values given by colorimetric assays are often difficult to interpret. Cross-reactivities of these assays with several species occur, especially in unknown and complex systems. These assays are well accepted in the chemical or pharmaceutical analytics, where single species of usually stable concentrations are aimed at being identified and/or quantified. Unfortunately, in plasma-treated liquids, the situation is not stable and quite complex in composition. Furthermore, the liquid will not be the only origin of reactive species in the solution; also the produced ROS and RNS from the gas and plasma phase can interact. Dissolving processes are possible, meaning the mass transfer of plasma or gas-phase born reactive species into the liquid. In addition they can trigger chain reactions, which most probably are leading to secondary or tertiary produced species to interact with the biological target in or below the liquid layer.

The determination of reactive species formed in the liquid, as a result of plasma treatment, was performed in the early stages of plasma-liquid interaction investigations in the field of plasma medicine. The first measurements were achieved in the framework of the bacterial inactivation experiments by use of atmospheric pressure plasma sources. These investigations were aimed at disinfection and sterilization in medical fields, e.g. medically relevant surfaces, as well as infected wounds. There, plasma treatments of bacterial suspensions as well as of biofilms were performed with various plasma sources. The antimicrobial efficacy of atmospheric pressure plasma treatment was shown by many groups [22, 32, 35–47]. This also specifically applies to multi-resistant pathogens, such as methicillin-resistant *Staphylococcus aureus* (MRSA), as shown in references [39, 48–50]. In these microbiologically focussed studies, mainly water or saline solutions were investigated as common solutions used for bacterial suspensions. In water or saline solution, beside an acidification, also hydrogen peroxide, nitrite and nitrate were determined [30–32, 51]. These three

1 Introduction and motivation

species are quite stable and could be detected in most studies dealing with plasma treatment of liquids also in case of higher complex liquid compositions. Incipient stages of short-lived species measurement were already performed. Based on theoretically assumptions, first studies already deal with these highly reactive species, e.g. oxygen radicals or peroxynitrite [31, 32, 51, 52]. In the following years, also the measurement effort was focused to the detection of these species by the use of various methods, which were transferred from classical chemical analytics as well as from free radical research in biology and medicine [14, 22, 29–33, 44, 51, 53–67]. Several of these measurements based on color-forming or fluorescent reactions and other techniques use chemical molecules as sensors.

Prior to this work there were only a few studies performed on the interaction of argon plasmas with liquids. Argon as the feed gas of the first certified plasma source for medical application is highly relevant. Especially, the plasma jet interaction with the more medically relevant and complex liquids such as buffered and non-buffered saline solutions were only marginally researched. Furthermore, the intricate effects of plasmas interacting with cell culture media were just scarcely examined. The studies published as an outcome of this thesis are up to now unique in terms of measuring the short-lived oxygen radicals in cell culture media and buffered saline solutions, with that the thesis filled relevant research gaps and made an important contribution to basic research in plasma medicine (see table 1.1).

Table 1.1: Overview of the plasma-liquid interaction literature of the past five years for helium, argon or air as working gas (adapted from reference [24], reprinted from Clinical Plasma Medicine, Vol 3, Jablonowski, H. & von Woedtke, Th. Research on plasma medicine-relevant plasma-liquid interaction: What happened in the past five years?, pp 42-52, © 2015, with permission from Elsevier).

	helium			argon			air					
	water	saline solution	buffered saline solution	cell culture medium	water	saline solution	buffered saline solution	cell culture medium	water	saline solution	buffered saline solution	cell culture medium
H ₂ O ₂	[31, 54, 68]		[69]		[30, 70][63]	[33][57]	[33][65, 67]	[33, 61, 71][72–74]	[51, 56, 58, 71, 75–78]	[43, 51, 78–81]	[14, 38, 43, 53, 67, 78, 82]	[53, 56]
•OH	[54, 55, 59, 64, 66]				[30, 60][63]	[33][67]	[33, 63]	[33, 61, 63]	[56, 58]		[53, 67]	[53]
ONOO [−] ONOOH							[65]		[32, 58, 83]		[14, 53]	[53]
O ₂ ^{•−}	[54, 55, 62, 84]				[63]	[33]	[33, 61, 63][65]	[33, 61, 63]	[56]		[14, 53]	[53]
¹ O ₂	[54]				[30]		W ^a [67]		[56]		[14, 53, 82]	[53]
NO ₂ [−]	[31]		[69]		[30]	[33]	[33, 61, 63][65]	[33][73, 74, 85]	[46, 51, 58, 78, 86, 87]	[43, 51, 78–81]	[38, 43, 53, 67, 78]	[53]
NO ₃ [−]	[31]				[30]	[33]	[33, 61, 63][65]		[46, 51, 58, 75, 78, 86, 87]	[43, 51, 78? –80]	[38, 43, 67, 78]	
O ₃									[58, 77]	[43]	[43]	
NO ₂ [•]						[57]	[67]		[58]			
•NO	[64]				[30]						[14, 67]	
HNO ₂									[77]			
HNO ₃						[57]						
O ₂								[88]				
H [•]	[64]											
ROS			[89]					[74, 85]			[53]	[53, 90]

^adata shown in this thesis

2 Fundamentals

As an interdisciplinary research field, investigations on plasma-liquid interaction includes the necessity of knowledge in plasma physics but also fundamentals of chemistry; especially liquid chemistry is key knowledge required for elucidation of mechanisms in the plasma treated liquids. Hence, in this chapter fundamentals of several selected basics in liquid chemistry relevant for the understanding of the plasma-liquid interaction chemistry are given. Due to the fact that the plasma-liquid interaction in this work is investigated with respect to plasma medicine; also the fundamental role of the described and discussed chemistry for biochemical processes in the human body is relevant.

Beside the chemical basics also fundamentals of the major method used in the work, the advanced technique of radical detection - electron paramagnetic resonance spectroscopy - are described. In this part of the chapter the physical basics of electron paramagnetic resonance as well as the experimental technique descriptions are given. Furthermore, the method of radicals stabilization for detection, the so-called spin trapping method is introduced.

2.1 Liquid chemistry relevant for plasma-liquid interaction

This section is introduced by the description and the relevance of the pH value for chemical and biochemical reactions, going on with the reactive species, which includes radicals and non-radicals. For both types of reactive species the relevant ones for plasma-liquid interaction in plasma medicine, hence, for biochemical processes in the human body are given.

2.1.1 Role of the pH value

The pH value is a measure for the acidic or alkaline properties of an aqueous solution. It is defined as the negative decadic logarithm of the activity of the hydrogen cation (H^+). The activity of the hydrogen cation (a_{H^+}) is the product of its molarity (m_{H^+} in mol/kg) and the activity coefficient of the hydrogen cation divided by the unit of the molarity. For simplification, the concentration of the hydrogen cation or in a diluted solution the concentration of the hydronium cation (H_3O^+) is used as it written in equations 2.1 and 2.2.

$$pH = -\lg([H^+] \cdot l/mol) \quad (2.1)$$

$$pH = -\lg([H_3O^+] \cdot l/mol) \quad (2.2)$$

Generally, the majority of chemical reactions are influenced by hydrogen cations, no matter if the ions are present in water (H_2O) as reaction partners or if they only act as catalysts. The rate of a chemical reaction is linked to the pH value. So-called buffer systems based on an equilibrium between an acid and its conjugated base. This systems

enable a stable pH value in a solution, even when a moderate amount of a stronger acid or base is added.

In the human body small changes of pH can already have strong effects. The range of pH in blood or in cellular liquids, without resulting in negative effects for health, is limited. In the blood a complex buffer system exists to keep the pH in a tolerable range. Arterial blood for instance has a pH value of 7.35 - 7.45. The composition of the blood buffer system includes a bicarbonate buffer, which covered 53% of the total buffer capacity of the blood, hemoglobin (35%), proteins (7%), and a phosphate buffer (5%). Although the phosphate buffer constitutes only the lowest amount in the blood, the buffer capacity of the intracellular liquids is provided by phosphates or proteins. The range of the intracellular pH is 6.8 to 7.4 [91].

The epidermis, the outer cell layers of the skin, is slightly acidic with a pH value of 5.5; other skin parts can have a pH value in the range of 4 to 7. This property of the epidermis is also called acid mantle of the skin, which protects the body against the penetration of or the infection by bacteria, viruses and other potential contaminants. However, as described in [92], an environment with a pH value of 5.5 or lower alone does not protect against these pathogens but the pH affects their enzymatic activity.

2.1.2 Reactive species in plasma treated liquids

During the plasma treatment of liquids reactive species are formed or incorporated. These species, especially the reactive oxygen and nitrogen species are also known in different research fields. With respect to plasma medicine an overlapping between biochemical relevant species and the plasma generated species are in the focus of this work. In biology and medicine, the generation of these reactive species is known to be able to occur by reactions of the normal essential metabolic processes in the human body. Furthermore, they are also produced by external sources such as radiation, ozone, environmental pollutants, certain drugs, and many others processes [93]. The generated concentrations of these different formation pathways, including plasma as origin of them, will differ.

In the human body, reactive species are produced continuously by enzymatic and non-enzymatic reactions. The enzymatic reactions are for example reactions of the respiratory chain or reactions of the immune system such as phagocytosis. Phagocytosis is an important immune system process where particles up to small cells are engulfed by a eukaryotic cell and afterwards degraded [94]. Non-enzymatic formation reactions are for instance the reaction of oxygen with organic compounds or the interaction of ionizing radiation with a mammalian system [93]. Reactive oxygen species (ROS) and reactive nitrogen species (RNS) are reactive species, which contain oxygen or nitrogen, respectively, and this part is also the reactive part of the molecule. Some reactive species, which contain both oxygen and nitrogen such as peroxynitrite are often attributed to both groups due to their ability to oxidize as well as to nitrate other molecules. Reactive oxygen and nitrogen species play an important role for the health of the human body. These active species can be divided into two groups: radicals and non-radicals. Although the term 'radical' is directly linked to high reactivity of species, the conclusion that non-radicals are less reactive than radicals is not always true. In the following the characterization of radicals and non-radicals as well as selected relevant examples of these reactive species types are given.

2.1.2.1 Radicals

An atom or molecule that contains one or more unpaired electrons is called free radical [95]. The term 'free' stands for the fact that a radical can exist independently. This addition of the word 'free' is often omitted. An unpaired electron is an electron which occupies an atomic or molecular orbital by itself. The localization of the unpaired electron in a free radical is in the chemical notation often represented by the dot position. The dot has to be set at the atom containing the unpaired electron, indicating, where the spin density is the highest [95]. Due to the surplus of one or more unpaired electrons rather than having matched pairs, radicals are highly reactive and generally less stable than non-radicals [28]. The simplest radical is a hydrogen atom, which contains a proton and one unpaired electron. Once a radical is formed, it causes a chain reaction by interaction with another atom or molecule, no matter if this is a radical or not. Therefore, the rate and selectivity depends on the concentration of the radical and the delocalization of the unpaired electron. Furthermore, by losing (see equation 2.3) or gaining (equation 2.4) a single electron, a radical cation or radical anion, respectively, can be generated from a non-radical. An example for the formation of a radical anion is the production of superoxide anion radicals by the electron transport chain from molecular oxygen [96].



Another formation of free radicals can take place due to homolytic fission, typically by either thermal or photochemical processes (equation 2.5). Thereby, a covalent bond will be broken; one bonding electron remains on each atom [95] - for instance, when hydroxyl radicals ($\bullet\text{OH}$) and hydrogen radicals ($\text{H}\bullet$) are produced by dissociation of water (see eq. 2.6). $\bullet\text{OH}$ contains nine protons and nine electrons, four of them are paired and one is unpaired. The hydrogen radical has one proton and one unpaired electron. A covalent bond cleavage, such as the dissociation of water in these radicals, requires a considerable amount of energy, which is called homolytic bond dissociation energy (D) [95]. This essential energy can be provided for example by heat, ultraviolet radiation (UV), vacuum ultraviolet (VUV) radiation or other ionizing radiation, depending on the bond to be cleaved.



The dissociation of water does not always lead to the formation of hydroxyl radicals. If heterolytic fission (see eq. 2.7) takes place instead of homolytic fission, no radicals are generated due to the fact that one atom receives both electrons [95], when the covalent bond is split. In this case hydroxide anions (OH^-) and hydrogen cations are formed by dissociation of water (eq. 2.8).



In contrast to the radicals, the ions formed due to heterolytic fission of water (see eq. 2.7) contain no unpaired electrons. The hydroxide anion consists of nine protons and ten electrons, which are all paired. The hydrogen cation contains only one proton and no electrons. It is important to note that the kind of cleavage determines the formation of radicals or non-radicals for one and the same molecule.

If a radical reacts with a non-radical, a new radical is generated (see eq. 2.9) and a chain reaction may occur. Radicals can be reducing (see eq. 2.9) as well as oxidizing agents (see eq. 2.11). Even though radical anions and cations exist, most of the radicals are non-charged species. A well-known electrically neutral radical is the above mentioned hydroxyl radical. An example for a charged radical is the superoxide anion radical.



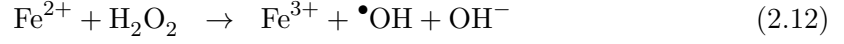
The ambient molecular oxygen (dioxygen, O_2) contains two unpaired electrons and is therefore a diradical. Due to its highly importance for the human body, this and other related oxygen radicals are strongly relevant for this work. Especially for living organisms, two very important oxygen-centered free radicals are hydroxyl and superoxide anion radicals [28]. Each unpaired electron in molecular oxygen is located in a different π^* anti-bonding orbital, and both electrons have the same spin quantum number. Due to its diradical character molecular oxygen easily oxidizes another atom or molecule by accepting a pair of its electrons. These electrons have to be parallel in spin so that they fit into the vacant space in the π^* orbitals. Since every radical aspires to be stable, they attempt to gain additional electrons. Hence, radicals attack nearby molecules causing damage or at least affect the reaction partner. This takes place not only in biological systems but is also highly relevant for this work. However, free radicals are not necessarily harmful. Oxygen radicals for instance are required for maturation processes of cellular structures in the human body. White blood cells, as a part of the body defense mechanism, release free radicals to destroy invading pathogens [93]. In mammalian systems, radicals are required but the concentration need to be appropriate to avoid undesired effects. The imbalance between the generation of reactive oxygen species and the activity of the autoxidation defense is termed 'oxidative stress' [25, 97, 98]. The terminology is under discussion since the term 'oxidative stress' is mainly understood in a negative way. The majority of biological molecules in the human body are non-radicals [28]. In the following several free radicals relevant for this work are introduced.

Hydroxyl radical

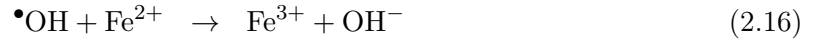
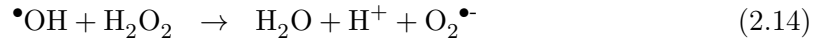
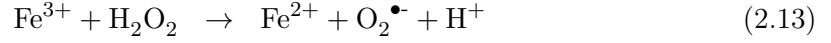
The hydroxyl radical, $\bullet OH$, is a highly reactive oxygen-centered free radical, and indeed it is even the most reactive oxygen radical known, with a positive reduction potential of 2.31 V [25]. The reduction potential is the ability of a species to gain electrons, hence to be reduced by a reaction partner. Due to the fact that $\bullet OH$ reacts with almost every type of molecule in living cells (sugars, amino acids, phosphor lipids, DNA bases, and organic acids) [27] with extremely high rate constants, it has a short half-life in mammalian systems of only $t_{1/2} = 10^{-9} s$ [28]. This highly reactive molecule can be formed not only via the

2.1 Liquid chemistry relevant for plasma-liquid interaction

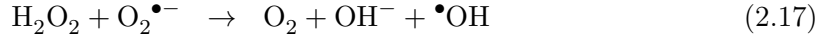
homolytic fission of one O–H bond in a water molecule, as described above, but also through the bond breaking of the O–O bond in hydrogen peroxide; H_2O_2 cleavage results in two hydroxyl radicals [27]. Furthermore $\bullet\text{OH}$ can be generated via photolysis of nitrous acid (HNO_2) with nitric oxide as byproduct [25]. This homolysis can take place not only by heat or ionizing radiation; furthermore a mixture of hydrogen peroxide and iron (II) salt (Fe^{2+}) forms hydroxyl radicals. This reaction is well-known as Fenton reaction (see eq. 2.12) [27].



The reaction 2.12 can provoke a whole series of radical reactions (see equations 2.13 to 2.16). Instead of iron (II) salt, copper (I) salt can be used with an even higher rate constant than iron (II) salt [27].



The formation of $\bullet\text{OH}$ under the presence of hydrogen peroxide and superoxide anion is described by the Haber-Weiss-reaction (see eq. 2.17) [27].



As described for the reactions derived from the Fenton-reaction, hydroxyl radicals can lead to the formation of free radicals of lower reactivity than the hydroxyl radical itself such as hydroperoxyl or superoxide anion radicals [28].

Superoxide anion radical

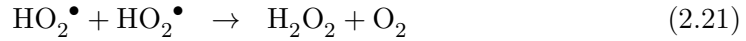
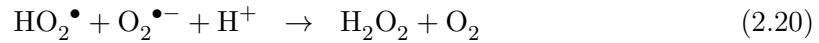
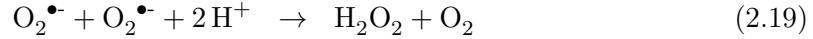
The superoxide anion radical, $\text{O}_2^{\bullet-}$, is a free radical of selective reactivity; it does not react at all with most biological molecules as $\bullet\text{OH}$. It is also less reactive in general, with a positive reduction potential of 0.94 V [25]. It can be produced if a single electron is accepted by the ground state O_2 molecule, which must enter one of the π^* anti-bonding orbitals [27]. Nevertheless, in combination with some other species, for instance with nitric oxide ($\bullet\text{NO}$) it reacts quite fast leading to the formation of peroxynitrite (ONOO^-). The reaction rates of superoxide anion radicals with non-radicals depend on the solvent and also on the pH value. The equilibrium constant for a dissociation reaction is given by the so-called pK_a value, which is the negative logarithm acid dissociation constant K_a . For the reaction of superoxide anion radical to its protonated form, the hydroperoxyl radical (HO_2^\bullet) the pK_a value is 4.8 (see eq. 2.18).



2 Fundamentals

Hydroperoxyl radicals are stronger reducing agents than superoxide anion radicals; their positive reduction potential has with 1.06 V a higher value than the one of superoxide anion [25]. The ratio of $O_2^{\bullet-}$ to HO_2^{\bullet} at pH values of most body tissues is $O_2^{\bullet-}/HO_2^{\bullet}=100/1$ at pH 6.8 and $O_2^{\bullet-}/HO_2^{\bullet}=1000/1$ at pH 7.8 [25]. For reactions in the human body, they are relevant due to the fact that hydroperoxyl radicals are uncharged and can, therefore, cross cellular membranes leading to intracellular reactions.

In aqueous solution, superoxide anion radicals rapidly disappear because of their probability of being reduced as well as oxidized. This process is called dismutation or disproportionation reaction [95]. The dismutation reaction for superoxide anion is given by equation 2.19. The rate constant for this reaction is with $k < 0.3 M^{-1}s^{-1}$ close to zero, but the reactions 2.20 and 2.21 have rate constants of $k = 9.7 \cdot 10^7 M^{-1}s^{-1}$ respectively $k = 8.3 \cdot 10^5 M^{-1}s^{-1}$ [25]. Hence, dismutation reaction of superoxide anion under physiological conditions proceeds by protonation of $O_2^{\bullet-}$ followed by reaction 2.20. This implies faster dismutation at acidic pH and a slowdown of the reaction by increasing pH. In aqueous solutions the calculated rate constant for the dismutation at pH 7.0 has a value of $5 \cdot 10^5 M^{-1}s^{-1}$ [25]. This means that every reaction of a molecule with superoxide anion radicals have to compete with the dismutation reaction. An aqueous system, which generates $O_2^{\bullet-}$, will also form hydrogen peroxide as shown in equations 2.19 to 2.21 [25].



In vivo, superoxide anion radicals can be produced by a number of enzyme systems, such as for instance autoxidation reactions [28]. $O_2^{\bullet-}$ is formed in almost all aerobic cells by the so-called 'respiratory burst' of phagocytes Such as e.g. neutrophils, monocytes or macrophages [27].

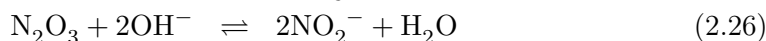
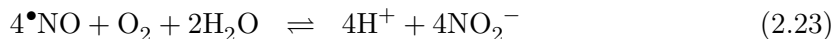
Nitric oxide

Nitric monoxide, or short nitric oxide, $\bullet NO$ is a colorless gas, which is moderately soluble in water (2 mM at 293.15 K with half-life of < 1 s in water, 1.6 mM at 310.15 K) [25]. Together with nitrogen dioxide radical (NO_2^{\bullet}) it is one of the sufficiently stable free radicals. Nitric oxide stably exists in relatively high concentrations while still being reactive enough to start free radical chain reactions [99]. Exposed to air, $\bullet NO$ reacts with molecular oxygen to form nitrogen dioxide (eq. 2.24) [100]. Compared to nitric oxide nitrogen dioxide is far more reactive..

Nitric oxide consists of overall 15 electrons, seven from the nitrogen atom and eight from the oxygen atom. The unpaired electron of nitric oxide is located in the π^*2p anti-bonding orbital of the nitrogen atom. The loss of the unpaired electron leads to the nitrosonium cation, NO^+ . One electron reduction will yield nitroxyl anion, NO^- . This conjugated base of the nitroxyl anion is named nitroxyl, HNO, it has a pK_a value of 11.4 [101]. Due to this pK_a value any nitroxyl anion *in vivo* will be protonated to HNO. Nitroxyl anion can also form highly reactive peroxyxynitrite when reacting with O_2 (see eq. 2.22) [25].



Dissolved nitric oxide in aqueous solutions produces mainly nitrite (NO_2^-). This can be described by the overall reaction 2.23, which is composed of equations 2.24, 2.25, and 2.26.



Although nitric oxide is a relatively stable free radical, the reaction rate constant is much higher if the potential reactions partners are other radicals. Its reaction rate with a free electron or a hydrogen radical is in the order of $10^{10} \text{ M}^{-1}\text{s}^{-1}$; for reactions with hydroxyl radicals, peroxy radicals, or superoxide anion radicals are in the order of $10^9 \text{ M}^{-1}\text{s}^{-1}$ [102].

In the human body, nitric oxide is a ubiquitous intracellular messenger, which is modulating for example blood flow. $\bullet\text{NO}$ is very useful as messenger molecule because it can cross membranes and diffuse between and within most cells and tissue with little losses due to consumption or direct reactions with biological molecules [103]. Often the half-life of nitric oxide is reported to be in order of seconds [100]. *In vivo* the half-life is much longer, up to ten minutes [104, 105]. The concentration of nitric oxide is inversely proportional to the half-life of nitric oxide [103].

In vivo nitric oxide can be produced by the vascular endothelium, which also produces small amounts of $\text{O}_2\bullet^-$ so that peroxynitrite (ONOO^-) can be formed (see eq. 2.27). The rate coefficient of this reaction is close to the diffusion-limited rate with $6.7 \cdot 10^9 \text{ M}^{-1}\text{s}^{-1}$ [106]. Hence, almost every collision of nitric oxide with superoxide anion yields the irreversible formation of peroxynitrite.



In plasma medicine one addressed medical application is the cure of chronic wounds. Therefore, a transition from a non-healing, chronic wound in an acute wound is one step in the healing process. As nitric oxide is known to be at least partly involved in acute inflammation [28], which is takes place in a acute wound, nitric oxide is highly relevant for plasma medicine.

Peroxy radicals

Peroxy, $\text{RO}_2\bullet$, and alkoxy radicals, $\text{RO}\bullet$, are oxidizing agents. Both can abstract hydrogen radicals from other molecules. This abstraction reaction takes place for example in lipid peroxidation [28]. Hydroperoxyl ($\text{HO}_2\bullet$) can be regarded as the simplest peroxy radical [102]. Often, peroxy radicals are formed when carbon-centered radicals react with molecular oxygen. The reaction of hydroxyl radicals with glucose yields six different peroxy radicals due to the six possible carbon atoms where $\bullet\text{OH}$ can abstract a hydrogen radical [25].

2 Fundamentals

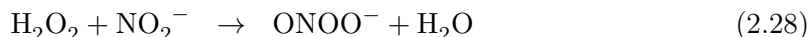
Furthermore, peroxy radicals and alkoxy radicals are produced by the decomposition of organic peroxides. For this decomposition usually additional energy, in the form of heat or in some cases ultraviolet radiation, is needed. Moreover, the addition of transition metal ions such as iron III can trigger this reaction [25].

2.1.2.2 Non-radicals

Most biological active molecules in the human body are non-radicals. These species can also contribute to radical forming reactions. Some non-radicals are more harmful to mammalian systems than their radical origin, as is, for instance, the case for peroxynitrite. Its radical precursors are nitric oxide and superoxide anion radicals. Their reactivity is lower than the of peroxynitrite. A publication with the title 'Nitric oxide, superoxide, and peroxynitrite: the good, the bad, and ugly' highlights this fact [100]. Other highly reactive, non-radical species are, for example, hydrogen peroxide, ozone, hypochlorous acid, and singlet oxygen. In the following details are given on selected non-radical species.

Peroxynitrite

Peroxynitrite, ONOO^- , is a reactive and, therefore, unstable isomer of nitrate, NO_3^- . In alkaline solution it is stable, whereas its conjugated acid, peroxynitrous acid (ONOOH), is highly reactive and has a positive reduction potential of 2.05 V [107]. The pK_a value of peroxynitrous acid is 6.8. The formation of ONOO^- can be caused by radicals as mentioned above, the reaction of $\bullet\text{NO}$ with $\text{O}_2\bullet^-$ [106]. Furthermore, ONOO^- can be produced by non-radicals via a reaction of molecular oxygen with nitroxyl anion (eq. 2.22) [25]. A common way to generate peroxynitrite in laboratories is the reaction of hydrogen peroxide with nitrite (eq. 2.28), often sodium nitrite is used [58, 107].



Peroxynitrite is an oxidant and as well as a nitrating agent, therefore, it is both, a reactive oxygen species and a reactive nitrogen species. The oxidizing character of peroxynitrite is the reason for its ability to damage a broad range of molecules in cells, including DNA and proteins. Furthermore, it can cause lipid peroxidation and it is known to be bactericidal [108].

Singlet oxygen

Two states of singlet molecular oxygen exist: $\text{O}_2^1\Sigma_g^+$ and $\text{O}_2^1\Delta_g$ [27] (see figure 2.1). $\text{O}_2^1\Sigma_g^+$ decays fast to $\text{O}_2^1\Delta_g$. The half-life of $\text{O}_2^1\Delta_g$ in the gas phase is 62 minutes, whereas $\text{O}_2^1\Sigma_g^+$ has only a half-life in the gas phase of 10 seconds [109]. In solution the half-life is much shorter; for instance in water it is in the order of μs [109–111]. From both states, $\text{O}_2^1\Delta_g$ is the more important one in biology [27], therefore, the term 'singlet oxygen' usually refers to $\text{O}_2^1\Delta_g$ and is also abbreviated as $^1\text{O}_2$, which is the abbreviation used in this work.

Singlet oxygen is also produced in the human body, for instance, in the mammalian eye $^1\text{O}_2$ is formed in the lens and in the retina through illumination [27]. Singlet oxygen is produced when nitric oxide reacts with hydrogen peroxide under emission of light in the visible

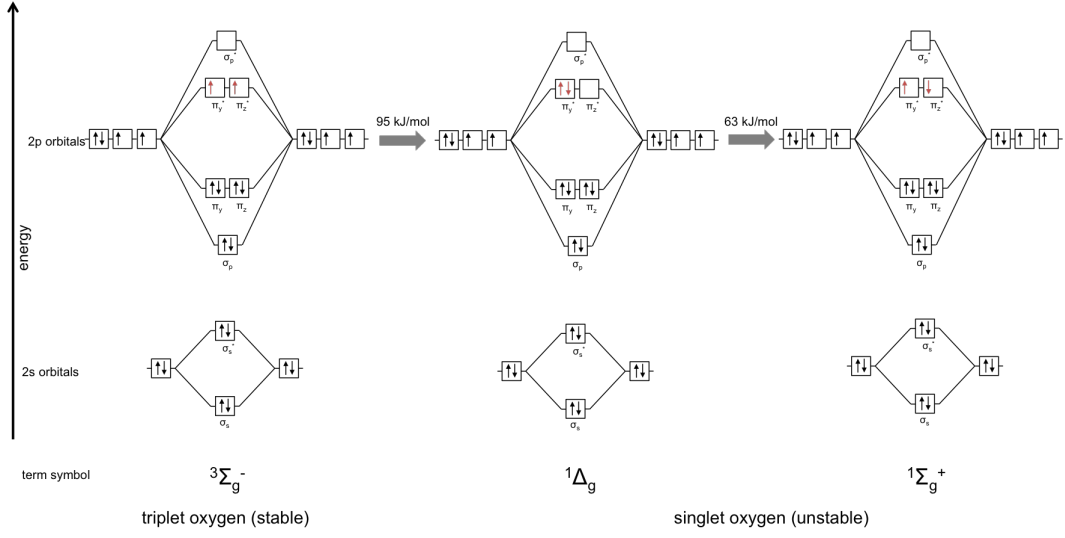
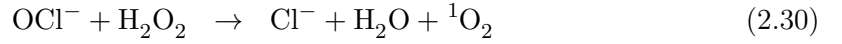


Figure 2.1: Term scheme of molecular oxygen.

spectral range. Furthermore, the pairing of peroxyxynitrite and hydrogen peroxide results in singlet oxygen with nitrite and water as byproducts [112]. In presence of superoxide anion radicals singlet oxygen will be quenched (see eq. 2.29) [27].



The chemical generation of singlet oxygen in laboratories often is achieved by the reaction of hypochlorite (OCl^-) with hydrogen peroxide (eq. 2.30) [25].



Singlet oxygen is a powerful oxidant, which is involved in many relevant processes in biology and medicine. Therapeutic applications are e.g. photosensitized oxidation, photodynamic inactivation of viruses and cells, phototherapy for cancer and photocarcinogenesis [109].

Ozone

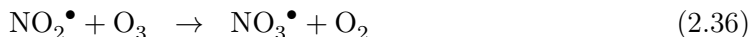
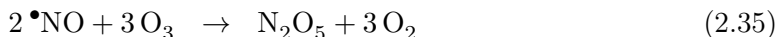
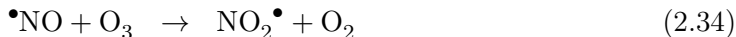
Ozone, O_3 , is, with its positive reduction potential of 1.6 V [113] a far stronger oxidizer than molecular oxygen, which has a negative reduction potential of -0.33 V [25]. It is gaseous under ambient conditions. With its low Henry constant of $1.2 \cdot 10^{-4} \text{ M} \cdot \text{Pa}^{-1}$ it is only slightly soluble in water [114]. The half-life of O_3 in the gaseous phase depends on the temperature and on the humidity. At high concentrations it is unstable and decays to molecular oxygen. It will be mainly formed by either the photodissociation of O_2 by ultraviolet radiation ($\lambda < 240 \text{ nm}$) or by a three body reaction of molecular oxygen, atomic oxygen and a third body M (see equations 2.31 and 2.32). Furthermore, ozone is produced by reaction of nitrogen oxides such as nitrogen dioxide radicals with molecular oxygen also

2 Fundamentals

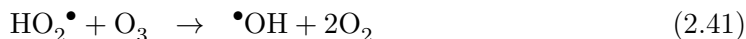
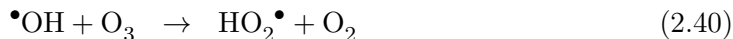
under UV radiation ($\lambda < 240$ nm) (see eq. 2.33 and afterwards eq. 2.32) [115, 116].



In the presence of nitric oxide, ozone is destroyed to nitrogen dioxide and molecular oxygen (eq. 2.34) or directly to dinitrogen pentoxide, N_2O_5 (see eq. 2.35) [115, 116]. The nitrogen dioxide then also reacts with ozone to form nitrate radicals, NO_3^\bullet , and molecular oxygen (see eq. 2.36) [116, 117]. The resultant pairing of these two nitrogen oxides results in the formation of N_2O_5 as shown in equation 2.37) [118].



The destruction of ozone by oxygen species such as atomic oxygen, hydroperoxide radicals, or hydroxyl radicals is also not negligibly (equations 2.38 to 2.41) [115, 116, 119].



Ozone is known to be germicidal, why it is common in water cleaning and air cleaning processes [119]. It is also produced naturally by white blood cells to destroy foreign bodies. The inhalation of ozone can irritate the respiratory system and, therefore, ozone is linked to some diseases such as asthma, bronchitis, heart attack, and other cardiopulmonary problems. O_3 is often regarded as the most toxic air pollutant [28].

Hydrogen peroxide

Hydrogen peroxide (H_2O_2) is a powerful oxidizing agent for most other molecules. Its reduction potential has a value of 0.33 V [25]. It is relatively stable and a colorless liquid under ambient conditions. H_2O_2 is slightly acidic and has a quite high pK_a value of 11.75 [27]. The related ion is the peroxide anion, O_2^{2-} , which is formed if superoxide anion gains an additional electron. At physiological pH, an immediate protonation of the peroxide anion to hydrogen peroxide will take place [27]. The decomposition of H_2O_2 depends on the temperature, its concentration and on the pH value. In a cool, dilute and acidic solution, the stability of hydrogen peroxide increases. The decay of hydrogen peroxide results in the dismutation of two hydrogen peroxide molecules to water and molecular oxygen (see

eq. 2.42). This reaction will be catalyzed by, for example, hydroxide anions or heavy metal ions. Therefore, commercially available hydrogen peroxide solutions always contain stabilizing agents such as phosphoric acid and chelates [120–122].



As mentioned above, in aqueous solution hydrogen peroxide can be formed by the so-called dismutation reaction of superoxide anion, whereas the dismutation rate is faster at acidic pH values (2.19). Industrial H_2O_2 is produced by the so called Anthrachinon process, which is based on the reduction of oxygen by 2-alky-anthrahydrohquinone [123]. This process was developed by the Baden Aniline and Soda Factory (BASF). The overall reaction is given by equation 2.43.



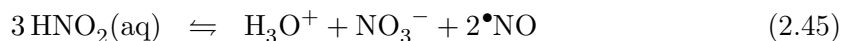
In general, hydrogen peroxide is cytotoxic; therefore, it is applied for disinfection purposes. Since hydrogen peroxide can produce highly reactive hydroxyl radicals in presence of transition metals [28] or by ultraviolet radiation, it can be a source of more harmful molecules. The human body protects itself by enzymes, such as catalase, against the cell membrane permeable H_2O_2 [28]. Catalase degrades hydrogen peroxide to the unharmed products water and molecular oxygen. Hydrogen peroxide is an important signaling molecule for a variety of processes, since it is formed in many biochemical reactions in the mammalian system. It can activate signaling pathways to stimulate different cell responses such as proliferation, differentiation, migration and apoptosis [124]. A study published in Nature [125] also shows the importance of hydrogen peroxide for the immune system. This publication deals with the increase of the hydrogen peroxide concentration after tissue damage leading to the convergence of the white blood cells and an initiation of the wound healing process. Although these investigations were performed on zebra fish, the results are assumed to be applicable also for the human body [125].

Nitrite

Nitrite (NO_2^-) is the conjugated base of nitrous acid (HNO_2). The pK_a for their acid-base-reaction (see eq. 2.44) is 3.4 at 25 °C [126]. Nitrous acid is a weak acid and in solution it is unstable with respect to the deprotonation reaction (eq. 2.44). Nitrite can oxidize or reduce its reaction partner depending on the oxidizing or reducing agent. Its reduction potential is 0.984 V [127]. It is relevant in biochemistry as a source of the potent vasodilator nitric oxide ($\bullet\text{NO}$). At low pH values in mammalian systems nitrite/nitrous acid can also yield spontaneous production of nitric oxide and nitrogen dioxide radicals (see equations 2.46 and 2.47). Hence, for nitric oxide generation originating from nitrite, either low pH values or enzymatic catalysts are required. The therapeutic use of inorganic

2 Fundamentals

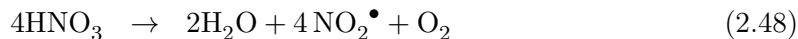
nitrite and nitrate in medicine is already known [128].



In human blood the half-life of nitrite is about 110 seconds [129]. NO_2^- is regarded as a central homeostatic molecule in the nitric oxide biology and may act as an important signaling molecule in mammalian systems [130, 131].

Nitrate

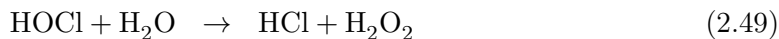
If nitrate (NO_3^-) is protonated, nitric acid (HNO_3) is formed. Nitric acid is a strong acid and highly oxidizing agent. The pK_a of nitric acid and nitrate is -1.37 at 25°C and the positive reduction potential is 0.96 V [126, 127]. When its concentration in the solution is higher than 86%, it is called, due to the forming fume, fuming nitric acid. By the decomposition of nitric acid by light or thermal load, nitrogen dioxide radicals can be formed (see eq. 2.48).



Nitrifying bacteria can be also form nitrate. In the human body a source of inorganic nitrate comes from diets rich in leafy green foods (e.g. spinach). The half-life of NO_3^- in human blood is with five to eight hours much longer than the half-life of nitrite [132, 133].

Hypochlorous acid

Hypochlorous acid (HOCl) or its deprotonated form, the hypochlorite anion (OCl^-) are potent chlorinating and, with their positive reduction potentials of 1.594 V and 0.89 V [127], respectively, also potent oxidizing agents. They can react with a wide variety of biological molecules (DNA; RNA, fatty acid groups, cholesterol, proteins) and lead to cell lysis and cell death [28]. Since hypochlorites are quite unstable in their pure form, they are usually handled in aqueous solution. HOCl is a weak acid with a pK_a value of 7.5 at 25°C [126]. With water, hypochlorous acid forms hydrochloric acid (HCl) and hydrogen peroxide (see eq. 2.49). In aqueous solution hypochlorous acid is, depending on the pH value, partially dissociated to hypochlorite (eq. 2.50) [134].



The human immune system also generates tiny amounts of hypochlorite as defense molecule against pathogens. The neutrophil granulocytes, which are with 50-65% the most abundant type of the white blood cells in humans, produces OCl^- during destruction of pathogens [135].

2.2 Electron paramagnetic resonance spectroscopy

The methods to detect radicals qualitatively and quantitatively are limited and in the community of free radical detection the method of choice is electron paramagnetic resonance (EPR) spectroscopy [25]. EPR spectroscopy is also called electron spin resonance (ESR) or electron magnetic resonance (EMR) spectroscopy [136]. With electron paramagnetic resonance spectroscopy it is possible to detect paramagnetic species in solids, liquids, or in the gas phase. Mainly these are radicals - atoms or molecules with an unpaired electron - but also detectable by EPR spectroscopy are transient metal ions with up to seven unpaired electrons, point defects in solids, as well as systems with more than one unpaired electron - bi- or multi-radicals (contain two or more unpaired electrons) or triplet-state systems. Due to this broad range of detectable species types, EPR spectroscopy is used in different research fields such as in chemistry, physics, biology and medicine, as well as for quality analysis in industrial research.

After a brief history of EPR, the physics background of the technique is described for the introduction of the abilities and limits of EPR.

In 1895 Hendrik Lorentz predicted line splitting of energy levels. This line splitting of the valence electron energy states occurs when an atom is placed in an external magnetic field. He based his assumption on his electron theory, describing the interaction of light and matter. Pieter Zeeman described one year later the experimental observation of line splitting of an spectral line in a strong external magnetic field [137]. This effect is known as the Zeeman effect. In 1920, Otto Stern and Walther Gerlach found in their famous experiment the intrinsic angular momentum of electrons and atoms [138]. Samuel Goudsmit and George Uhlenbeck proposed the existence of the electron spin five years later [139]. Nuclear magnetic resonance absorption was first measured in molecular beams and described in 1938 by Isidor Rabi [140]. The first electron paramagnetic resonance spectrometers were developed in 1945 by Evgeny Konstantinovich Zavoiskii in Kasan (Russia) [141]. He verified the existence of electron spin resonance by application of radio frequency. Whereas Baggeley, Bleaney, and Griffiths [142], who developed independently from him in 1946 electron paramagnetic resonance spectroscopy in Oxford (United Kingdom), worked already in 1946 with radiation in the microwave region. This is still the common frequency range for EPR measurements. Almost simultaneously, EPR spectroscopy was developed in the United States of America by Cummerow and Halliday [143, 144]. Continuous wave electron paramagnetic resonance (CW-EPR) spectrometers were developed in the years between 1960 and 1980, contemporaneously the first experiments with pulsed EPR were performed. The first commercial pulsed EPR was available in the 1950s. Nowadays, most commonly used EPR spectrometers work at a frequency of around 9.5 GHz . These spectrometers are called X-band EPR spectrometers.

A necessary requirement for successful EPR measurements is an unequal distribution of the spin between the two Zeeman levels. For better understanding of the electron paramagnetic spectra in the following physical and technical details about EPR spectroscopy are given.

2.2.1 Basic principles of EPR

Electron paramagnetic resonance spectroscopy is based on the absorption of microwave radiation by paramagnetic species in the presence of an external magnetic field. Due to a simpler technical setup, typically for electron paramagnetic resonance spectroscopy, the microwave frequency is kept constant whereas the magnetic field is varied. Absorption

2 Fundamentals

of the supplied microwave radiation leads to a transition between the energy levels. The intensity of the magnetic field is increased, which yields a widening of the energy gap of the split levels until the energy of the irradiated microwave and the energy difference of the levels match. An electric transition of the probed species leads to the absorption of the incident photons.

Beer-Lambert law

As EPR spectroscopy is based on the absorption of microwave radiation to evaluate the number of unpaired electrons in the sample, the Beer-Lambert law is introduced in the following: It describes the intensity decrease of electromagnetic radiation during transition of a sample due to absorption (see figure 2.2).

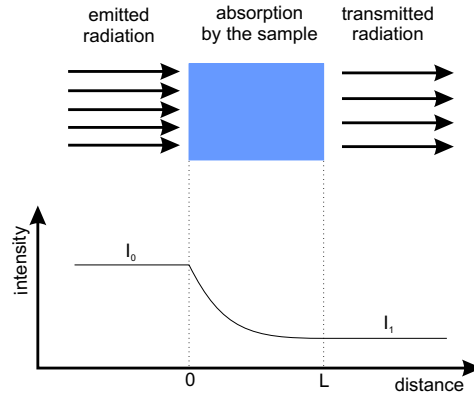


Figure 2.2: Intensity decrease of electromagnetic radiation due to absorption by a sample of the thickness L .

The differential decrease of the radiation intensity ($I(x)$) over the distance x is proportional to the intensity itself, with a constant of proportionality - the so-called absorption coefficient - α and the concentration c . By integration the so-called Beer-Lambert law is given (equations 2.51 and 2.52) [145].

$$\int_{I_0}^{I_1} \frac{dI(x)}{I} = - \int_0^L \alpha(\lambda) c dx \quad (2.51)$$

$$I_1 = I_0 e^{(-\alpha(\lambda) c L)} \quad (2.52)$$

Electron spin

The electron, with a certain mass (m_e) and negative charge, has an angular momentum consisting of two rotations: on the one hand, it spins around the nuclei and, therefore, it has an orbital magnetic momentum. On the other hand, it spins around its own axis having a spin magnetic momentum. The electron spin is one of the main fundamental properties of the electron. It is described by the quantum number S . The total spin angular momentum \vec{S} is given by the sum of the individual ones (eq. 2.53) and its absolute value results from

equation 2.54 [146].

$$\vec{S} = \sum_i \vec{s}_i \quad (2.53)$$

$$|\vec{S}| = \hbar\sqrt{S(S+1)} \quad (2.54)$$

S_z , the component in z-direction, is composed of m_S the projection of the spin angular momentum and reduced Planck's constant $\hbar = h/2\pi$ (eq. 2.55). The possible values of m_S are given by equation 2.56. Since a single unpaired electron has $S = 1/2$, m_S can only have two values, $m_S = +1/2$ (spin up) or $m_S = -1/2$ (spin down). States with $S = 1/2$ are referred to as doublet states since the multiplicity $(2S+1)$ is equal to 2. Following the same logic, states with $S = 1$ are called triplet states [146].

$$S_z = m_S \cdot \hbar \quad (2.55)$$

$$m_S = S, S-1, \dots, -S \quad (2.56)$$

The magnetic momentum of the electron spin μ_S is directly proportional to the spin angular momentum (eq. 2.57), with $g_e = 2.0023$ being the free electron g-factor and μ_B being the Bohr's magneton (eq. 2.58).

$$\vec{\mu}_S = -g_e \cdot \mu_B \cdot \vec{S} \quad (2.57)$$

$$\mu_B = \frac{e\hbar}{2m_e} \quad (2.58)$$

In an external magnetic field, interaction of the \vec{B} -field with the magnetic momentum $\vec{\mu}$ will occur (eq. 2.59). For a single free electron with $S = \pm 1/2$ it will result in an energy difference ΔE of the two levels (equations 2.60, 2.61, 2.62) [146–148]. If there is no external field present, the difference in the energy levels $E_{-1/2}$ and $E_{+1/2}$ will be zero [147, 148].

$$E = -\vec{\mu} \cdot \vec{B} \quad (2.59)$$

$$E = +g_e \cdot \mu_B \cdot S \cdot |\vec{B}| \quad (2.60)$$

$$E_{\pm 1/2} = \pm 1/2 \cdot g_e \cdot \mu_B \cdot |\vec{B}| \quad (2.61)$$

$$\Delta E = g_e \cdot \mu_B \cdot |\vec{B}| \quad (2.62)$$

The g-factor

The gyromagnetic ratio γ of a particle is the ratio of its magnetic dipole momentum and its angular momentum. In contrast to the g-factor, which is closely related to the gyromagnetic ratio and also sometimes referred to as 'gyromagnetic ratio', it is not dimensionless. When an electron or nucleus is placed in an external magnetic field which is not aligned to its magnetic moment, a precession of the angular momentum around the external field axis will occur. This precession has an angular frequency ω which is proportional to the external field. This frequency is called Larmor frequency (eq. 2.65). The orbital gyromagnetic

2 Fundamentals

ratio (γ_L) is given by the absolute value of the magnetic momentum of the orbit $|\vec{\mu}_L|$ divided by the absolute value of the orbital angular momentum $|\vec{L}|$ (eq. 2.64). For a charged particle with the mass m , the charge q is given by equation 2.66. Likewise, the spin gyromagnetic ratio γ_S is given by the magnetic momentum of the spin divided by the spin angular momentum (eq. 2.67). For a free electron, the Larmor frequency results from equation 2.69 with consideration of equation 2.68. In these equations, g_e is the g-factor of the electron, $-|e|$ is the charge of the electron and m_e is the mass of the electron [146].

$$\vec{L} = \sum_i \vec{l}_i \quad (2.63)$$

$$|\vec{L}| = \hbar \sqrt{L(L+1)} \quad (2.64)$$

$$\omega = -\gamma_L \cdot B \quad (2.65)$$

$$\gamma_L = \frac{|\vec{\mu}_L|}{|\vec{L}|} = \frac{q}{2m} \quad (2.66)$$

$$\gamma_S = \frac{|\vec{\mu}_S|}{|\vec{S}|} = \frac{qg_s}{2m} \quad (2.67)$$

$$\gamma_e = -\frac{eg_e}{2m_e} = -\frac{g_e\mu_B}{\hbar} \quad (2.68)$$

$$\omega_e = \frac{g_e\mu_B}{\hbar} B \quad (2.69)$$

The g-factor of an electron consists of three parts corresponding to the three magnetic moments of the electron: the spin angular momentum μ_S , the orbital angular momentum μ_L and the total angular momentum μ_J (eq. 2.70). The spin g-factor g_S is often defined as the absolute value of the negative g_e . The orbital g-factor g_L is equal to one. The total angular momentum g-factor is also called Landé g-factor, g_J , which is defined by equation 2.71, with $\vec{J} = \sum_i \vec{j}$ being the total angular momentum. Since nuclei also have spin and magnetic moments ($\vec{\mu}_I$) they have a g-factor, too. This factor is defined alike, following equation 2.72. There, μ_N is the nuclear magneton and \vec{I} the nuclear spin angular momentum.

$$\vec{\mu}_J = \vec{\mu}_L + \vec{\mu}_S \quad (2.70)$$

$$\vec{\mu}_J = -\frac{g_J\mu_B}{\hbar} \vec{J} \quad (2.71)$$

$$\vec{\mu}_I = \frac{g_N\mu_N}{\hbar} \vec{I} \quad (2.72)$$

The Landé g-factor describes a specific g-value, namely for an electron which has a spin angular momentum as well as an orbital angular momentum (eq. 2.73). With the orbital g-value $g_L = 1$ and the approximation of the spin g-value $g_S \approx 2$, the Landé formula is

simplified to equation 2.74 [144, 147].

$$g_J = g_L \frac{J(J+1) - S(S+1) + L(L+1)}{2J(J+1)} + \quad (2.73)$$

$$g_S \frac{J(J+1) + S(S+1) - L(L+1)}{2J(J+1)}$$

$$g_J \approx 1 + \frac{J(J+1) + S(S+1) - L(L+1)}{2J(J+1)} \quad (2.74)$$

In the presence of multiple electrons, the kind of coupling of the angular momenta needs to be considered. Equation 2.74 is correct in the case of spin-orbit (LS-) coupling, as here, both, the orbital and the spin angular momentum are well defined. Included in the calculation are only the valence electrons, since in closed shells the angular momenta and spin momenta are coupled to zero.

The calculated value of g by application of the Landé formula is only an estimation. In the calculation, corrections due to quantum electrodynamics effects are missing. The implementation of quantum electrodynamics yields a value, which is increased by 1.1‰, so that the resulting value is $g_e = 2.0023193$.

For an atom with a total atomic angular momentum $F = I + J$, the g -value is given by equation 2.75. Since $g_I < g_J$ this formula can be further simplified to equation 2.76.

$$g_F = g_J \frac{F(F+1) - I(I+1) + J(J+1)}{2F(F+1)} \quad (2.75)$$

$$+ g_I \frac{F(F+1) + I(I+1) - J(J+1)}{2F(F+1)}$$

$$g_F \approx g_J \frac{F(F+1) - I(I+1) + J(J+1)}{2F(F+1)} \quad (2.76)$$

Zeeman effect

Two cases for the Zeeman Effect can be distinguished. The normal and the anomalous Zeeman effect. The first developed normal Zeeman effect is actually a special case of the anomalous Zeeman effect. Both effects are described in the following.

Normal Zeeman effect

In the case of the normal Zeeman effect, a semi-classical description is applicable. The electron is in a classical orbit with a quantized orbital angular momentum (eq. 2.64). The amount of split lines for the normal Zeeman effect is determined only by the orbital angular momentum, since the total spin of the system is $S = 0$. Therefore, the interaction energy is only the result of the scalar product of the magnetic field \vec{B} with the orbital angular magnetic momentum $\vec{\mu}_l$ (eq. 2.77). With consideration of equation 2.66, the energy is given by equation 2.78. For the scalar product, $l_z \cdot |\vec{B}|$ can be applied (eq. 2.79). Moreover, with the z-component of the orbital angular momentum, given by $l_z = \hbar m_l$, the energy is given by equation 2.80. Hence, the number of resulting energy levels corresponds to the possible

2 Fundamentals

values of the projection of the orbital angular momentum m_l [143, 146].

$$E_{mag} = -\vec{\mu}_l \cdot \vec{B} \quad (2.77)$$

$$E_{mag} = -\gamma_l \cdot \vec{l} \cdot \vec{B} \quad (2.78)$$

$$E_{mag} = -\gamma_l \cdot l_z \cdot |\vec{B}| \quad (2.79)$$

$$E_{mag} = \mu_B m_l |\vec{B}| \quad (2.80)$$

$$\text{with } m_l = l, l-1, \dots, -l \quad (2.81)$$

The energy levels are split into $2l+1$ equidistant levels with distance of $\Delta E_{mag} = \mu_B |\vec{B}|$.

Anomalous Zeeman effect

For the anomalous Zeeman effect, which in contrast to its name is the common case, the spin angular momentum and the orbital angular momentum cannot be considered separately. They have to be taken into account as the sum, the total angular momentum \vec{j} . Only the absolute value of the total angular momentum and its component in z-direction of the external magnetic field are clearly defined. For the orbital angular momentum the absolute value $|\vec{l}|$ and its scalar product with the spin angular momentum $\vec{l} \cdot \vec{s}$ are also well-defined. Hence, the interaction energy is given by equation 2.82 in consideration of equations 2.83, 2.84, 2.85, and $g_e \approx 2$. Since the g-value is not equal to one, the axis of the total angular momentum and the total angular magnetic momentum are not coinciding anymore. Therefore, the energy of the interaction (eq. 2.86) is also different for different values of j , regarding their influence on the values of the g-value and the projection of the total angular momentum m_j [146].

$$E_{mag} = -\vec{\mu}_j \cdot \vec{B} \quad (2.82)$$

$$\text{with } \vec{\mu}_j = \vec{\mu}_l + \vec{\mu}_s \quad (2.83)$$

$$\text{and } \vec{\mu}_l = \gamma_l \cdot \vec{l} = -\frac{\mu_B}{\hbar} \cdot \vec{l} \quad (2.84)$$

$$\text{and } \vec{\mu}_s = \gamma_s \cdot \vec{s} = -g_e \cdot \frac{\mu_B}{\hbar} \cdot \vec{s} \quad (2.85)$$

$$E_{mag} = m_j \cdot g_j \cdot \mu_B \cdot |\vec{B}| \quad (2.86)$$

$$m_j = j, j-1, \dots, -j \quad (2.87)$$

$$\Delta E_{mag} = g_j \cdot \mu_B \cdot |\vec{B}| \quad (2.88)$$

The splitting for different energy levels is, for the case of the anomalous Zeeman effect, more complex than for the normal Zeeman effect. The Landé g-factor is dependent on both the total angular momentum \vec{j} and the orbital angular momentum \vec{l} . During the interaction of an external magnetic field the orbital and spin angular momenta cannot be treated separately. In the following details are given for the coupling of the spin and the orbit.

Spin-orbit coupling

Since the electron is moving around the nucleus, the electron itself experiences a movement of the positively charged nucleus, which induces a magnetic field \vec{B}_l . The axis of \vec{B}_l is parallel to the axis of the orbital angular momentum \vec{l} and the energy of the interaction with the magnetic momentum of the spin $\vec{\mu}_s$ is given by equation 2.89 with the factor $\eta > 0$.

$$E_{l,s} = \eta \cdot \vec{l} \cdot \vec{s} \quad (2.89)$$

The angular momenta \vec{l} and \vec{s} give the total angular momentum \vec{j} (eq. 2.90 with equations 2.91 and 2.92). The possible values for the total angular quantum number j can be calculated according to equation 2.93:

$$\vec{j} = \vec{l} + \vec{s} \quad (2.90)$$

$$|\vec{j}| = \hbar \sqrt{j(j+1)} \quad (2.91)$$

$$|\vec{j}|^2 = \hbar^2 \left(|\vec{l}|^2 + 2 \cdot \vec{l} \cdot \vec{s} + |\vec{s}|^2 \right) \quad (2.92)$$

$$j = l + s, l + s - 1, \dots, |l - s| \quad (2.93)$$

For the spin quantum number $s = 1/2$, there are two possible values for the orbital quantum number l , zero and one. An orbital quantum number of zero means that the total angular quantum number is equal to the spin quantum number, $j (l = 0) = s$. For an orbital quantum number other than zero j is given by $j (l \geq 1) = l \pm 1/2$; $l \geq 1$ yields two possible values of j . The angular momenta \vec{l} and \vec{s} need to have different orientations to each other. This results in different $\vec{l} \cdot \vec{s}$ and, therefore, the spin-orbit coupling energies differ. The orientation of \vec{s} to the axis through \vec{l} is for both cases not symmetrical. The scalar product will have different absolute values and, hence, the splitting of the energy levels is not symmetrical [146].

Hyperfine structure

The interaction of the electrons with the nuclear angular momentum is called hyperfine structure. The electron induces a magnetic field \vec{B}_J due to their movement. This magnetic field interacts with the magnetic momentum of the nucleus $\vec{\mu}_I$. The coupling of these momenta results in a splitting of the energy levels. Therefore, the nuclear magnetic momentum has two separate effects on the splitting. On the one hand, the nuclear magnetic momentum is interacting with the magnetic field originating from the movement of the electron. This effect is also called the Zeeman effect; that of the nuclear magnetic moment with the atomic magnetic field. On the other hand, the nuclear induced magnetic field interacts with the electronic magnetic momentum, which also contributes to the splitting.

$$\vec{\mu}_I = g_I \cdot \frac{\mu_N}{\hbar} \cdot \vec{I} \quad (2.94)$$

$$\Delta E_{HFS} = -\vec{\mu}_I \cdot \vec{B}_J \quad (2.95)$$

The energy E_{Ij} of $\vec{\mu}_I$ in the inner magnetic field is given by equation 2.96. The magnetic

2 Fundamentals

field is induced by the electron on the location of the nucleus, $B_{int} = B_j$. As the scalar product can also be expressed by the angle between the vectors, this equation turns into eq. 2.97. By further substitution with equations 2.98 and 2.100, this angle is determined by the total angular momentum of the atom \vec{F} , the total angular momentum of the electron, as well as the nuclear spin momentum. The the total angular momentum of the atom is the sum of the total angular momentum of the electron $\vec{J} = \sum_i \vec{j}_i$ and the nuclear spin momentum \vec{I} (see eq. 2.99). Hence, the energy of the hydrogen atom will be given by equation 2.101, whereas A is the so called hyperfine structure constant (eq. 2.102) [146].

$$E_{Ij} = -\vec{\mu}_I \cdot \vec{B} \quad (2.96)$$

$$E_{Ij} = -|\vec{\mu}_I| \cdot B_j \cdot \cos(\angle(\vec{j}, \vec{I})) \quad (2.97)$$

$$\cos(\angle(\vec{j}, \vec{I})) = \frac{\vec{j} \cdot \vec{I}}{|\vec{j}| \cdot |\vec{I}|} \quad (2.98)$$

$$\begin{aligned} \vec{j} \cdot \vec{I} &= \frac{1}{2} (\vec{F}^2 - \vec{j}^2 - \vec{I}^2) \\ \vec{F} &= \vec{j} + \vec{I} \end{aligned} \quad (2.99)$$

$$\cos(\angle(\vec{j}, \vec{I})) = \frac{1}{2} \cdot \frac{F(F+1) - j(j+1) - I(I+1)}{\sqrt{j(j+1) \cdot I(I+1)}} \quad (2.100)$$

$$\Delta E_{HFS} = \frac{A}{2} \cdot [F(F+1) - j(j+1) - I(I+1)] \quad (2.101)$$

$$A = \frac{g_I \cdot \mu_N \cdot B_j}{\sqrt{j(j+1)}} \quad (2.102)$$

Due to hyperfine structure interaction between nuclear magnetic momentum and electrons, each energy level $E_{n,l,j}$ is split into its hyperfine components according to equation 2.103:

$$E_{HFS} = E_{n,l,j} + \frac{A}{2} \cdot [F(F+1) - j(j+1) - I(I+1)] \quad (2.103)$$

Sensitivity

The population of the spin at thermal equilibrium and with an applied external magnetic field is distributed between the two so-called Zeeman levels, following Boltzmann's law. For EPR spectroscopy this means that the absorption of the irradiated microwave energy can only occur as long as the particle number in the upper state is less than in the lower state. The ratio for equilibrium is predicted by the Boltzmann distribution which gives the ratio between the population of the upper to the lower level. This ratio results from equation 2.104, where k_B is the so called Boltzmann constant, T is the temperature, and ΔE the energy difference of the two levels. With $\Delta E_{mag} = g_j \cdot \mu_B \cdot B$ the expression becomes equation 2.105.

$$\frac{N_{upper}}{N_{lower}} = \exp\left(-\frac{\Delta E}{k_B T}\right) \quad (2.104)$$

$$\frac{N_{upper}}{N_{lower}} = \exp\left(-\frac{g_j \mu_B B}{k_B T}\right) \quad (2.105)$$

For room temperature the exponent is very small and an approximation is valid. Therefore, the exponential can be written according to the first order series expansion as $\exp(-x) \rightarrow 1 - x$, this leads to equation 2.106. For the conditions applied in this study (298 K and an external magnetic field of around 3000 G) the ratio is close to unity (eq. 2.107). Hence, there is just a marginal difference in population, but still enough to lead to absorption.

$$\frac{N_{upper}}{N_{lower}} = 1 - \frac{g_j \mu_B B}{k_B T} \quad (2.106)$$

$$\frac{N_{upper}}{N_{lower}} = 0.9986 \quad (2.107)$$

Since the absorbance determines the sensitivity of the measurement, the sensitivity can be enhanced by working at lower temperatures and/or with higher magnetic field strength [147–149].

Spin relaxation mechanisms

At 298 K and at an applied external magnetic field of 3000 G, the population of the two energy levels are almost identical. If there is no relaxation from the upper level to the lower level, saturation occurs. Therefore, to prevent saturation the electrons in the upper level need to release energy, $E = h\nu$, to relapse to the lower state. These processes are called spin relaxation processes. Two relaxation processes are relevant, namely the spin-lattice relaxation and the spin-spin-relaxation [144].

Spin-lattice-relaxation describes the interaction of the unpaired electrons with the surrounding molecules, the lattice. The dissipation of the released energy within the lattice will be in the form of vibrational, rotational, or translational energy. The characteristic parameter for this relaxation is the relaxation time τ_1 . This τ_1 is determined by the necessary time for a decrease to a $1/e$ -part of the original, the excess energy of the spin system. A short relaxation time τ_1 represents a fast dissipation of the energy. This is essential for the determination of differences in population of both levels. If the spin-lattice relaxation time is long, saturation can occur. This diminishes the EPR signal. Long relaxation times frequently occur in systems with free radicals, especially for low temperatures.

The spin-spin-relaxation takes place by interaction of unpaired electrons in the upper level with nearby electrons or magnetic nuclei in the lower level. This relaxation does not transfer the energy into the lattice. The process is characterized by the relaxation time τ_2 .

Both relaxation processes, the spin-spin-relaxation and the spin-lattice-relaxation, can contribute to the electron paramagnetic resonance signal. The magnetic field difference (ΔB) is proportional to the sum of the reciprocal relaxation times (see eq. 2.108).

$$\Delta B \propto \frac{1}{\tau_{1e}} + \frac{1}{\tau_{2e}} \quad (2.108)$$

$$\text{since : } \tau_{1e} > \tau_{2e} \quad (2.109)$$

The magnetic field difference mainly depends on the spin-spin-interaction. A decrease of the spin-spin distance is directly depending on the increase in spin concentration. The spin-lattice-relaxation times thus become very short, so that the influence of this relaxation

2 Fundamentals

process becomes more relevant for the line width than spin-spin-relaxation. If the spin system is just loosely coupled to the lattice, the relaxation time τ_{1e} increases and the electrons are not able to reduce the energy to drop back to the lower energy level. Hence, the lower level is emptied and saturation occurs. To prevent this, the applied intensity of the microwave radiation should be reduced.

Experimental technique

In figure 2.3, a principal setup of an X-band electron paramagnetic resonance spectrometer is depicted. It consists of a so-called microwave bridge, where the electromagnetic radiation source in the microwave region as well as the detector is situated. The sample is placed in a resonator, usually a cavity, between the pair of magnetic coils. The console containing the signal processing and control electronics, is connected to a computer for data analyzing and controlling all units of the spectroscope.

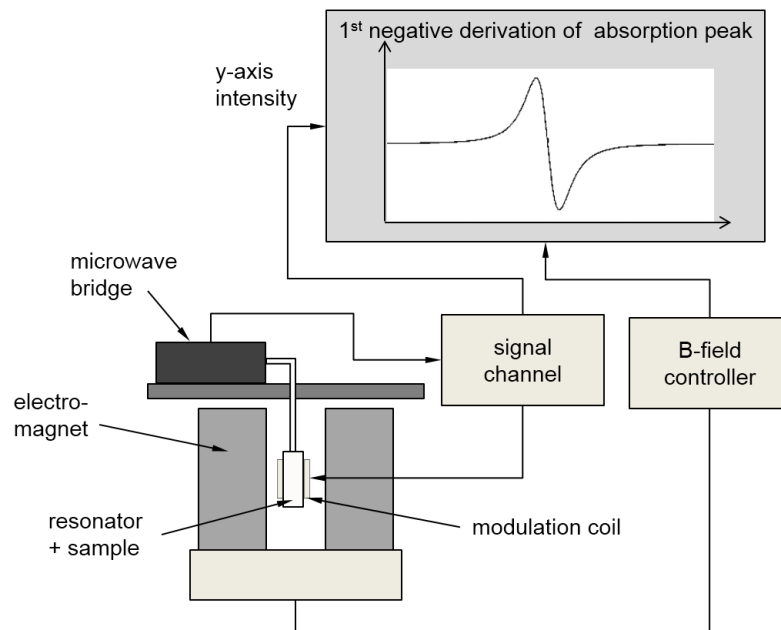


Figure 2.3: Scheme of an X-band EPR spectroscope setup (adapted from [149]).

Microwave bridge

In the microwave bridge the radiation source and the detector are placed. The microwave originates from the microwave source. In older EPR spectrometers the source is a so-called klystron, in newer systems it is a Gunn diode. Since the variation of the output power of the microwave source is challenging but essential for avoiding saturation, an attenuator is set to precisely control the amount of irradiated microwave radiation to the sample [149]. Through a circulator, the radiation is guided to the cavity where only a part of the source microwave radiation is reflected. This part is passing the circulator again and is measured by the detector in comparison to the original amount of irradiated microwave radiation. Common detectors are Schottky diodes. If the diode current is proportional to the microwave radiation for lower power levels ($\leq 1 \mu W$), the detector is called square law detector. For high power levels ($\geq 1 mW$) the diode current is proportional to the square root of the microwave power and the detector is a linear one. For quantification and best sensitivity, the linear mode of the diode should be applied [149]. The optimum concerning sensitivity and quantification is reached if $200 \mu A$ is used as diode current. Therefore, a reference arm with a phase shifter provide additional microwave power in phase with the reflected microwave to support working at ideal conditions.

EPR cavity

The EPR signals are weak, therefore, a cavity is used for amplification. Microwave cavities are rectangular or cylindrical metal boxes which resonate with the irradiated microwave. In resonance case, the microwave energy will not exit the cavity and no reflected radiation will reach the detector. The so-called quality factor Q is characteristic of a cavity and represents the amount of stored energy (E_{stored}) in the cavity per lost energy per microwave period (E_{lost}) according to equation 2.110. The Q -factor can be determined via equation 2.111, whereas the resonance frequency is given by ν_{res} and $\Delta\nu$ is the width at half height of the resonance [149].

$$Q = \frac{2\pi E_{stored}}{E_{lost}} \quad (2.110)$$

$$Q = \frac{\nu_{res}}{\Delta\nu} \quad (2.111)$$

As result of the resonance inside the cavity, a standing wave occurs so that the electric and magnetic field components are exactly out of phase. Since most samples also absorb energy in non-resonant conditions by their electric field component, the phase difference of both electric and magnetic field can be used to enhance sensitivity and signal strength by placing the sample in the resonator cavity. Due to the strong impact of the magnetic field for the absorption the sample is located at electric field minimum and magnetic field maximum, yielding the strongest signals and the highest sensitivity. The coupling of the microwaves in the cavity takes place by the use of the so-called iris. The iris is a hole of variable size. This change in size can be tuned and, therefore, the amount of forward and reflected microwave radiation can be controlled. When the impedances are matched by the iris, the resonator is, so-called, critically coupled. The absorption of the microwave by the sample reduces the quality factor due to the increased losses. Additionally, the coupling is also altered, since the absorption of the microwave by the sample influences the impedance of the cavity itself. This leads to a no longer critically coupled cavity. Hence, the microwave

will be reflected back to the detector and an EPR signal can be observed [149].

Sensitivity enhancement by modulation

The sensitivity of the EPR spectroscopy can be enhanced by a phase sensitive detection technique. This method provides a decrease in the noise from the detection diode as well as an elimination of the baseline instabilities resulting from the electronics. The phase sensitive detection is implemented in the signal channel [149].

For sensitivity enhancement by this phase sensitive technique, the magnetic field applied to the sample is modulated with a modulation frequency (usually 100 kHz). The resulting EPR signal, e.g. the reflected microwave radiation from the cavity is modulated in its amplitude at the same frequency. Thus, if the EPR signal is approximately linear over a range similar to the width of the modulation amplitude, the signal is transformed into a sinusoidal signal, of which the amplitude is proportional to the slope of the absorption peak. The resulting EPR signal is the derivation of the absorption peak (see figure 2.4). The signal channel also produces a reference signal (proportional to the amplitude of the modulated signal) with the same frequency and phase as the modulated field which it will be compared with. If the comparison results in differences, these signals will then be suppressed. This can lead to a sensitivity increase of several orders of magnitude. However, applied values, modulation frequency as well as amplitude and time constant, need to be chosen with caution. If the modulation amplitude is too low, the EPR signal amplitude is increasing during the magnetic field increase. Amplitudes of the modulation larger than the line width of the EPR signal falsify the signal, because a broadening of the signal will occur.

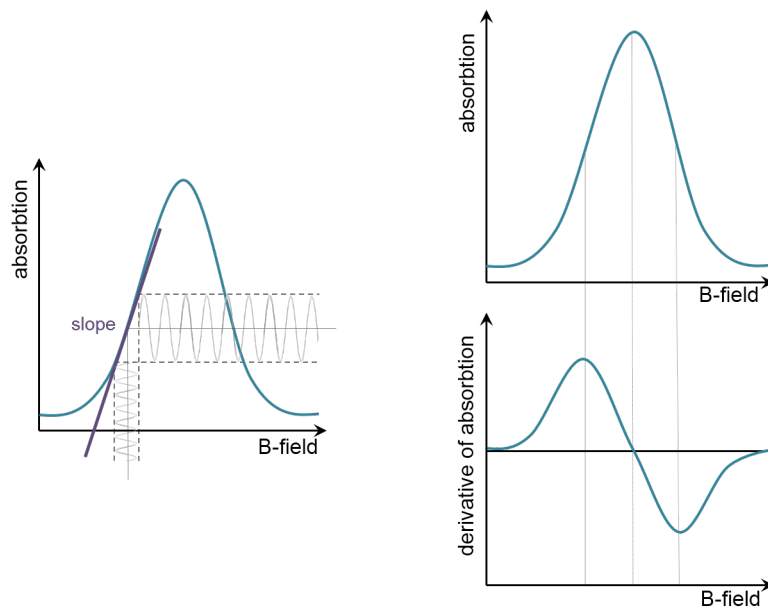


Figure 2.4: Sketch of the modulation of the absorption peak with a modulation frequency. The modulation yields the first derivative of the absorption peak.

Magnetic field controller

For the defined tuning of the magnetic field the magnetic field controller is used. It houses two parts, one for the controlled timing and one for the magnetic field values. The magnetic field controller controls the so-called sweep rate, the time steps between the different magnetic field steps (in maximum 4096 steps are possible), and also the magnetic field values. The regulation of the magnetic field is monitored by a Hall probe located in between the magnet. The voltage determined by the Hall probe is compared to the reference voltage, which is given by the other part of the controller. Occurring differences in the voltages are corrected by changing the current flowing through the windings of the magnet resulting in the rearrangement of the magnetic field [149].

EPR spectrum

From the EPR spectrum itself, many information can be gained. The intensity of the absorption signal expresses, in general, the presence of unpaired electrons in the sample, whereas the g-factor gives information about the kind of sample. From the line shape the molecular motion in the sample can be deduced. Information about the nearby atoms can be concluded from the hyperfine structure as it is shown in figure 2.5. In the upper left part of figure 2.5 the chemical structure of the hydroxyl radical bonded to the common spin trap DMPO is shown. The values hyperfine splitting due to the interaction with the two neighbor atoms, N and H, of the molecule's radical center are given by a_N for the interaction with the nitrogen atom and a_H for the hydrogen atom interaction. For the case of DMPO-OH the values are the same for both interactions, hence, the distance between the peaks are similar and an overlapping of the two middle ones occurs. Therefore, the resulting pattern consists of four peaks with an intensity distribution of 1:2:2:1. This pattern in combination with the hyperfine splitting values a_N and a_H is characteristic for this specific spin trap adduct. From the area below the peaks the total number of spins, and hence, the concentration can be deduced.

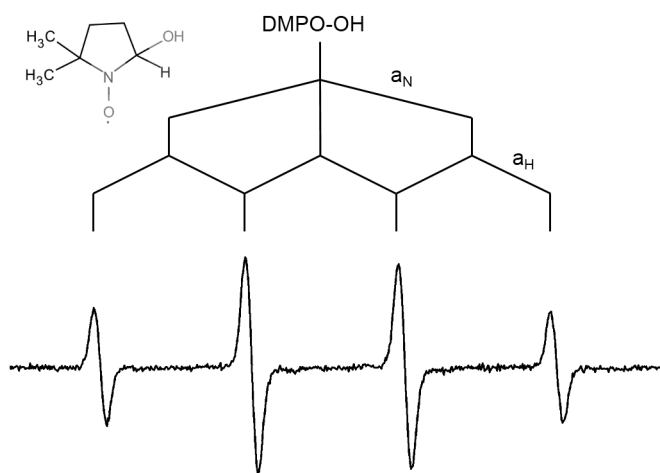
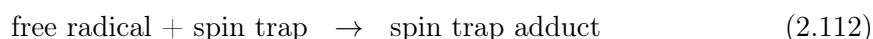


Figure 2.5: Peak pattern of the hydroxyl radical adduct with the common spin trap DMPO.

2.2.2 Spin trapping technique

Many free radicals of interest, especially in mammalian systems, are quite short-lived and, hence, from their concentrations, below the detection limit of the commonly used EPR spectroscopes (approximately $10^{-6} M$ [150]). Some free radicals, present in sufficient concentrations for EPR measurements, will not be measurable since their spin relaxation times are very short under the investigated conditions [150]. Free radicals belonging to these and, therefore, unobservable reactive species, are the hydroxyl radical, the superoxide anion radical, as well as the alkoxy radicals and sulfur-centered radicals. A measurement approach for these radicals is the so-called spin trapping technique. Due to the findings of Iwamura and Inamoto that a stable nitroxide is formed by the reaction of two carbon centered radicals with phenyl *tert*-butyl nitron (PBN), the group of Janzen and Blackburn started to investigate what they will later term 'spin trap' [151, 152]. Spin traps are compounds which react with short-lived free radicals forming more stable molecules. These molecules are so-called spin adducts (eq. 2.112), which are due to the bonded radical EPR active, meaning they are paramagnetic.



The spin trapping technique was developed almost simultaneously in 1968/69 by five different groups: beside the groups around Janzen [152] also the groups of Lagercrantz [153], Perkins [154], Leaver and Ramsay [155–157], and Konaka [158] investigated the stabilization of short-lived free radicals by addition reaction. Mainly two kinds of spin traps have been developed, nitroso and nitron compounds. The groups of Mackor, Forshult and Lagercrantz, Perkins and Chalfont, as well as Leaver and Ramsay investigated nitroso compounds as spin traps [153–155, 159–164]. Nitroso ($R-NO$) spin traps have the huge advantage, that the free radical directly bonds to the nitrogen atom of the nitroso molecule (see eq. 2.6). The reason for the stability of the nitroxide radical in the compound is the delocalization of the electron between the nitrogen and oxygen atom. This leads to more easily accessible information about the structure of the free radical studied, but the major drawbacks of nitroso spin traps are their instability of oxygen-centered and sulfur-centered free radical adducts as well as their property to dimerize and the formation of nitroxides due to photolysis or thermal decomposition [96, 151, 165, 166].

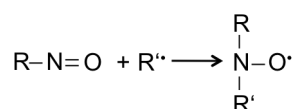


Figure 2.6: Reaction of a free radical with a nitroso spin trap forming fairly stable nitroxide radicals.

Nitron compounds instead bind the free radical to the carbon atom. Therefore, the information regarding structure and nature (O-, N-, C-, S-centered) is more difficult to obtain than for nitroso spin traps. The nitron spin traps also generate nitroxide radicals. The radical character for the trapped free radical stick to the nitroxide part of the compound, whereas the former free radical is bonded to the carbon atom (see figure 2.7). The so formed nitroxide radicals yield a 1:1:1 EPR peak pattern, due to the interaction of the

unpaired electron with the nitrogen atom of the spin trap. Further peaks occur due to other nuclei in the radical itself.

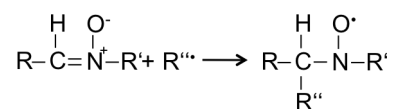


Figure 2.7: Reaction of a free radical with a nitron spin trap forming a fairly stable nitroxide radical.

The nitroso spin traps directly bond the radical to the nitrogen atom, whereas nitron traps bind to the carbon atom. This leads to a different stability of the spin trap adduct. Adducts of radicals with the nitroso traps are less stable than the ones bonded to the nitron traps, especially in the case of oxygen radicals. This is a strong disadvantage. Furthermore, the EPR spectrum is more easily influenced by nitroso trap radicals and generates hyperfine splittings. However, in biological systems, the reason for the use of nitron spin traps as the agents of choice for spin trapping is their ability to form stable and specific adducts with oxygen- and sulfur-centered free radicals [167]. A nitron spin adduct usually yields a distinctive EPR spectrum characteristic for a particular free radical that is trapped. Additionally, nitrones are better soluble in water than nitroso compounds [166].

The spin trap type, nitroso or nitron, as well as the specific spin trap itself need to be chosen for each specific case. In this work only nitron spin traps have been used, due to the focus of reactive species in aqueous solutions relevant to mammalian systems and medicine.

3 Materials and methods

In this chapter, the used plasma source and the different experimental setups are introduced. Furthermore, the applied chemical assays and the electrochemical detection as well as tables of the used chemicals and devices are described. The experimental conditions for the performed electron paramagnetic resonance measurements are given.

3.1 Plasma jet and treatment of liquids

Plasma-liquid interaction are investigated with respect to the interaction of an atmospheric pressure plasma jet with relevant liquids for plasma medicine. This plasma jet is a commercially available device named kinpen09 (neoplas GmbH, Greifswald, Germany). The applied feed gas is mainly argon (argon N50, Air Liquide, Paris, France) with a total flow rate of 3 standard liters per minute (slm). In individual studies molecular admixtures to the feed gas argon are also added. In all experiments the total gas flow rate of 3 slm is kept constant. A scheme of the plasma jet and the liquid treatment is shown in figure 3.1. This plasma jet consists of a ceramic capillary (1.6 mm in diameter) with a centered needle electrode inside. This electrode is driven at a frequency of around 1 MHz. The grounded ring electrode is positioned close to the end of the capillary (2 mm distance to the nozzle) at the outside around the ceramic [168]. The RF power dissipated in the plasma usually lies between 0.9-2.2 W [12]. From a calorimetric experiment performed with a laboratory version (kinpen Sci) of the kinpen09 used in this work a dissipated power of around 1.1 W can be deduced [169].

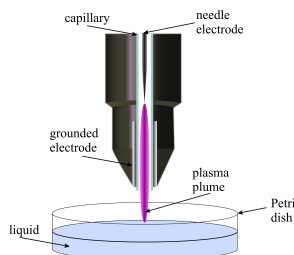


Figure 3.1: Schematic drawing of the kinpen09.

The standard plasma treatment of the liquids is the following: a 60 mm in diameter polystyrene Petri dish (TPP, Trasadingen, Switzerland) is filled with 5 mL of the investigated liquid and placed under the plasma jet at a distance of 9 mm from the plasma jet's nozzle to the liquid surface (see figure 3.2a). This distance is kept constant for all experiments. The plasma jet is moved in a meandric pattern (see figure 3.2b), by the use of a computer controlled xyz-table over the liquid surface.

The results of this work show that the environment has strong impact on the liquid chemistry, hence, a controlled environment during the liquid treatment with the plasma jet

3 Materials and methods

is necessary. This can be provided by application of a curtain gas device (see figure 3.2c) [21, 22, 33, 170]. More details on the influences of ambient surroundings and, hence, the necessity of a curtain gas device are described in section 4.2.1. This curtain gas device outlet has a distance of 1.9 mm to the plasma jet's nozzle. Used gases for the curtain are oxygen (oxygen N48, Air Liquide, Paris, France), nitrogen (nitrogen N50, Air Liquide, Paris, France), a mixture of both or synthetic air (synthetic air L50, Air Liquide, Paris, France). The total curtain gas flow rate is in all cases set to 5 slm .

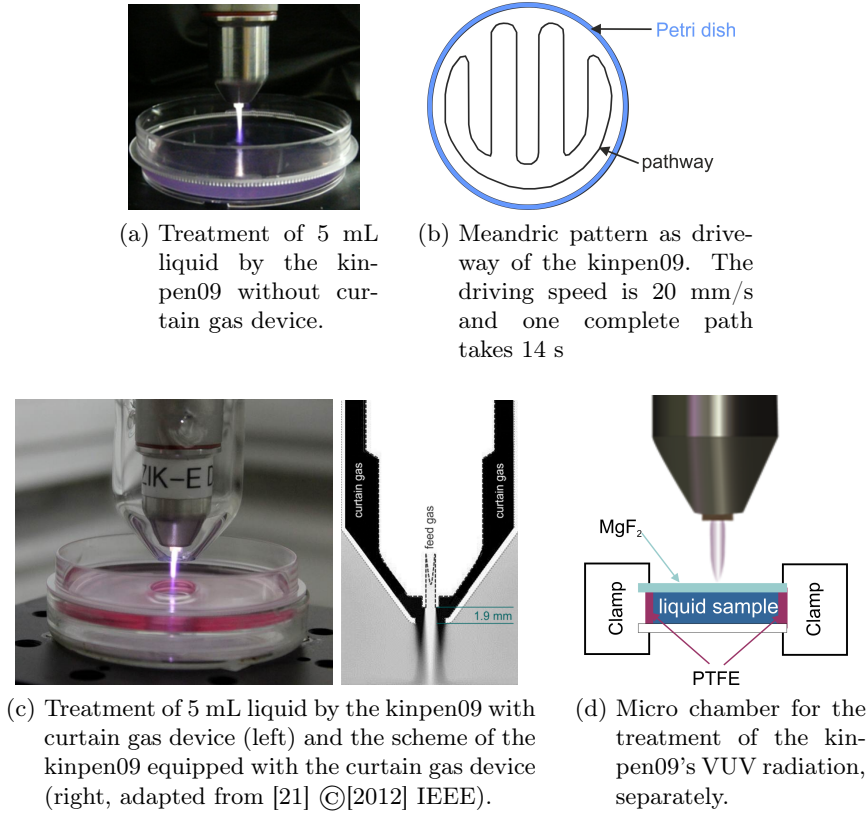


Figure 3.2: Kinpen09 treatment setups for different studies.

To the treatment standard procedure in this work, there is one exception: for the investigation of the impact of VUV radiation of the plasma jet on the liquid chemistry a specially constructed micro chamber (see figure 3.2d) is necessary. This micro chamber consists of a polytetrafluoroethylene (PTFE) ring of $400\text{ }\mu\text{m}$ thickness, with a cutout for filling in the liquid and taking samples after treatment. This PTFE ring is covered by a magnesium fluoride (MgF_2) window on the upper side, the bottom cover is an acrylic glass plate. The window-ring-plate construction is held together by two clamps. The liquid volume in the chamber is due to the size of the PTFE rings set to $80\text{ }\mu\text{L}$. For the measurement, the micro chamber is completely filling to avoid air bubbles in the solution. The plasma jet is positioned at 9 mm distance to the liquid surface. The usage of the MgF_2 covered micro chamber provides, due to its cut-off wavelength of 115 nm the exclusion of all reactive components of the plasma jet besides (V)UV radiation. All determined values by this measurement of VUV treatment are corrected by the window transmission, and the treatment volume is eliminated for comparison with the plasma treatment in a Petri dish.

3.2 Colorimetric assays

For the chemical analysis of reactive species in the plasma treated liquids selective color-forming assays are used. The applied assays are well-known and established for the detection of relevant stable reactive species in plasma-liquid interaction. In the following details are given for the colorimetric detection of nitrate and nitrite, hydrogen peroxide and ozone used in this work.

3.2.1 Nitrate and nitrite

The determination of nitrate and nitrite is performed using a colorimetric assay based on the Griess reaction. The underlying chemistry of this assay is the reaction of nitrite with the Griess reagents resulting in a deep purple azo compound. The commercial assay used, is the so-called 'nitrite/nitrate detection kit' from Cayman Chemical Co. (Ann Arbor, USA). As a simple method for the detection of the total nitrate/nitrite concentration the Griess assay is well established. Due to the use of a reductase enzyme and a related cofactor nitrate is converted into nitrite and therefore it becomes detectable by the assay. The Griess reagent 1, which is sulfanilamide, reacts with nitrite and forms a diazonium salt as shown in figure 3.3. The addition of N-(1-naphthyl)-ethylenediamine (Griess reagent 2) to the diazonium salt leads to the formation of a deep purple color (see figure 3.4).

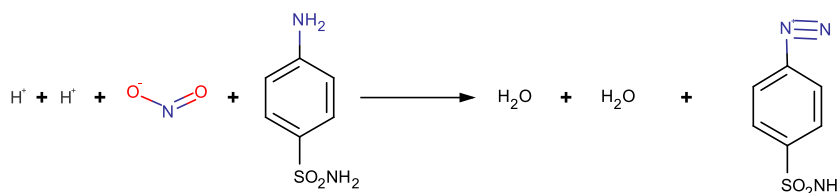


Figure 3.3: Reaction of nitrite with sulfanilamide (Griess reagent 1) to diazonium salt.

The measurement procedure is performed in 96-well plates, where each sample is analyzed, each with its own standard row. These standard rows are necessary for all colorimetric assays performed in well plates, since the absorption length in a well plate is defined by the filling heights, which, although the same volume is used differs for the different liquids. In contrast, if the assay is performed in a cuvette, the cuvette thickness gives the absorption length and due to the sideways measurement contrary to the downwards irradiation in the well plate the filling heights is unimportant. The concentrations applied for the standard row are in maximum $109.375\ \mu\text{M}$ for nitrite and for nitrate. Each data point represents the average value of three independent samples, where a threefold measurement of the sample concentration is performed for each sample. By measuring the absorbance using a microplate reader (Tecan Infinite M200 Pro; Tecan Group Ltd., Männedorf, Switzerland) at $540\ \text{nm}$ the concentration can be deduced by comparing the sample's absorbance with the one of the related standard row. For evaluation of the nitrate concentration, NO_3^- is converted as described above to NO_2^- . The difference of the so-determined total nitrite and nitrate concentration to the separately measured nitrite concentration alone gives the nitrate concentration in the investigated samples.

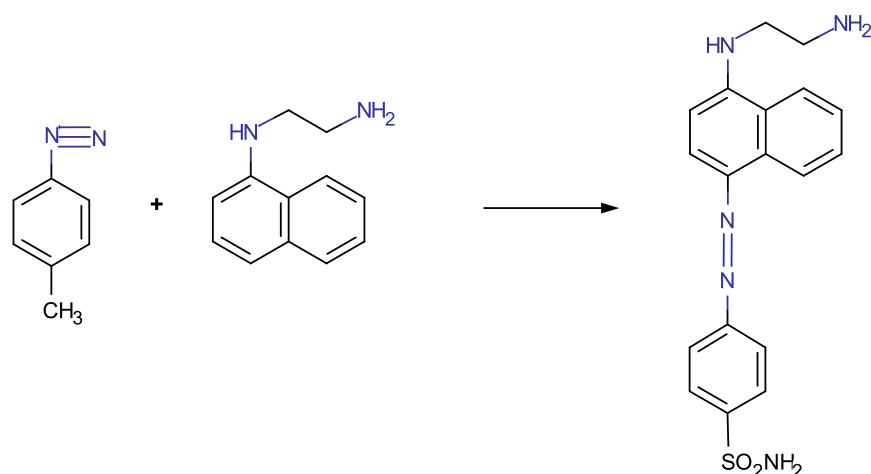


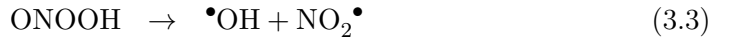
Figure 3.4: Reaction of diazonium salt with Griess reagent 2 (N-(1-naphthyl)-ethylenediamine) to the detectable deep purple azo compound.

Each well has, if filled with the sample and all detection solutions, at the end a volume of 200 μL . To 80 μL of the unknown sample 10 μL of each, reductase enzyme and related cofactor are added for nitrate determination. For nitrite determination instead 20 μL of the investigated untreated solution are added. These 100 μL volumes are incubated for one hour prior to further steps. This activation takes place in parallel for the samples and their related standard row. Finally, 50 μL each of Griess reagent 1 and Griess reagent 2, respectively, are mixed with the prepared melange of sample and assay solution. The measurement by the plate reader is performed after an additional ten minutes incubation. The background signals from the untreated solution and the well plate are subtracted before the concentration calculation.

3.2.2 Hydrogen peroxide

Hydrogen peroxide concentration is determined by three different colorimetric reactions, namely via the reaction with titanium(IV) oxysulfate, Amplex[®] Red, or by the use of commercial peroxide test stripes. All three methods are described in the following and are compared to verify the results and exclude cross-reactivities.

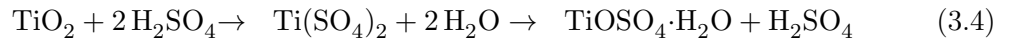
The assay using titanylsulfate contains sulfuric acid which leads to an acidification of the solution. Under acidic conditions, reactions 3.1 to 3.3 can occur if nitrite is present [58, 171]. This can influence the determination of the hydrogen peroxide concentration. Therefore, the applicability of the measurement is verified by using assays not based on titanylsulfate and where the buffer capacity of the investigated solution is not consumed due to added acids.



Amplex[®] RedAssay is known to be specific for hydrogen peroxide [172], but only applicable for concentrations up to 100 μM . For higher concentrations either dilution steps need to be performed or another assay such as titanylsulfate has to be used. The test stripe method has the big advantage of being applicable to small volumes, e.g. at least 7 μL of the sample volume are required per test stripe in contrast to Amplex[®] Red and titanylsulfate where 50 μL and 100 μL , respectively, are needed per sample for a single measurement point.

Titanylsulfate

The titanylsulfate assay is based on the reaction of titanium(IV) oxysulfate (TiOSO_4 solution, Fluka, Sigma Aldrich, St. Louis, USA) with hydrogen peroxide. TiOSO_4 is produced when TiO_2 is dissolved in sulphuric acid (see 3.4). This forms in water the ions $[\text{Ti}(\text{OH})_2]_2^+$ and $[\text{Ti}(\text{OH})_3]^+$ as well as hydrogen sulphate (eq. 3.5). The product of this reaction, $[\text{Ti}(\text{OH})_3(\text{H}_2\text{O})_3]^+$, is the actual reactant of hydrogen peroxide. Their reaction yield the yellow-orange complex $[\text{Ti}(\text{O}_2)(\text{OH})(\text{H}_2\text{O})_3]^+$ (eq. 3.6). The absorption at 407 nm is then according to Beer-Lambert law a measurement for the hydrogen peroxide concentration.



In this work, the assay is performed in 96 well plates. Each sample is pipetted into three wells (three dependent samples). Additionally, the same plasma treatment is repeated three times (three independent samples). Each sample set has its own simultaneously measured standard row. The color-forming Ti(IV) reagent is mixed with the samples and the standard solution in a ratio of 1:2, meaning 100 μL of the sample 50 μL reagent are added. Prior to the measurement, the solutions are well mixed. The absorption measure-

3 Materials and methods

ment is performed against the background control at 407 nm (Tecan infinite M200 pro, Tecan Group Ltd., Männedorf, Switzerland).

Amplex[®] Red

The second colorimetric method for the detection of hydrogen peroxide in plasma treated liquids is performed by the use of the commercial Amplex[®] Red Hydrogen peroxide/peroxidase Assay Kit (Molecular Probes, Eugene, USA). Amplex[®] Red (10-acetyl-3,7-dihydroxyphenoxazine) forms in the presence of peroxidase, for instance horseradish peroxidase (HRP), with hydrogen peroxide in a 1:1 stoichiometry resorufin (figure 3.5). Since the extinction coefficient is quite high, both, a fluorometric and spectrophotometric detection is possible for this assay. According to the manufacturer and to the literature, the reagent is light-sensitive and unstable for pH values higher than 8.5 [172]. Additionally, the fluorescence of resorufin is also pH-dependent. The fluorescence wavelength shifts below the pK_a of ~ 6.0 . Therefore, the assay has to be performed at pH values between 7 – 8. Concentrations of hydrogen peroxide that are too high ($\geq 100 \mu M$) also falsify the assay due to possible oxidizing of resorufin to the non-fluorescent resazurin.

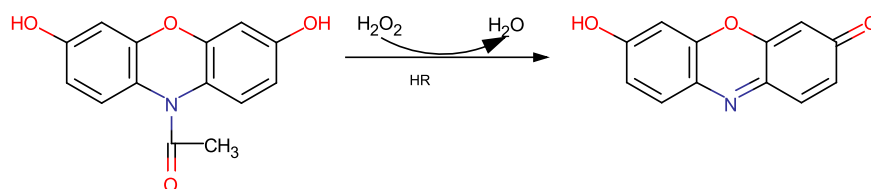


Figure 3.5: Reaction of Amplex[®] Red via horseradish peroxidase with hydrogen peroxide to resorufin.

The assay procedure in the work is the one suggested by the manufacturer. The measurements are all performed in a 96 well-plate, where each well is filled with the final volume of 100 μL . Prior to the plasma treatment, all stock solutions as well as a standard row are prepared for each sample set. Three independent repetitions of the plasma treatment are performed and each sample is pipetted into three wells. The wells for the sample and for the standard row are filled with 50 μL solution of either the sample or the standard. After all wells are loaded with the samples or the standard row, the working solution of the reagent and HRP are prepared in the reaction buffer, which ensured the proper pH range. Adding this to the samples initiates the reaction starts. Absorption or fluorescence could be measured after 30 minutes incubation time at 560 nm and 590 nm, respectively, by use of a multiplate reader (Tecan infinite M200, Tecan Group Ltd, Switzerland). Concentrations of hydrogen peroxide could be determined by comparing the sample absorption and fluorescent values with the one of the standard row after subtracting the background.

Merck test stripes enhanced by camera read out

The third method used for determining the H_2O_2 concentration in plasma treated liquids is also a colorimetric assay where peroxidase reacts with the peroxide oxygen to form a blue colored oxidation product. The commercial test stripes (MQuant™ 110011, Merck, Darmstadt, Germany) read out is enhanced by a microscope camera (digital microscope camera 1.3 million pixel, zoom factor 10 to 200x, Conrad, Germany) situated in a dark box with defined constant light conditions in order to precisely analyze the color of the sensor part of test stripes by determination of the red-, green- and blue-values. Prior to each experiment a calibration is conducted, where the related color values of hydrogen peroxide concentrations in the range of $0 - 180 \mu\text{M}$ ($0 - 6 \text{ mg/L}$) are determined. These H_2O_2 concentrations are prepared by dilution of a 10 M hydrogen peroxide stock solution ($340 \text{ g} \cdot \text{L}^{-1}$, MerckKGAA, Darmstadt, Germany) in the investigated liquid.

For the calculation of the concentrations, the given concentration of hydrogen peroxide from the calibration is plotted over the sum of the color values of the red and green camera channel. The resulting linear calibration curve is then used for the calculation of the sample H_2O_2 concentrations.

Each sample is measured with at least three different test stripes, on which always the same volume of the investigated solution is pipetted. The optimal liquid volume for the test stripes is between $10 - 30 \mu\text{L}$. Also a volume low as $7 \mu\text{L}$ is possible to receive reproducible color values and, therefore, hydrogen peroxide concentration. Each plasma treatment is repeated three times to get three independent values. The incubation time before read-out is held constant during an experiment, at values between 15 seconds and 1 minutes due to handling reasons. This is well within the manufacturer suggestion of at least 15 seconds but not exceeding 3 minutes.

The comparison of these three different colorimetric assays for the detection of hydrogen peroxide, titanium(IV)oxysulfate, Amplex® Red and Merck test stripes is performed and published for the last two methods in reference [71] where Amplex® Red values are determined via fluorescence and absorption measurements and both gave the same values, also comparable with the test stripes method. The test stripe values are at the lower end of the error bars of the via Amplex® Red determined values (see figure 4.22 in section 4.2.2). Since the assays are based on different reactions, a cross-reactivity falsifying the assays can be excluded or at least negligible under the present conditions. Only if all tested assays are equally sensitive to the other generated species, which is not very likely, would this conclusion be wrong.

3.2.3 Ozone

The ozone concentration in the liquid phase is investigated by the use of the so-called indigo assay. This colorimetric assay is based on the decolorization of the indigo blue dye by ozone. First described in 1981 by Bader and Hoigné [173], this method of aqueous ozone concentration determination became widely accepted. Compared to other methods it is more selective, fast, sensitive and has less interferences with manganese ions, chlorine, hydrogen peroxide and ozone decomposition products [174, 175]. Due to the interferences with chlorine it is necessary to perform the assay in chlorine free solutions, for example in deionized water. In this work ultrapure water (HPLC grade) is used for the assay. It has to be noted that the interaction of the assay with other oxidizers such as hydrogen peroxide or hydroxyl radical makes a reliable measurement quite difficult, yet it can be used for getting an indication of ROS in general.

3 Materials and methods

For the measurements indigo trisulfonate is the stock solution used; this intense blue dye is oxidized by ozone to the colorless isatin sulfonate (figure 3.6). Spectrophotometrically, the decolorization can be determined against the an untreated control. At low pH (below 4) the reaction of indigo trisulfonate with ozone appears stoichiometrically in a 1:1 ratio.

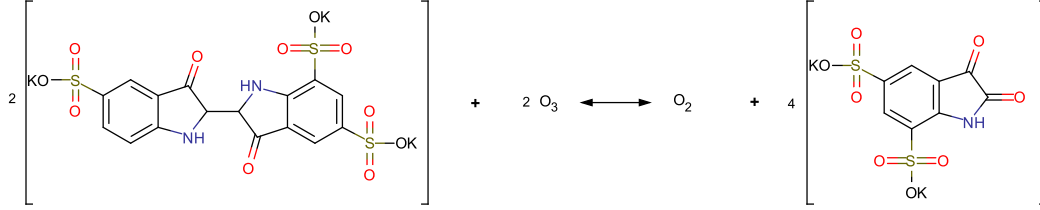


Figure 3.6: Indigo trisulfonate reaction with ozone to potassium isatin sulfonate.

The performance of the assay is based on the original protocol described [173]. Before starting the plasma treatment, the indigo stock solution is prepared by mixing 15.1515 *mL* of 0.66 *M* phosphoric acid (H_3PO_4) with 308.36 *mg* potassium indigo trisulfonate in deionized water. The final volume is 500 *mL* with 20 *mM* final concentration of H_3PO_4 and 1 *mM* indigo trisulfonate. The indigo reagent is only stable for one day, hence it has to be prepared directly before usage. For the preparation of the indigo reagent in deionized water (final volume of 10 *mL*) 200 μL of the stock solution, 100 *mg* of sodium dihydrogen phosphate (NaH_2PO_4) and 1.5606 *mL* of 0.66 *M* H_3PO_4 are mixed.

As mentioned above, the reaction of the indigo reagent with ozone is stoichiometric at low pH. Therefore, reagent and investigated sample are mixed in a 1:1 ratio to a final volume of 200 μL . Since the assay is adapted to 96 well plates, the plate is measured at 600 *nm* by the use of a multiplate reader (Tecan infinite M200, Tecan Group Ltd, Switzerland). From the measured absorptions of both, sample (A_{sample}) and control (A_{control}), the concentration (c_{O_3}) can be deduced. Therefore, the difference multiplied with the total volume (V_{total}) divided by the product of the path length of the well (b) with the sample volume (V_{sample}) and with the sensitivity coefficient (f) (see equation 3.7) gives the concentration of aqueous ozone in the sample.

$$c_{\text{O}_3} = \frac{\Delta(A_{\text{sample}} - A_{\text{control}}) \cdot V_{\text{total}}}{b \cdot V_{\text{sample}} \cdot f} \quad (3.7)$$

3.3 Chemicals and devices

In the following lists of all used devices and chemicals can be found. For the used spin traps an additional table is placed with their chemical structure.

Table 3.1: Used devices and software.

type	name	manufacturer
electron paramagnetic resonance spectroscope	EMXmicro	Bruker BioSpin, Rheinstetten, Germany
EPR resonator cavity	ER4119HS	Bruker BioSpin, Rheinstetten, Germany
EPR measurement software	Xenon software	Bruker BioSpin, Rheinstetten, Germany
EPR evaluation software	Xenon Spin Counting module	Bruker BioSpin, Rheinstetten, Germany
pH meter	SevenMulti M47	Mettler-Toledo International Inc., Columbus, OH
plasma source	kinpen09	neoplas GmbH, Greifswald, Germany
mass flow controller	MKS	MKS Instruments Deutschland GmbH, Munich, Germany
chilled mirror dew point hygrometer	DewMaster	EdgeTech, USA
multiplate reader	Tecan infinite M200 pro	Tecan Group ltd., Männedorf, Switzerland
xyz-manipulator	High-Z S-400T	Hylewicz CNC Technik, Geldern, Germany
xyz-manipulator software	WIN-PCNC Professional Software	Hylewicz CNC Technik, Geldern, Germany

Table 3.2: Chemicals used in the study-part 1.

name	abbreviation	manufacturer
Dulbecco's phosphate buffered saline	DPBS	Lonza, Switzerland
Rosewell Park Memorial Institute cell culture medium 1640	RPMI 1640	Lonza, Switzerland
Dulbecco's modified eagle medium	DMEM	Lonza, Switzerland
Hank's balanced salt solution	HBSS	Lonza, Switzerland
Sørensen's phosphate buffer	SPB	Lonza, Switzerland
Iscove's modified Dulbecco's medium	IMDM	Lonza, Switzerland
EpiLife	EpiLife	LifeTechnology, Germany
milliQ water	milli Q	Millipore
HPLC grade water	UPW	neolab Migge, Berlin, Germany
sodium chloride	NaCl	Sigma Aldich, St. Louis, USA
titanium(IV) oxysulfate	TiOSO ₄	Fluka, Sigma Aldrich, St. Louis, USA
potassium indigotrisulfonate	indigo blue	Sigma Aldich, St. Louis, USA
10-acetyl-3,7-dihydroxyphenoxazine	Amplex [®] Red	Molecular Probes, Eugene, USA
horseradish peroxidase	HRP	Molecular Probes, Eugene, USA
Amplex [®] Red reaction buffer (sodium phosphate buffer)	reaction buffer	Molecular Probes, Eugene, USA
dimethylsulfoxide	DMSO	Molecular Probes, Eugene, USA
hydrogen peroxide	H ₂ O ₂	340g/l, Merck, Darmstadt, Germany
nitrate standard	NO ₃ ⁻ standard	Cayman Chemical Co., Ann Arbor, USA
nitrite standard	NO ₂ ⁻ standard	Cayman Chemical Co., Ann Arbor, USA
nitrate reductase enzyme	NO ₃ ⁻ enzyme	Cayman Chemical Co., Ann Arbor, USA
nitrate reductase cofactor	NO ₃ ⁻ cofactor	Cayman Chemical Co., Ann Arbor, USA
Assay buffer	-	Cayman Chemical Co., Ann Arbor, USA
Griess reagent 1	Griess 1	Cayman Chemical Co., Ann Arbor, USA
Griess reagent 2	Griess 2	Cayman Chemical Co., Ann Arbor, USA

Table 3.3: Chemicals used in the study-part 2.

name	abbreviation	manufacturer
alanine spin calibration sample	-	Bruker BioSpin, Rheinstetten, Germany
5,5-dimethyl-1-pyrroline-N-oxide	DMPO	Dojindo Laboratoire, Kumamoto, Japan Cayman Chemical Co., Ann Arbor, USA Sigma Aldich, St. Louis, USA Enzo Life Sciences Inc., Farmingdale, NY, USA
5-tert-butoxycarbonyl-5-methyl-1-pyrroline-N-oxide	BMPO	Enzo Life Sciences Inc., Farmingdale, NY, USA Dojindo Laboratoire, Kumamoto, Japan
2-ethoxycarbonyl-2-methyl-3,4-dihydro-2H-pyrrole-1-oxide	EMPO	Enzo Life Sciences Inc., Farmingdale, NY, USA
5-(diethoxyphosphoryl)-5-methyl-1-pyrroline-N-oxide	DEPMPO	Cayman Chemical Co., Ann Arbor, USA AdipoGen [®] Life Sciences, Liestal, Switzerland
5-(diisopropoxyphosphoryl)-5-methyl-1-pyrroline-N-oxide	DIPPMPO	Enzo Life Sciences Inc., Farmingdale, NY, USA
5-(2,2-dimethyl-1,3-propoxy-5-methyl-1-pyrroline N-oxide	CYPMPO	Cayman Chemical Co., Ann Arbor, USA
2,2,6,6-tetramethyl-4-piperidone hydrochloride	TEMPD-HCl	Sigma Aldich, St. Louis, USA
2-(4-carboxyphenyl)-4,4,5,5-tetramethylimidazoline-1-oxyl-3-oxide, monopotassium salt	Caboxy-PTIO	Cayman Chemical Co., Ann Arbor, USA Molecular Probes, Eugene, USA
1-hydroxy-4-phosphono-oxy-2,2,6,6-tetramethylpiperidine	PPH-HCl	Enzo Life Sciences Inc., Farmingdale, NY, USA
1-hydroxy-3-carboxy-2,2,5,5-tetramethylpyrrolidine	CPH-HCl	Enzo Life Sciences Inc., Farmingdale, NY, USA

Table 3.4: Investigated spin trapping agents.

spin trap	structure	spin trap	structure
DMPO		CYPMPO	
BMPO		TEMPD-HCl	
EMPO		Carboxy-PTIO	
DEPMPO		PPH-HCl	
DIPPMPO		CPH-HCl	

3.4 pH measurement

For the measurement of pH changes a pH meter (SevenMulti™ S47, Mettler-Toledo International Inc., Columbus, OH, USA) with a pH electrode (InLab® Micro, Mettler-Toledo International Inc., Columbus, OH, USA) is used. The electrode is made of glass, which consists of a thin glass membrane sensitive to a specific ion [126]. In the electrode system two electrodes are implemented, the glass electrode as well as a reference electrode. A schematic drawing can be seen in figure 3.7a. The reference electrode is a silver wire in a silver chloride placed in potassium chloride solutions electrolyte. This reference part encases the measurement electrode, which also consists of a silver wire in silver chloride and potassium chloride solution, but this solution contains in addition a phosphate buffer. On the tip of this measurement electrode the glass membrane is placed, connecting the electrode with the liquid to be measured. In contact with aqueous solutions, this glass membrane forms a gel layer. On the inner boundary of the glass membrane a gel layer is also formed. This gel layer can exchange H^+ ions with the outer liquid (figure 3.7b). In acidic solutions the hydrogen cations can diffuse into the gel layer, in the alkaline surroundings they diffuse out of the layer. Therefore, on the outer membrane a positive or negative charge is formed. Since the internal buffer keeps the pH in the electrode constant, the potential also remains constant. Hence, the difference in potential gives the actual measurement pH electrode potential. The reference electrode is also connected to the investigated liquid by the use of a diaphragm. If the electrode system is placed in a solution, the changes in the electric potential between both electrodes can be measured and the pH can be deduced [176].

The measurements are repeated at least three times and together with the mean average its minimal and maximal derivation are shown.

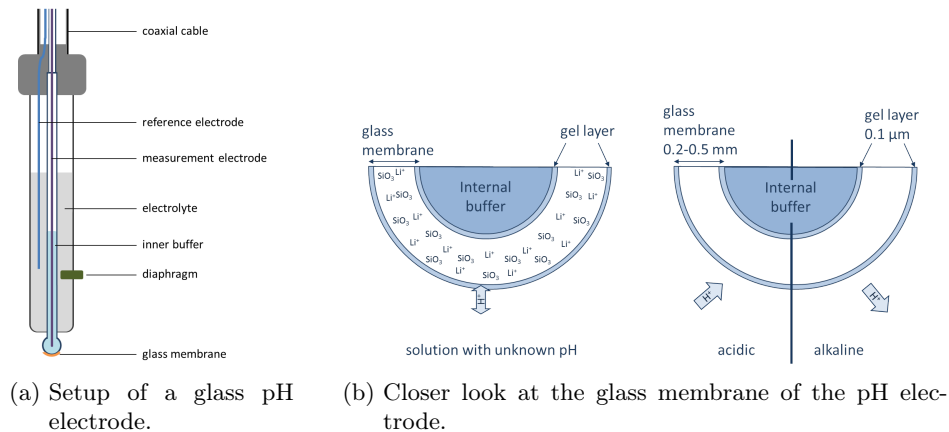


Figure 3.7: Schematic drawing of a common pH electrode.

3.5 EPR

The electron paramagnetic resonance spectroscope used in this work is an X-band (equals to microwave frequency of 9.87 GHz) EPR (EMXmicro, Bruker BioSpin GmbH, Rheinstetten, Germany) with the resonator ER 4119HS (Bruker BioSpin GmbH, Rheinstetten, Germany). The used microwave frequency limits the penetration depths in the sample of the irradiated radiation. In the case of aqueous samples the penetration depth is around 1 mm [177, 178]. The applied instrument's parameters of the EPR spectroscope are the same for all measurements: modulation frequency of 100 kHz, modulation amplitude of 0.1 mT, microwave power of 5.024 mW, receiver gain of 30 dB, time constant of 0.01 ms. The magnetic field scan is adjusted according to the sample measured. When suitable, as in most cases, a range of 10 mT is used.

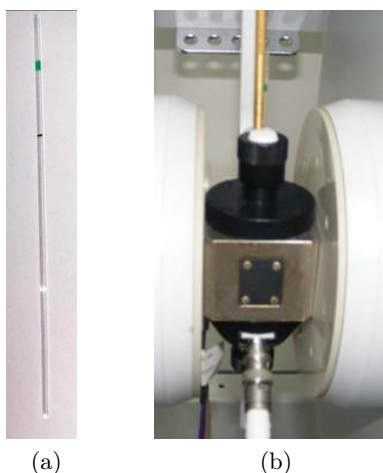


Figure 3.8: Borosilicate sample tube (a) placed in the ER 4119HS EPR resonator (b) [29].

The measurement procedure always follows the same protocol, including performing measurements in triplicates for each sample. Prior to a measurement the spin trap solution is prepared and 50 μL of the untreated solution are taken as control. This untreated solution is pipetted into a borosilicate class tube (125 mm length, 0.8525 mm inner diameter) as shown in figure 3.8a. This test tube is placed inside the EPR resonator (see figure 3.8b) and then its EPR signal is recorded. Afterwards, the liquid (with or without the spin trap) to be investigated is treated, directly followed by the sampling and pipetting of 50 μL in a new borosilicate glass tube, and placing it in the EPR. From the treatment to the measurement a few minutes are needed due to handling reasons. This delay time is always fixed to four minutes. From the measured EPR signal the spectrum of the untreated control is subtracted.

Quantification is possible by using a calibration procedure with a stable radical. The used calibration sample is an alanine spin calibration sample (Bruker BioSpin, Rheinstetten, Germany), which is placed in the EPR. Its spectrum is measured according to the calibration protocol of the manufacturer. Afterwards the absolute number of spins can be calculated. The concentration thus determined is compared to the one given by the calibration sample data sheet, and the differences are considered by a correction factor for subsequent quantitative evaluations. Therefore, the characteristic parameters such as

Landé-factor and hyperfine coupling, need to be measured. These parameters together with the evaluation software (Xenon software with Xenon Spin Counting module, Bruker BioSpin, Rheinstetten, Germany) enable a simulation of the measured spectrum. This spectrum then includes also the spectra of all different trapped radicals, hence, a distinction and separated evaluation of the concentration is possible. The use of the Xenon Spin Counting module enables the deduction of the absolute radical concentration. These measurement protocol is applied for all EPR measurements in this work, if not indicated differently. The parameters of the shown and evaluated spectra are given in table 5.2 in the appendix 5.

A list of all utilized spin trapping agents can be found in table 3.4; the suppliers of the spin traps are listed in table 3.2.

4 Results and discussion

In the following chapter the results of this work are presented and discussed. This chapter is divided into four parts: section 4.1 starts with the description of the development of a suitable procedure for the detection of plasma generated, highly reactive free radicals by the use of electron paramagnetic resonance spectroscopy (section 4.1.1) subsequently the investigations regarding the used spin trapping chemicals (section 4.1.2) are shown. These results are published in reference [29]. In section 4.2 the obtained impact of operating conditions from the surroundings (section 4.2.1), the impact of molecular admixtures into the feed gas of the plasma jet (section 4.2.2) and the influence of liquid ingredients on plasma generated reactive species compositions in the liquid (section 4.2.3) are described and discussed. The gained knowledge of this section is published in references [21, 33, 170]. The third part of the chapter deals with the origin of the reactive species detected in the plasma treated liquid (section 4.3). This is studied at the example of hydrogen peroxide (section 4.3.1) and singlet oxygen (section 4.3.2) as representatives for more stable but still reactive oxygen species. Furthermore, the impact of plasma generated VUV radiation and a possible transport of ions from the gaseous phase into the liquid phase are investigated and discussed in section 4.3.3 and section 4.3.4, respectively. Also the parts of the studies of this section are published [61, 63, 71]. The last section 4.4 of this chapter is focused on the impact of selected tailorable components of the plasma-liquid treatment on biological targets, e.g. the effect of the controlled surroundings on eukaryotes and prokaryotes (section 4.4.1) as published in reference [22]. Additionally, the effect of plasma jet VUV radiation on cell suspension is discussed (section 4.4.2).

4.1 Radicals in plasma treated liquids

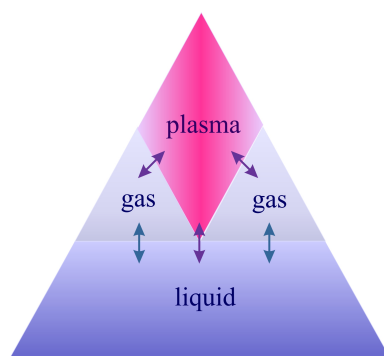


Figure 4.1: Interaction of the plasma with the gaseous and aqueous phase.

The plasma reacts with the ambient species in close vicinity as well as with aqueous species. Furthermore, the gas-phase-plasma generated species can react with the liquid yielding aqueous reactive species (see figure 4.1). Therefore, during the treatment of liquids with the plasma, interactions leading to the formation of reactive species in the liquid can occur in all phases.

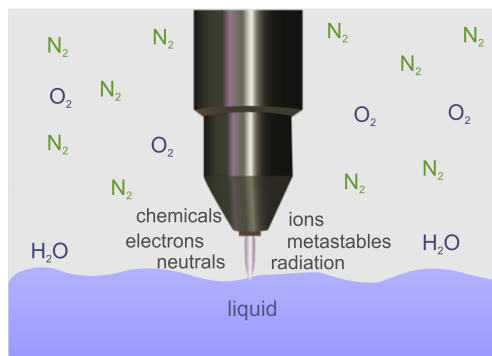


Figure 4.2: Liquid treatment situation in open atmosphere for the kinpen09.

In figure 4.2 the situation is schematically shown for a treatment of a biologically relevant solution by the plasma jet kinpen09. The plasma jet is situated in an open atmosphere above a liquid. The molecular nitrogen and oxygen in the gaseous phase represent the air surrounding the plasma jet. It is known from the literature that the kinpen09 produces electromagnetic radiation from vacuum ultraviolet radiation, UV and visible light up to near infrared (120 nm to 1000 nm) [168, 179]. Additionally, this plasma source also forms metastable species [17, 180], ions [9], electrons [17], neutral ground state atoms [7, 181] and other chemically active molecules [17, 71]. These components interact with both the gaseous environment and the liquid. Besides the surrounding environment the feed gas will also have an obvious impact. If impurities in the feed gas (usually pure argon) itself or in the pipes are present, they will also become part of the active component formation pathway. Therefore, the composition of the reactive species present in the liquid phase are remarkably affected by the experimental situation. As a third interaction partner besides the surroundings and the working gas, the liquid composition and condition also needs to be considered. The liquid ingredients can have a strong impact on the resulting species so that the composition of the treated solutions will affect the output of biologically relevant reactive species. For fundamental investigations, suitable methods and setups for the multi-phase pathways elucidation of the involved active components are intricate. The present work studies the plasma generated liquid phase reactive species with a special focus on the intermediate species - namely free radicals.

During plasma treatment of liquids a large variety of reactive species are formed inside the liquid such as hydrogen peroxide, nitrate and nitrite, as well as peroxyxynitrite and peroxyxynitrous acid [31, 32, 44, 58, 78]. For most of these species aqueous free radicals are potential precursors. Some indication on their formation in solution during plasma treatment are given by the literature in the early years of plasma medicine related studies of relevant plasma-liquid interaction [31, 51]. Radical formation was postulated, but their detection has posed great challenges to the plasma medicine community. The reason for the difficult access to these highly reactive species is that most of them are extremely short-lived - in liquid phase the lifetimes are in the range of milli- or microseconds. This lifetime becomes even shorter in the case of biological solutions, such as body fluids as well as cell culture media. For instance, the hydroxyl radical only has a half-life of few nanoseconds in such an environment [28]. In the scheme in figure 4.3 the experimental situation in the case of kinpen09 treatment is depicted.

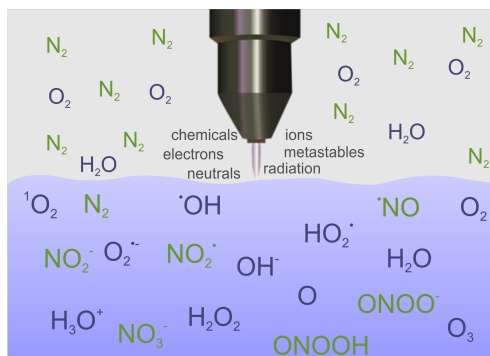


Figure 4.3: Treatment scheme with the focus on the liquid phase and the plasma generated reactive species.

4.1.1 Spin trapping in plasma-liquid interaction analysis

For the stabilization of the highly reactive, short-lived radicals spin trapping technique - as described in section 2.2.2 - is applied. The chemicals used as spin traps react with radicals to produce more stable radicals. These are detectable by the use of electron paramagnetic resonance spectroscopy. Due to the simultaneous presence of a multitude of plasma generated active molecules in the solution, these active species interact with each other resulting in the generation of secondary and tertiary products. For instance, the reaction of superoxide anion radicals with nitric monoxide radicals can produce peroxynitrite. A second example is the recombination of two hydroxyl radicals into hydrogen peroxide. This leads to a consumption of radicals, which are targeted for the detection.

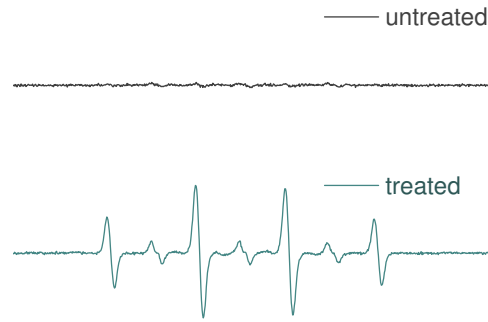
The spin trapping technique can be applied in two different ways: one is the mixing of the spin trap with the solution to investigate prior to plasma treatment. The other option is the addition of the plasma treated liquid to the spin trap afterwards. Both options have advantages and disadvantages: by the mixing of the spin trap with the plasma treated liquid after treatment, the analysis will yield only secondary or other subsequent radicals. One advantage of this approach is the applicability of literature knowledge about the spin trap properties, such as the efficacy of trapping specific radicals. However, the drawback of not detecting the plasma induced radicals directly instead of only the detection of later products outweighs this benefit. Information about the directly plasma generated liquid phase free radicals can only be gained by the previous addition of the spin trap to the solution. The thereby resulting situation during the treatment is shown in figure 4.4. It has to be noted that the prior addition of the spin trap can cause the following difficulties: the efficacy of the spin trap in the presence of plasma as well as the influence on the spin trap of the complex mixture of different reactive species is unknown. In the present work, the information and results described are, therefore, gained from the total spin trap adduct and a deduction of the total radical concentration is deliberately deferred to later works.

The interaction of the spin trap with the plasma is determined for DMPO (5,5-dimethyl-1-pyrroline-N-oxide), provided by different suppliers, as it is shown in figure 4.5. Although it could have been expected that the same chemical agent from different suppliers are comparable, figure 4.5 (a, b, c) shows that this is obviously not the case. All three spectra are obtained for the same EPR parameters and the same plasma treatment conditions. Furthermore, the plasma treatment is exactly the same for all three DMPO samples. DMPO is dissolved in DPBS (with a final concentration of 100 mM), an untreated sample is measured, depicted as a black curve in the upper part of each figure 4.5a, 4.5b and 4.5c. In the

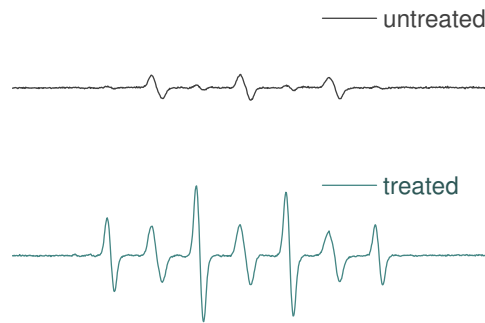


Figure 4.4: Treatment scheme with the focus on the liquid phase and the plasma generated reactive species including the spin trap. The depicted species amount represents the concentrations neither of the reactive species nor of the spin trap.

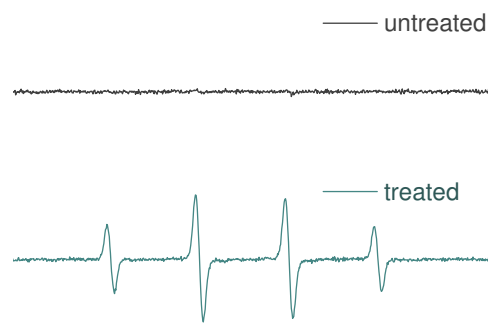
bottom part of each figure the DMPO spectrum after 3 minutes of plasma treatment is shown (blue curve). In the measured spectrum of figure 4.5a (supplier A) two radicals are observed in the plasma treated liquid. The four peaks with the typical 1:2:2:1 intensity distribution can be ascribed to the hydroxyl radical adduct with DMPO. The three peaks in between are related to the methyl radical ($\text{CH}_3\bullet$) which can only origin from the spin trap itself, as DPBS itself does not include carbon-containing species, whereas DMPO provides two methyl groups (see table 3.4). In figure 4.5b, these methyl radical related signals are even more pronounced in the EPR spectrum. In the untreated spectrum these peaks are already observed. In the EPR spectra of supplier A (figure 4.5a) and supplier B (figure 4.5b) the characteristic four peak patterns of the DMPO hydroxyl radical adduct can be found. In comparison to the two other DMPO samples from supplier A and B, the DMPO provided by supplier C shows a pure, methyl radical free spectrum of $\text{DMPO}\bullet/\text{OH}$. The increase of the methyl radical adduct signal due to the plasma treatment leads to the assumption that some amount of the spin trap is degraded by the treatment or impurities in the spin trap solution, containing methy groups, are cleaved by the plasma treatment. This is obviously an undesired effect. For the present work, therefore, DMPO from supplier C is used for all DMPO-measurements.



(a) DMPO signal of supplier A.



(b) DMPO signal of supplier B.



(c) DMPO signal of supplier C.

Figure 4.5: DMPO of three different suppliers treated exactly in the same manner shows different spectra (©2013 IOP Publishing Ltd. Reprinted with permission from [29]).

4.1.2 Choice of spin trap

The characteristic pattern of the $\text{DMPO}\bullet/\text{OH}$ adduct is a 1:2:2:1 intensity distribution at specific position in the spectrum. In the bottom part of figure 4.6 such a typical DMPO spectrum is shown. Due to the fact that DMPO is a nitron, the hydroxyl radical is bonded to one carbon atom of the cyclic molecule forming the spin trap adduct. The so-formed spin trap adduct of the free radical has a specific fingerprint EPR spectrum as the nearby atoms such as e.g. the nitrogen nucleus influence the electron ls-coupling of the free radical. Since the spin of the nitrogen atom nucleus is one, in an external magnetic field a splitting of the peak into three peaks results. This nuclear spin has an impact on the surrounding electromagnetic field so that the interaction of this magnetic field with the external magnetic field leads to the hyperfine splitting (see section 2.2.1). In the case of DMPO, not only the nitrogen atom influences the atoms in close vicinity but also the nearby hydrogen atom has an impact on the measured peak pattern. Hence, the spectrum of DMPO's hydroxyl radical adduct is characteristic due to the 1:2:2:1 intensity distribution of $\text{DMPO}\bullet/\text{OH}$ four peaks (highlighted by filled dots). This pattern consists of the two triplet patterns caused by the nitrogen and hydrogen atom related splitting. These two triplets superpose in two out of three peaks, so that the resulting two peaks in the middle of the four peaks are the overlaid ones (see section 2.2, figure 2.5).

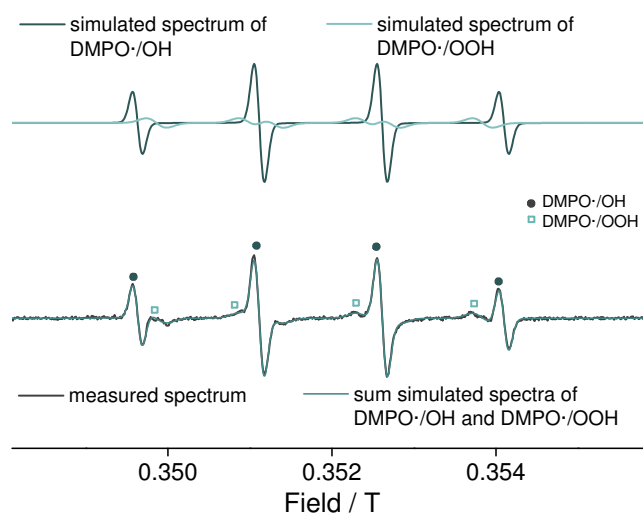


Figure 4.6: Typical DMPO spectrum of $\text{DMPO}\bullet/\text{OH}$ (dark dots) and $\text{DMPO}\bullet/\text{OOH}$ (light squares) measured after 180 s plasma treatment of DPBS and simulated by the EPR software (©2013 IOP Publishing Ltd. Reprinted with permission from [29]).

The stability of the spin adduct is essential for their usage. Therefore, the adduct stability is investigated by an observation of the $\text{DMPO}\bullet/\text{OH}$ EPR spectrum over a period of 74 hours. In figure 4.7 the decay of the resulting $\text{DMPO}\bullet/\text{OH}$ concentration over the complete measurement period is shown; the inset gives a detailed view of the first 25 minutes. Zero is set to the time point when the plasma treatment stops, so that the direct radical generation through the plasma is finished. Since the handling also takes a few minutes the first point measured is four minutes after plasma treatment. From four to seven minutes

the concentration can be estimated to be constant. Between seven and eight minutes after treatment there is a clear drop in concentration. From the manufacturer and also from the literature it is known that the spin trap adduct is stable for approximately ten minutes [182, 183]. Although the plasma treatment is stopped, it cannot be excluded that post treatment reactions occur, which result in further production of oxygen radicals. A potential post plasma treatment reaction is, for instance, the formation and decay of ONOO^- is known from the literature [58]. As no increase in the concentration is observed after plasma treatment it is assumed that the decay of the spin trap adduct and the formation according to post treatment reactions compensate one another. From this measurement it can be deduced that under the present conditions reproducible results, and therefore, stable concentration can only be gained in the first minutes up to approximately 7 to 8 minutes after plasma treatment. Hence, the handling time is a crucial parameter which needs to be kept constant if measurements should be comparable. Throughout the present investigation, the time gap between plasma treatment and measurement is always set to four minutes, unless noted otherwise.

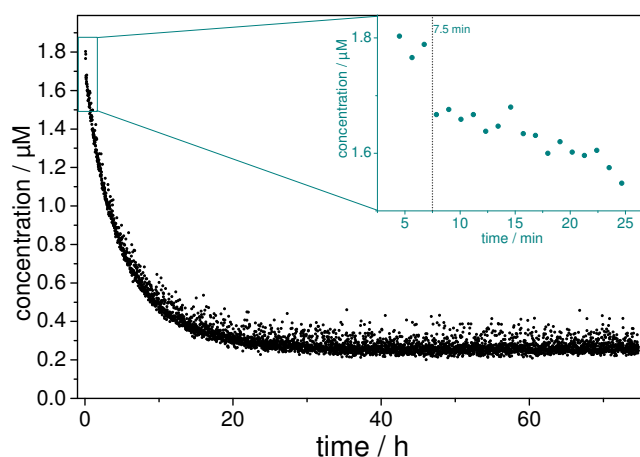


Figure 4.7: Decay of spin trap adduct observed over 74 hours (©2013 IOP Publishing Ltd. Reprinted with permission from [29]).

In figure 4.6, also small peaks - characteristic of superoxide anion / hydroperoxyl radical adduct with DMPO, $\text{DMPO}\bullet/\text{OOH}$ (marked with open squares) - are formed during plasma treatment. The upper part of this figure shows the individual simulated spectra of both, $\text{DMPO}\bullet/\text{OH}$ (dark curve) and $\text{DMPO}\bullet/\text{OOH}$ (light curve). The blue curve in the bottom part of the figure is the combination of both simulated spectra. The fit and measurement exhibit an excellent agreement. As DPBS is a buffered solution with a constant pH value of 7.4, the measured peaks are 99.9% related to $\text{O}_2^{\bullet-}$ and not to its protonated form, HO_2^{\bullet} , due to their pK_a value of 4.88 [184]. The reaction rate of DMPO with either the hydroxyl radical or the superoxide anion and hydroperoxyl radical is quite different: for $\bullet\text{OH}$ the rate is $k_{\bullet\text{OH}} > 10^9 \text{ M}^{-1} \text{ s}^{-1}$ [25, 185, 186] whereas for $\text{O}_2^{\bullet-}/\text{HO}_2^{\bullet}$ it is $k_{\text{O}_2^{\bullet-}} < 10^2 \text{ M}^{-1} \text{ s}^{-1}$ [25]. Hence, in the presence of hydroxyl radicals, DMPO is mainly reacting with $\bullet\text{OH}$ rather than with $\text{O}_2^{\bullet-}$ or HO_2^{\bullet} . A known drawback of DMPO used as spin trap is the fast decay of the $\text{DMPO}\bullet/\text{OOH}$ adduct in less than one minute into the $\text{DMPO}\bullet/\text{OH}$ adduct (see figure 4.8). It is, therefore, not directly possible to distinguish

4 Results and discussion

between superoxide anion and hydroxyl radicals by use of DMPO as spin trap [187, 188].

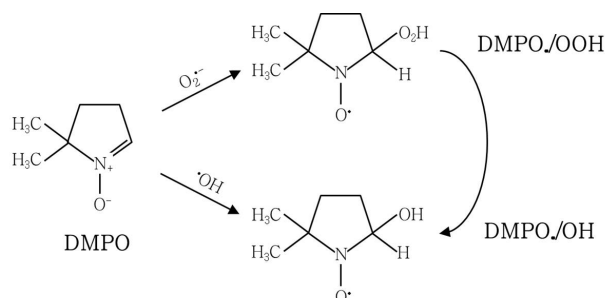


Figure 4.8: DMPO•/OOH adduct decays into DMPO•/OH (©2013 IOP Publishing Ltd. Reprinted with permission from [29]).

Different spin traps for oxygen radicals besides DMPO are also investigated in order to overcome its difficulty in the distinction of hydroxyl and superoxide anion radicals produced by plasma treatment of liquids. One of the possible alternatives to DMPO is BMPO (5-tert-butoxycarbonyl-5-methyl-1-pyrroline-N-oxide), which is the second spin trap mainly used in this study. Also other spin traps for oxygen radicals are investigated. A detailed description of these spin traps can be found in the appendix (section 5).

BMPO is a derivative of DMPO with the advantage that short-lived superoxide anion, hydroxyl, and thiyl radicals are well stabilized. Furthermore, BMPO adducts of $\bullet OH$ and $O_2^{\bullet -}$ show distinguishable spectra and the BMPO•/OOH does not decay into BMPO•/OH (see figure 4.9). In comparison to DEPMPO, DIPPMPO, and CYPMPO (section 5), BMPO has the benefit of exhibiting a plainer spin trap adduct spectrum. The spectrum consists, similar to DMPO, mainly of four peaks (see figure 4.10). The spectra of DEPMPO, DIPPMPO and CYPMPO for hydroxyl and superoxide anion radicals are dominated by eight peaks. Furthermore, with the half-life of the superoxide anion spin trap adduct of 23 minutes, the BMPO adduct has one of the longest lifetimes, according to the literature, of the tested spin trap compounds (see table 4.1).

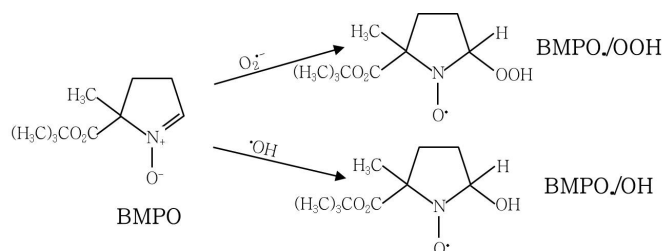


Figure 4.9: Reaction of BMPO with superoxide anion radical to form a stable adduct BMPO•/OOH.

In addition to the well-suited application for oxygen radical spin trapping, BMPO has

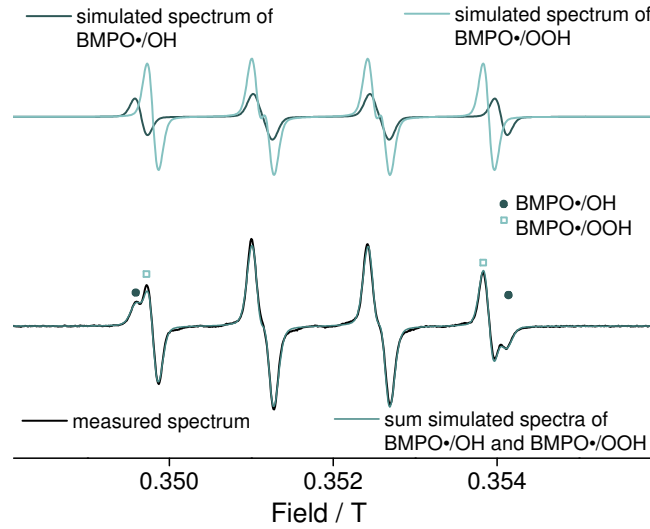
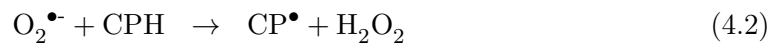
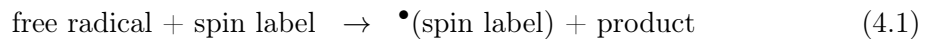


Figure 4.10: BMPO spectra of $\text{BMPO}\bullet/\text{OH}$ and $\text{BMPO}\bullet/\text{OOH}$ measured after 180 s plasma treatment of DPBS and simulated by Xenon software and Xenon Spin Counting module (Bruker BioSpin, Rheinstetten, Germany) (©2013 IOP Publishing Ltd. Reprinted with permission from [29])

the advantage over DMPO and its other derivatives to form a not fully overlapping EPR spectrum of the thiyl radical ($\bullet\text{SG}$) with the hydroxyl radical. Some of the investigated complex cell culture media contain glutathione, which can form the glutathione thiyl radical, therefore, the thiyl radical is of relevance for the plasma-liquid interaction in the field of plasma medicine. Furthermore, in the case of plasma treatment of cell suspension, several mammalian cells can also release thiyl radicals as a response to oxidative stress (see section 4.4.2). Similar to the spectra of oxygen radicals the spectrum of $\bullet\text{SG}$ is also much simpler for BMPO, DMPO, and EMPO compared to DEPMPO. The DMPO thiyl adduct has the drawback compared to the BMPO adduct that it appears with quite similar spectral parameters as $\text{DMPO}\bullet/\text{OH}$, which makes it difficult to distinguish. $\text{EMPO}\bullet/\text{SG}$ also forms a characteristic spectrum, but the most stable spin trap adduct is $\text{BMPO}\bullet/\text{SG}$ [194]. An alternative to spin trapping is the usage of so-called spin labels: in biology, spin trapping technique is also applied to detect intracellular free radicals. But although BMPO is a cell permeable spin trap, intracellular spin trapping of superoxide anion radicals with BMPO is not recommended, since $\text{BMPO}\bullet/\text{OOH}$ is reduced by glutathione/glutathione peroxidase to $\text{BMPO}\bullet/\text{OH}$. In contrast to spin traps, spin labels forms by reaction with a radical or a reactive species a non-specific spin label radical and a non radical product (see equation 4.1), e.g. for the spin label CPH reaction 4.2 takes place [195].

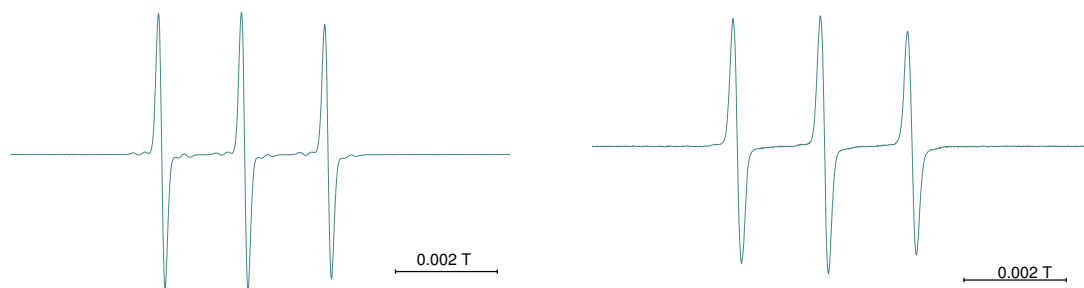


In some cases the drawback of being unspecific is outweighed by the higher reaction rate of the spin label with the species to be trapped. In the literature it is also reported,

Table 4.1: Spin traps for superoxide anion detection and the lifetime of their spin trap adduct.

spin trap	lifetime of O ₂ ^{•-} -adduct	detectable free radicals	applicable research fields
DMPO	≤ 1 minute [189]	•OH, O ₂ ^{•-} , R [•] , RO [•]	cell-free and extracellular detection of •OH, O ₂ ^{•-} , R [•] , S [•]
EMPO	8 minutes [189]	•OH, O ₂ ^{•-} , R [•] , RO ₂ [•] , S [•]	
DEPMPO	15 minutes [190]		
DIPPMPO	21.5 minutes [191]	•OH, O ₂ ^{•-}	
CYPMPO	15 minutes ¹ [192] 51 minutes ² [192]	•OH, O ₂ ^{•-}	
BMPO	23 minutes [193]	•OH, O ₂ ^{•-} , S [•]	

that the measurement of peroxynitrite by the use of spin label enhanced electron paramagnetic resonance spectroscopy is possible [196–199]. Potential spin labels are PPH, 1-hydroxy-4-phosphono-oxy-2,2,6,6-tetramethylpiperidine and CPH, 1-hydroxy-3-carboxy-2,2,5,5-tetramethylpyrrolidine. Both are effective scavengers of peroxynitrite and superoxide anion radicals but as described above their reactions do not lead to specific spectral patterns [199]. In figures 4.11a and 4.11b spectra of the spin labels CPH and PPH after 180 s plasma treatment of DPBS are shown. Identical spectra are formed by either $O_2^{\bullet-}$ or $ONOO^-$ reactions. Both reactions lead to a subtraction of the hydrogen atom of the hydroxyl group from the spin label. Therefore, the oxygen atom has radical properties. Similar to the spin traps, also the peaks of the spin label spectra are due to the hyperfine interaction of the electron spin with the nitrogen atom. These are in the presented case the three peaks of CPH/PPH. In most peroxynitrite studies with the application of spin labels, the superoxide anion radical is suppressed during measurement by the addition of superoxide dismutase (SOD). For investigation of plasma generated peroxynitrite, an addition of SOD to the solution before the spin label is added and the treatment takes place is not recommended, because one of the main peroxynitrite formation mechanisms assumed in plasma-liquid interaction is via the reaction of nitric monoxide and superoxide anions radicals [31, 32]. An addition of SOD would, therefore, inhibit the formation via this reaction pathway. Additionally, the admixture of such a complex molecule could lead to additional organic reactive species and further unknown parameters. Both spin labels, PPH and CPH, have a high reactivity with superoxide anion radicals, whereby a detection of peroxynitrite is not possible without the use of superoxide anion radical scavengers such as SOD. A direct detection of peroxynitrite or peroxynitrous acid, respectively, is not possible in case of plasma-liquid interaction by the use of spin label enhanced EPR spectroscopy, due to the fact that the scavenging of one of its precursors inhibit the formation of $ONOO^-$. Therefore, the measurements in this work are focused on the detection of the precursors. Precursors of $ONOO^-/ONOOH$, for instance, are superoxide anion radicals, which have already been found in plasma treated liquids (see



(a) Spectrum of CPH measured after 180 s plasma treatment of DPBS. (b) Spectrum of PPH measured after 180 s plasma treatment of DPBS.

Figure 4.11: Adducts of spin label for peroxynitrite and superoxide anion, CPH and PPH.

figures 4.6 and 4.10), as well as in nitric monoxide radicals. In comparison to the amount of available spin traps for oxygen radicals, for the detection of nitrogen free radicals the number of spin trapping agents is quite limited. Mainly in the literature used spin traps are dithiocarbamate complexes (DTC). *N,N*-diethyldithiocarbamate (DETC) is a water-insoluble nitric monoxide spin trap; a water-soluble version of a dithiocarbamate spin trap is MGN (*N*-methyl-D-glutamine dithiocarbamate). To be able to react with nitric monoxide to form stabilized adducts, DTCs have to react previously with iron to generate Fe(II)-DTC. By reaction of Fe(II)-DTC with $\bullet\text{NO}$ a stable nitrosyl iron-dithiocarbamate complex is formed. However, a drawback of DTCs is that they will be quickly become oxidized by dissolved oxygen in the solution. Therefore, handling should be performed under oxygen-free conditions, which makes DTC compounds not well-applicable under ambient conditions as is the case for plasma-liquid interaction in plasma medicine. An alternative is 2-(4-carboxyphenyl)-4,4,5,5-tetramethylimidazoline-1-oxyl-3-oxide, monopotassium salt (Carboxy-PTIO, CPTIO). Carboxy-PTIO is a stable and water-soluble spin trap which reacts with nitric monoxide to form Carboxy-PTI. In figure 4.12 a spectrum of Carboxy-PTIO is depicted. As shown in table 3.4, the spin trap itself is a paramagnetic species containing two nitrogen atoms and an unpaired electron, whose density is equally distributed over both N atoms [200]. If there is a nitrogen atom in close vicinity of an unpaired electron, the line will be split into three. As Carboxy-PTIO contains two nitrogen atoms, the line should be split into nine lines. Due to the equivalence of both interacting nuclei, their splitting constants are the same and an overlapping of the lines results in a characteristic pattern of five lines with an intensity distribution of 1:2:3:2:1. When the spin trap reacts with nitric monoxide, the distribution of the unpaired electron's density is no longer equal for both nitrogen atoms. It is then concentrated on the nitroxide nitrogen which results in unequal hyperfine splitting and multiple peak pattern can be observed in the spectra. The measured spectrum shown in figure 4.12 is obtained after 180 s plasma treatment of DPBS. No nitric oxide could be measured by the spin trapping with C-PTIO. Since other measurements already give indications that nitric monoxide is formed during the plasma treatment in the liquid phase, the absence of the Carboxy-PTI signal does not mean that no $\bullet\text{NO}$ is formed. Due to C-PTIO's paramagnetic property itself, the concentration of the spin trap needs to be in the same order of magnitude as the expected nitric monoxide concentration. For the experiments shown in figure 4.12 1 mM C-PTIO is used, which seem to be higher than the plasma generated nitric oxide concentration in the liquid so

4 Results and discussion

that the spectrum is dominated by Carboxy-PTIO peaks and the Carboxy-PTI peaks are diminished. A recent model estimates a concentration of nitric monoxide formed in the gas phase during plasma treatment with kinpen09 of 40 *ppm* [17]. Applying the Henry's law a concentration in the liquid phase of approximately 60 μM can be presumed, therefore the used concentration of the spin trap C-PTIO was to high, for future investigations this has to be adjusted.

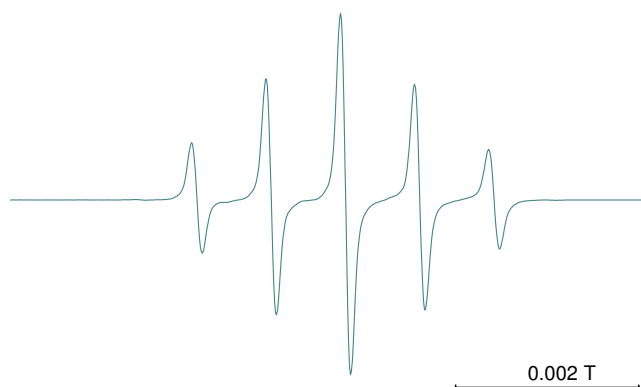


Figure 4.12: Carboxy-PTIO spectrum measured after 180 *s* plasma treatment of DPBS, with 100% nitrogen in the curtain gas device, 100% humidified feed gas ($\text{Ar} + 0.8\% \text{N}_2 + 0.2\% \text{O}_2$) added.

Due to above-described considerations, for the investigations in this work mainly DMPO, as a general oxygen radical trap, and BMPO, as the one which can distinguish between superoxide anion, hydroxyl, and glutathione thiyl radicals are used for oxygen radicals. For the detection the nitrogen free radicals as well as for peroxynitrite, the stable end product are observed by the use of color forming reactions.

4.2 Controlled conditions

For reproducible results and a simplification of chemical reaction kinetics, control of the treatment conditions is essential. This can also prove to be fundamentally relevant for therapeutic applications. In the following, three dominant treatment conditions influencing the reactive component outcomes are investigated: the ambient surroundings (section 4.2.1, published in references [21, 29, 33, 170]), feed gas admixtures (section 4.2.2) as well as the complexity of the liquids meaning the impact of their ingredients (section 4.2.3, published in reference [33]). In figure 4.2 it is shown that the plasma jet is situated in ambient air and these air species can diffuse into the plasma plume. This diffusion leads to a direct formation of reactive oxygen and nitrogen species in the gas phase [8, 10, 17, 181]. To achieve reproducible results and to control the outcome of the plasma treatment, the influence of ambient conditions is studied and tailored. The respective studies are described in the following.

4.2.1 Influence of ambient conditions

For plasma treatment in medicine, controlled surrounding conditions are hard to achieve. A patient can hardly be placed in a sealed chamber; and therefore the control of the environment has to be realized on site. The topology of a wound, as well as the area to be treated, are always different. Additionally, the treatment should yield bacteria inactivation without harming the healthy tissue and a stimulation of the wound healing process is desired. Since plasma treatment has to be reproducibly applicable under varying circumstances, the condition such as environment humidity need to be controlled or its effect on the reactive components needs to be studied. Therefore, a curtain gas device developed in our group [170] allows the adjustment of the atmosphere around the plasma jet plume and the targeted wound region. This is schematically shown in figure 4.13.

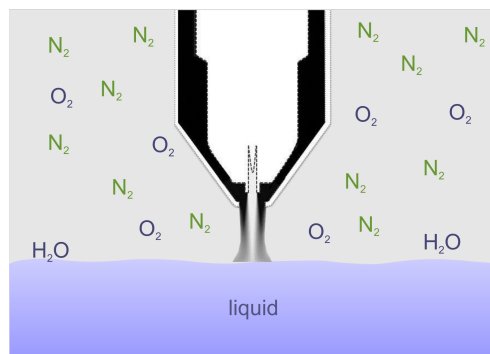


Figure 4.13: The curtain gas situated around the plasma jet's plume to exclude the ambient influences, such as humidity and diffusion of molecular air species into the plume.

4.2.1.1 Gas phase

Although the focus in this work is set on the plasma-liquid interaction, the gas phase has to be considered as one source of reactive species or their origin. Therefore, the impact of the interaction of the curtain gas with the plasma plume, which occurs in the gaseous phase, has to be investigated. The data shown here regarding the effectivity of

4 Results and discussion

the curtain gas device in the gas phase was measured by Dr. J. Winter. The complete study is presented in reference [170], including among other techniques optical emission or absorption spectroscopy. Furthermore, the verification of an exclusion of ambient oxygen inside the plasma plume due to the curtain gas is shown by absorption measurements as depicted in figure 4.14a. Shown are the argon excimer in the VUV spectral region. This radiation dominantly is generated inside the plasma jet. The spectrum exhibits absorption dips originating from the absorption of the excimer radiation by molecular oxygen diffusing into the plasma plume. With an increasing curtain gas flow rate from 0 to 3 *slm* the absorption dip is reduced; for 3 *slm* curtain gas flow rate, no molecular oxygen-related absorption is observed. It can be concluded that the nitrogen gas protects the plasma plume from diffusing ambient oxygen.

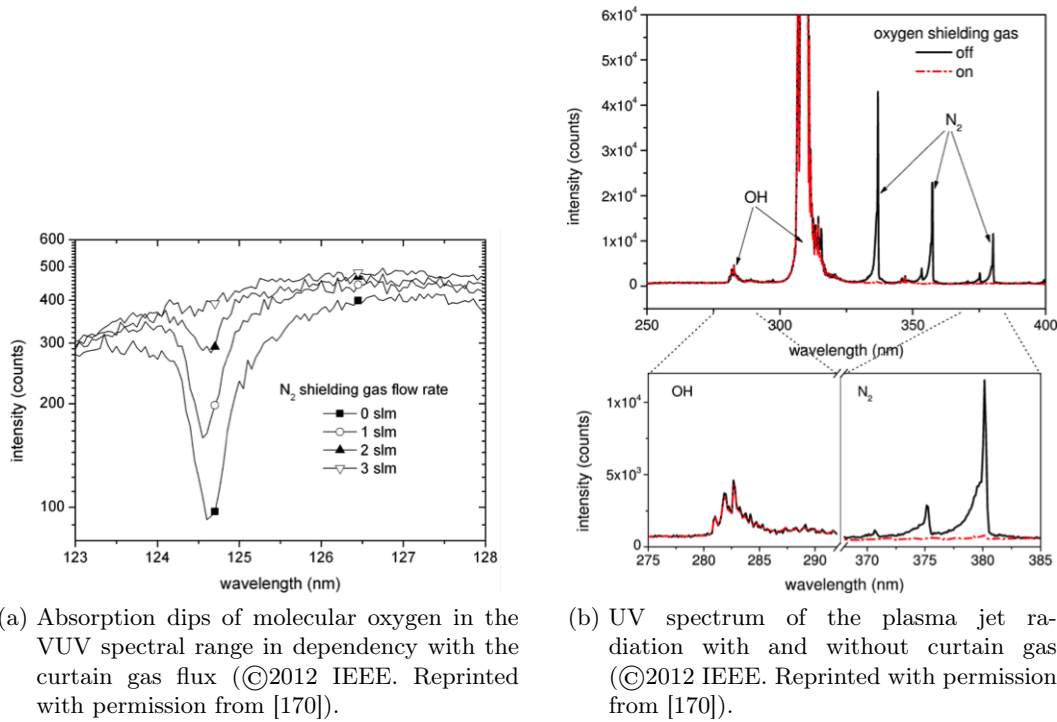


Figure 4.14: Gas phase measurements of the curtain gas impact.

In figure 4.14b the focus is set on the ultraviolet region between 250 and 450 nm. In this spectral range, the ro-vibrational emission bands of the hydroxyl radicals ($\bullet OH$ $A^2\Sigma^+ \rightarrow X^2\Pi$) as well as the bands related to the second positive system of molecular nitrogen (N_2 $C^3\Pi \rightarrow B^3\Pi$) can be observed. These peaks are good markers for the exclusion of ambient species: when oxygen is used as curtain gas, the nitrogen emission is not detectable anymore. The right part of the zoomed section in figure 4.14b clearly shows this effect. The gaseous hydroxyl radical signal is not affected by the kind of gas in the curtain device. The reason for the unaffected presence of the $\bullet OH$ molecule lies in its origin. As shown in the literature, the humidity inside the system is responsible for the production of gaseous hydroxyl radicals [71]. Therefore, the curtain gas cannot have a strong impact on this molecule. Additionally, it is found that humidity in the curtain gas device would not lead to such intensive hydroxyl radical emission signals as the feed gas humidity is

produces [71]. This is further verified in a follow-up study by measuring the hydrogen peroxide production rate in the gaseous phase by variation of feed gas humidity or curtain gas humidity [201].

4.2.1.2 Impact of the ambient surroundings on liquid reactions

In the same way that the gas phase reactive species generation is influenced by the changes of the curtain gas composition around the plasma plume, the plasma induced reactive species composition in the liquids is also expected to be dependent on the curtain gas. Therefore, the influence on liquid phase reactive species due to the variation of the gas curtain composition is studied for DPBS and other liquids. DPBS is an example of a biologically relevant liquid with a relative low complexity. The effect on other liquid solutions will be discussed in chapter 4.2.3.

In the experiments the oxygen to nitrogen ratio is varied in the curtain gas and their impact on the generation of reactive oxygen as well as on reactive nitrogen species is investigated. Additionally, the influence on the pH value is observed. DPBS is a buffered liquids, and therefore no change in pH is expected during plasma treatment in comparison to the untreated sample. In figure 4.15 the results of the pH measurement are shown, and, as expected, the pH remains constant at a value of 6.7. This means that the buffer capacity of the phosphate buffer included in DPBS, is not exceeded.

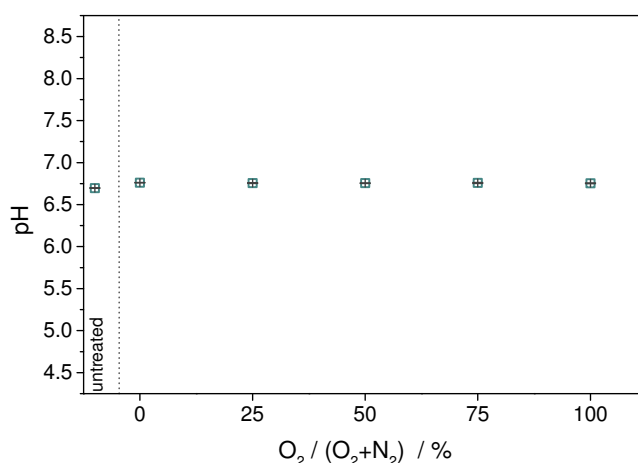
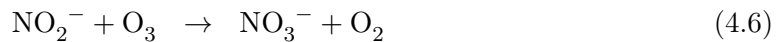
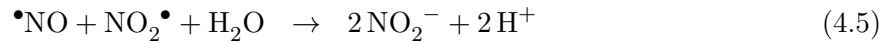
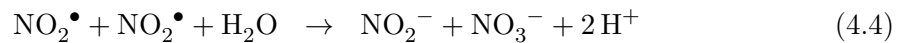


Figure 4.15: The change in pH depending on the curtain gas composition in 5 mL DPBS after 180 s plasma treatment (Republished with permission of Begell House Inc., from [33]; permission conveyed through Copyright Clearance Center, Inc.).

As a surrogate marker for the formed reactive nitrogen species in DPBS, nitrate and nitrite concentrations are determined by the so-called Griess assay. In the bar chart shown in figure 4.16, the concentration in μM over the variation of the gas composition in the curtain is shown. The trend for both species is similar, although the concentrations are slightly different, they are still in the same order of magnitude. For a pure nitrogen curtain gas, a high concentration of nitrogen species can be assumed. Since nitrate and nitrite consist only partly of nitrogen, more precisely of just of one nitrogen atom and two or three oxygen atoms, respectively, the presence of oxygen is also required. This requirement

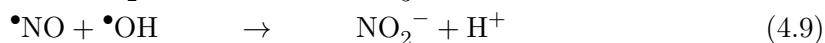
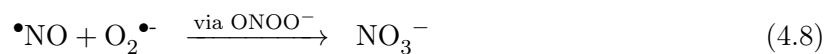
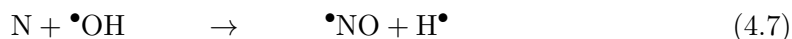
4 Results and discussion

of oxygen could be satisfied either by the already solvated oxygen in the solution or by the dissociation of water, where oxygen species can be formed. With these limited sources of necessary oxygen, the pure nitrogen curtain gas leads to a lower concentration of the formed NO_2^- and NO_3^- . The resulting nitrite and nitrate concentrations are the second lowest concentrations. The lowest value is obtained for 100% oxygen. The fact that even without nitrogen in the surroundings nitrite and nitrate are detectable might be attributed to nitrogen already solvated in the liquid. Water stored in an air environment at 20°C will contain approximately 0.3 mM molecular oxygen and 0.5 mM molecular nitrogen, according to Henry's law [202]. This concentration of N_2 in the liquid, only caused due to storage in open atmosphere, is not sufficient for the determined nitrate and nitrite concentration. Furthermore, the bond dissociation energy of molecular nitrogen is with about 9.8 eV (corresponds to 126 nm) quite high. Therefore, the nitrogen-precursors have to be somehow originating from the gas phase. One origin could be impurities in the used gases. Feed gas and curtain gases contain nitrogen up to 5 parts per million by volume (*ppmv*) according to the supplier. If these impurities formed only nitrogen oxide species in the gas phase, they would instantly be destroyed, since the 100% oxygen curtain gas leads to high amounts of ozone [203]. Ozone oxidizes nitric oxide, the precursor of nitrate and nitrite, yielding nitrogen dioxide (see eq. 4.3) [107]. NO_2^\bullet from the gas phase can dissolve in water and, theoretically, it can react to nitrite and nitrate via electron capture by nitrogen dioxide or nitric oxide (see equations 4.4 and 4.5) [107], but as the Henry coefficients of nitrogen dioxide and ozone have with $1.2 \cdot 10^{-4}\text{ M} \cdot \text{Pa}^{-1}$ the same value [114], the solvation of both is similar. In the presence of ozone, nitrite is rapidly oxidized to nitrate and molecular oxygen (see eq. 4.6) [107]. The pure oxygen curtain gas composition yields a concentration of ozone which is extremely higher than the concentration of nitrogen oxides in the gas phase [17]. The measurements in the gaseous phase are performed by Fourier transform infrared spectroscopy supplied with a multipass cell to enhance the absorption length, and hence the sensitivity of the method. Due the application of the multipass cell the measurement takes place in the so-called far field, a region with is several centimeters away from the plasma plume. More details on this Fourier transform infrared spectroscopy measurements can be found e.g. in reference [17]. The nitrogen oxides are not detectable in the far field in this case. Therefore, the formation of these nitrogen oxides, including nitrite and nitrate, are assumed to play only a secondary role.



However, when the nitrogen impurities in the argon plasma react with excited argon the radiative state of molecular nitrogen $\text{N}_2(\text{C})$ as well as atomic nitrogen is formed. Besides other pathways, $\text{N}_2(\text{C})$ deexcites to $\text{N}_2(\text{A})$ [204], metastable nitrogen, with a long life of 2 s [205]. This high energetic species with an energy of around 6 eV can react with water to form $\bullet\text{OH}$. During plasma treatment also gaseous atomic nitrogen can be formed [17]. If N is present, it reacts on the water surface with hydroxyl radicals, nitric oxide radicals will be generated (see eq. 4.7). Aqueous $\bullet\text{NO}$ can react, for instance, with superoxide anion radicals, generating nitrate (eq. 4.8) or it can react with solvated O_2 (eq. 2.23) yielding nitrite. In addition, NO_2^- is also generated by the reaction of nitric monoxide with another

hydroxyl radical (eq. 4.9).



Interestingly, the highest reactive nitrogen species concentrations (NO_2^- : $6.8 \pm 0.7 \mu\text{M}$, NO_3^- : $4.8 \pm 0.8 \mu\text{M}$) are measured for the condition which is the closest to “normal” air, for 25% oxygen and 75% nitrogen. For all oxygen contents higher than 25% it can be stated that the higher the oxygen content in the curtain gas is, the lower are the resulting NO_2^- and NO_3^- amounts detected in the liquid. An optimum for the production of nitrate and nitrite precursors can be assumed to be at or close to 25% oxygen and 75% nitrogen in the curtain gas; at a higher oxygen content these precursors will probably be just formed in lower amounts or more likely be destroyed by the higher amount of oxygen species formed in the gaseous phase.

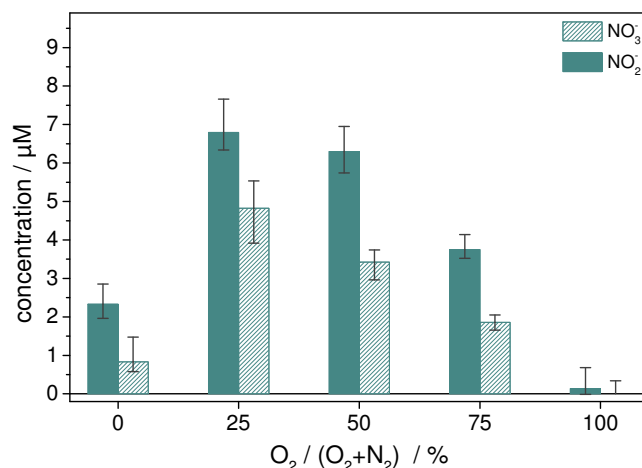


Figure 4.16: Nitrite and nitrate generated in DPBS due to 180 s plasma treatment as a function of the variation of the curtain gas composition. The error bars show minimum and maximum deviations of the mean value of at least three independent measurements (Republished with permission of Begell House Inc., from [33]; permission conveyed through Copyright Clearance Center, Inc.).

Nitrate and nitrite can also be termed RONS, reactive oxygen and nitrogen species, as they contain both species and more importantly, both can pose as the reactive part of the molecule. H_2O_2 , $\bullet\text{OH}$, and $\text{O}_2\bullet$ consist, besides hydrogen, only of oxygen. These three species are investigated as representative for reactive oxygen species. In figure 4.17 the hydrogen peroxide concentration is depicted. Surprisingly, the highest concentration is determined for pure nitrogen gas curtain with $2.4 \pm 0.3 \text{ mg} \cdot \text{L}^{-1}$. For the other curtain gas compositions the total amount of plasma generated H_2O_2 in DPBS remains constant. There are different assumptions which could explain this behavior: the hydrogen peroxide formation is not enhanced by 100% nitrogen curtain gas like for other compositions so that there is not a direct relation between H_2O_2 and the curtain gas. Instead the presence of

4 Results and discussion

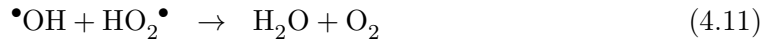
oxygen in the other compositions leads to fundamental changes in the plasma. Therefore, further components are formed and less energy is available for the H_2O_2 production in the liquid. Precursors of hydrogen peroxide are, among others, hydroxyl radicals or hydroperoxyl and/or superoxide anion radicals. As explained above, the presence of nitrogen in an argon plasma leads to the formation of metastable nitrogen. This molecular nitrogen carries 6.1 eV [206], which is enough energy to dissociate water. The necessary energy for H_2O dissociation is averaged 4.5 eV [207]. This reaction yields hydroxyl radicals, which are the main precursors of hydrogen peroxide (see eq. 4.10) since their reaction rate with each other is really fast [208, 209]. Often, the recombination of two hydroxyl radicals to hydrogen peroxide is reported as diffusion controlled [210, 211].

The formation of H_2O_2 by hydroperoxyl and superoxide anion radicals only occurs if the pH value is close to the pK_a value of 4.8 (eq. 2.20) or even lower (eq. 2.21). Hence, in the liquid this reaction pathway cannot play an important role for DPBS whose pH is still 6.7 after plasma treatment (see figure 4.15).



The absence of oxygen in the plasma plume's surrounding area enables the vacuum ultraviolet radiation to reach the liquid surface, where it will also dissociate water molecules and generate hydroxyl radicals [63]. More details about the impact of VUV radiation on the reactive species formation in liquids due to plasma treatment are given in section 4.3.3. Their recombination then again results in an increase in hydrogen peroxide concentration in the solution.

Since the gaseous surroundings of the plasma plume is varied, a reactive species formation dominated by the gas phase also needs to be considered for the higher amount of hydrogen peroxide in the liquid. This will be important especially for hydrogen peroxide due to its high Henry constant of $8.3 \cdot 10^{-1} \text{ M} \cdot \text{Pa}^{-1}$ [212]. Besides hydroxyl radicals, hydroperoxyl radicals are also formed in the gas phase, but only if gaseous O_2 is present and interacts with the plasma plume. If $\text{HO}_2\bullet$ is formed in the gas phase it can react with $\bullet\text{OH}$ and will produce water and molecular oxygen (see eq. 4.11) [17].



The presence of hydroperoxyl and, consequently, also the presence of molecular oxygen in the gas phase will partially hinder the formation of gaseous hydrogen peroxide. Therefore, the higher amount of aqueous H_2O_2 in the case of pure nitrogen is assumed to be caused by the absence of the recombination of hydroxyl and hydroperoxyl radicals in the gas phase. Furthermore, as mentioned above the absence of molecular oxygen results in larger amounts of VUV-caused water dissociation yielding the recombination of two hydroxyl radicals to hydrogen peroxide.

To study the relevance of the oxygen radicals, in the following, hydroxyl and superoxide anion radical formation is determined depending on the curtain gas composition. The resulting net production rate R_{net} (see eq. 4.12) of these radicals, given by the particular radical concentration $c_{radical}$ normalized to the treatment time $t_{treatment}$ per sample volume

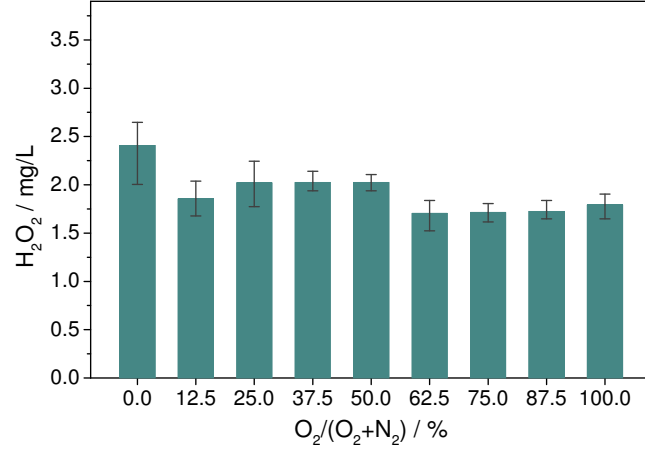


Figure 4.17: The resulting concentration of hydrogen peroxide as a function of the variation of the curtain gas composition for 180 s plasma treatment. The error bars show the minimum and maximum deviations of the mean value of at least three independent measurements (Republished with permission of Begell House Inc., from [33]; permission conveyed through Copyright Clearance Center, Inc.).

V_{sample} , is shown in figure 4.18 for DMPO used as spin trap.

$$R_{net} = \frac{c_{radical} \cdot V_{sample}}{t_{treatment}} \quad (4.12)$$

The first measurement point shown in figure 4.18 is determined without the use of the curtain gas. This condition yields the lowest net production rate. With increasing oxygen content in the curtain gas, the net production rate of the spin trap adduct of the oxygen radicals remains constant to the point where the oxygen level is 50% or more; from thereon the spin trap adduct concentration and, therefore, also the related spin trap adduct net production rate rises until it reaches its maximum for pure oxygen gas in the curtain device.

The high dynamic region towards higher oxygen admixture is investigated more thoroughly by measuring the net production rates for the hydroxyl and superoxide anion radicals separately. For this, BMPO is used as spin trap (see figure 4.19). Three surrounding conditions are investigated: 75%, 87.5% and 100% oxygen in the curtain gas. The first remarkable point is that the amount of trapped superoxide anion radicals is more than twice as high as the trapped hydroxyl radicals. The second point is the gradient of both net production rates as a function of the oxygen content in the curtain gas. Both net production rates are increasing with a higher oxygen content, but for the hydroxyl radical adduct the increase is less than the for superoxide anion radical adduct. BMPO•/OH increases from $29 \text{ pmol} \cdot \text{s}^{-1}$ for 75% O₂ to 33 pmol/s for 100% O₂, whereas BMPO•/OOH increases from $69 \text{ pmol} \cdot \text{s}^{-1}$ (75% O₂) to $76 \text{ pmol} \cdot \text{s}^{-1}$ (100% O₂).

From this measurement it can be concluded that the increase in oxygen radicals due to the curtain gas variation is related to the upwards trend of the superoxide anion and the hydroxyl radicals. Although the net production rate of BMPO•/OH is less than that of

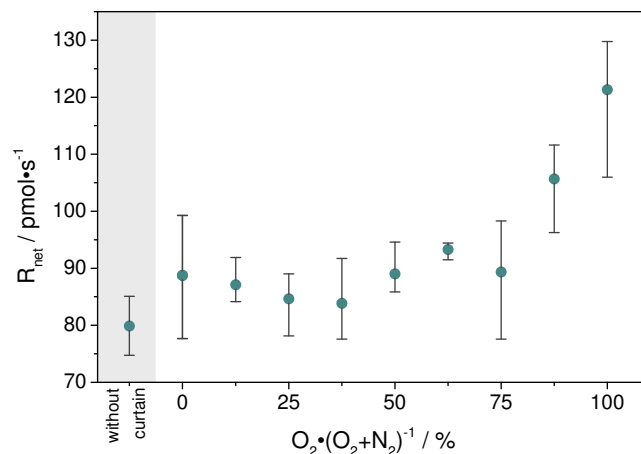


Figure 4.18: Net production rate of DMPO•/OH+OOH adduct after 180 s plasma treatment of DPBS as a function of the curtain gas composition ((©2013 IOP Publishing Ltd. Reprinted with permission from [29])). The error bars show the minimum and maximum deviations of the mean value of at least three independent measurements.

BMPO•/OOH, it cannot be concluded that hydroxyl radicals have a minor impact on the O-centered radical net production rate, since the reaction rates and more important the efficacy of the two radicals with the spin trap are quite different. It is known that the recombination reaction of hydroxyl radicals to hydrogen peroxide always competes with that of the spin trap, both are in the same order of magnitude ($10^9 M^{-1} s^{-1}$ [210, 213]). However, in the presence of hydroxyl radicals the detection of superoxide anion is difficult because of the huge difference in the reaction rates of BMPO with $O_2^{\bullet-}$ ($77 M^{-1} s^{-1}$) [193] and with $\bullet OH$ ($2 \cdot 10^9 M^{-1} s^{-1}$) [213]. The plasma treatment of the liquid results in a complex and unknown composition of reactive species in the liquid, and therefore, the known efficacies from the literature for systems without plasma are not applicable. The efficacy for a system without plasma are for the reaction of BMPO with superoxide anion radicals about 90% [213], whereas for BMPO with hydroxyl radicals the efficacy is about 0.6% [214]. Nevertheless, under the assumption that the efficacy values are in the right order of magnitude, and hence, can be applied as a first estimation; the net production rate for BMPO•/OOH is assumed to correspond approximately to the situation in the liquid, whereas the net production rate of BMPO•/OH is drastically underestimated. By the comparison of the slopes of the net production rates for the two different spin traps in the range of for 75% up to 100% oxygen in the curtain gas, a difference became obvious (figures 4.18 and 4.19). This difference is, besides the different reaction rates of DMPO and BMPO with superoxide anion radicals and hydroxyl radicals, mainly due to their different trapping efficacy. For DMPO the efficacy of the reaction with $\bullet OH$ is between 3% up to 30% [215] and for the reaction with $O_2^{\bullet-}$ it is about 90% [215]. The efficacy of trapping superoxide anion radicals is for both spin traps the same but for trapping hydroxyl radicals it differs strongly. Therefore, the increase of the net production rate with increasing amount of oxygen in the curtain gas is presumed to be mainly caused by hydroxyl radicals. As hydroxyl radicals are one of the responsible precursors for hydrogen peroxide, one expects a similar trend for both as a function of the oxygen content in the curtain gas. In contrast figure 4.17 and figure 4.18 are opposed. This an indication that

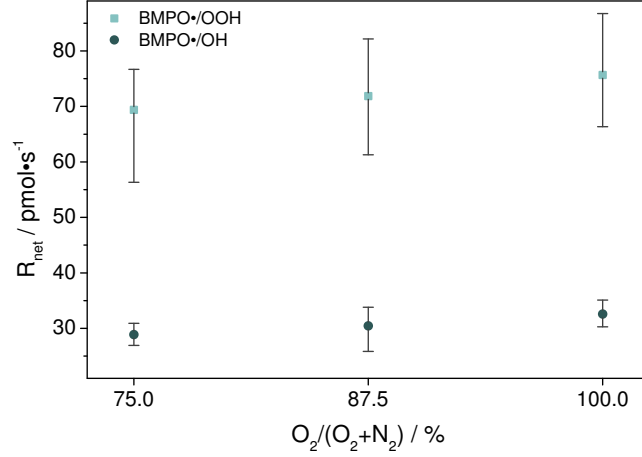
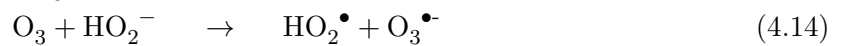
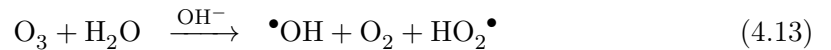


Figure 4.19: Net production rate of BMPO•/OH and BMPO•/OOH adduct after 180 s plasma treatment of DPBS as a function of the curtain gas composition. The error bars show the minimum and maximum deviations of the mean value of at least three independent measurements.

the hydrogen peroxide production under this specific plasma treatment conditions is not dominated by the recombination of aqueous hydroxyl radicals. The formation has to be mainly caused by gaseous precursors. As mentioned above, the presence of molecular oxygen in the surroundings of the plasma plume yields the formation of hydroperoxyl radicals, which is in the gas phase a potential loss channel for hydroxyl radicals, and therefore, it hinders the formation of H₂O₂. Since the gap between the nozzle of the plasma jet and the liquid surface is only 9 mm, the formation of gaseous hydrogen peroxide is improbable, but a generation of the precursors are most likely. When such a precursor, e.g. gaseous •OH radicals, reaches the surface of the liquid an reaction at the plasma-liquid interface occurs. This interface reaction results in hydrogen peroxide, yielding an increase in the H₂O₂ concentration in the case of pure nitrogen curtain gas. For all cases, where molecular oxygen is contained in the curtain gas, the formed hydroperoxyl reacts prior with hydroxyl radicals and disables the interface reaction. The O₂ from the curtain gas diffuses into the plasma plume. It can form atomic oxygen as well as ozone in the gas phase [8], which can lead to the generation of hydroxyl radicals by reaction with water (see equations 4.13 to 4.15). Hence, the increase in the net production rates for higher amounts of ambient oxygen is presumed to be caused by formation of atomic oxygen and ozone, as the other potential sources for the dissociation of water, such as VUV radiation and metastable nitrogen, can be excluded.



Summarizing this section it can be stated, that the H₂O₂ concentration can only be slightly reduced by addition of molecular oxygen into the curtain gas, but a further increase is not possible, whereas all other investigated species can be increased in their concentration

4 Results and discussion

by a tailoring the surroundings of the plasma plume. Furthermore, the type of reactive species, either RNS or ROS, which is dominating the liquid chemistry is tunable with the exception of hydrogen peroxide. For investigations of effects of ROS and RNS on mammalian systems these findings are essential, as hydrogen peroxide has a strong influence on these systems, in studies focusing on species other than H_2O_2 , its concentration needs to be held constant and other parameter need to be varied. The increase of hydrogen peroxide can be achieved by humidity addition to the feed gas (detail are given in section 4.3.1). In the following section the molecular gas admixtures to the feed gas are described and discussed .

4.2.2 Impact of molecular gas admixture into the feed gas on liquid chemistry

As shown in the previous section the surrounding environment can tailor plasma induced liquid chemistry. An even stronger effect is expected from the feed gas manipulation, described in the following. It is known for the gas phase that the formation of highly reactive nitrogen and oxygen containing species such as nitric oxide or nitrogen dioxide radicals as well as hydroxyl and hydroperoxyl radicals is triggered by the admixture of both molecular gases into the feed gas [203]. A similar behavior is, therefore, expected also for the liquid phase. In figure 4.20 the dependence of the oxygen radical spin trap adduct with BMPO is depicted as a function of the oxygen and nitrogen admixture to the feed gas. For this investigation, 1% of oxygen or nitrogen or a mixture of both is added to the feed gas argon. The total gas flow rate is remains constant at three standard liters per minute. Since it was shown in the previous section (section 4.2.1.2) that the surroundings has such an influence on the liquid reactive species output due to the plasma treatment, the curtain gas device with synthetic air as surrounding gas is used to enable stable experimental conditions. The presence of molecular gases in the feed gas leads to an alteration of the plasma plume. By obtaining the visible plasma plume, the length and color of the plume is changing with molecular admixtures. As shown in reference [8], although the visible plume becomes shortened by an admixture of molecular oxygen, while the atomic oxygen density in the plume still increases.

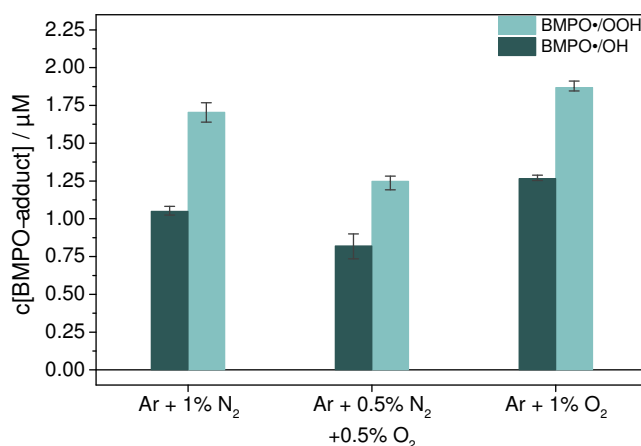
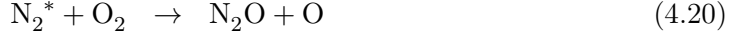


Figure 4.20: Oxygen radical BMPO adduct in DPBS as a function of oxygen and nitrogen feed gas admixture, formed during 180 s kinpen09 treatment with synthetic air as curtain gas.

As shown in figure 4.20, for the case of 0.5% of each, molecular oxygen and nitrogen, the resulting BMPO adduct concentrations for hydroxyl radicals and superoxide anion radicals are the lowest compared to the pure cases. This behavior is expected due to the gas phase chemistry. From the literature it is known that in the presence of oxygen and nitrogen the reactions 4.16 to 4.21 occur [17]. Therefore, the formation of the highly reactive oxygen and nitrogen species, O, N and N₂^{*}, yields the generation of reactive nitrogen species, mainly nitric oxide. Furthermore, they react also with hydroxyl radicals in the gas phase

4 Results and discussion

resulting in a lower amount of potential precursors for the liquid phase oxygen radicals.



Since the curtain gas for the feed gas admixture measurements is synthetic air (syn. air), the quenching of the high energetic metastable species by molecular oxygen can also occur for the pure nitrogen feed gas admixture. Nevertheless, in the case of N_2 admixture into the feed gas, the production of metastable nitrogen is in parallel also enhanced inside the plasma. This results in a higher concentration of the trapped oxygen radicals in the liquid in comparison to the case where both, nitrogen and oxygen, is admixed to the feed gas. There, the potential oxygen and nitrogen reaction partners yielding nitrogen oxide species are directly present at their place of origin.

The pure oxygen case yields the highest amount of trapped oxygen radicals. This observation is assumed to be due to an additional solving of gaseous generated oxygen radicals in DPBS. As the admixture of oxygen to the feed gas results in high concentrations of gaseous ozone [181], ozone will be partially solvated in the liquid, according to Henry's law (Henry constant for O_3 : $1.2 \cdot 10^{-4} \text{ M} \cdot \text{Pa}^{-1}$ [114]). Due to the buffer in the solution, the pH value remains constant at 7.4, hence, the dissolved ozone is quite unstable and will, therefore, decompose to generate hydroxyl radicals and hydroperoxyl/superoxide anion radicals (see eq. 4.13). In the presence of hydrogen peroxide the decomposition of ozone becomes faster and results in an increased concentration of oxygen radicals (see equations 4.14 and 4.15). For this decomposition mainly the conjugated base of hydrogen peroxide, hydroperoxide (HO_2^-), is assumed to be responsible [107, 216]. This so-called peroxone process is relatively fast for pH values above 5. So in case of DPBS with a pH of 7.4 this process is likely to take place. Furthermore, the photolysis of ozone can also yield higher concentrations of hydroxyl radicals in the solution since during this photolysis process singlet oxygen ($\text{O}_2(^1\Delta_g)$ or $^1\text{O}_2$), triplet oxygen ($\text{O}_2(^3\Sigma_g)$) and most important excited atomic oxygen ($\text{O}(^1\text{D})$) are produced. The latter reacts with water to form hydroxyl radicals [107]. Hence, higher amounts of oxygen in the feed gas will lead to higher concentrations of oxygen radicals in the solution.

In the case of a pure nitrogen curtain gas besides hydroxyl radical and superoxide anion radical, the formation of singlet oxygen is also expected in the liquid due to its high density in the gas phase, as known from the literature [17]. Especially, an admixture of 1% molecular oxygen to the feed gas is assumed to result in high concentrations of these reactive oxygen species in the liquid. Therefore, all three highly reactive oxygen species are determined by the use of spin trap enhanced electron paramagnetic resonance spectroscopy. For $\bullet\text{OH}$ and $\text{O}_2\bullet$ again BMPO is used as spin trap, for $^1\text{O}_2$ TEMPD-HCl is the spin trap of choice. The most reactive species out of the three is the hydroxyl radical, of which the detected BMPO adduct is of the lowest amount in the solution, whereas superoxide anion radical spin trap adduct, $\text{BMPO}\bullet/\text{OOH}$, is approximately three times higher in concentration. The highest spin trap adduct concentration of all three species is determined for singlet oxygen trapped by TEMPD-HCl. It has to be noted that a direct

comparison of the measured amounts of different spin traps always needs to be treated with caution since the reaction rates as well as the efficacy not only of each spin trap but also for each trapped species differ and, therefore, need to be considered. If these rates and efficacies are unknown, as is the case for TEMPD-HCl, or if they are clearly different, a direct comparison, without consideration of these parameters, is not recommended. The origin of singlet oxygen will be discussed in more detail in section 4.3.2.

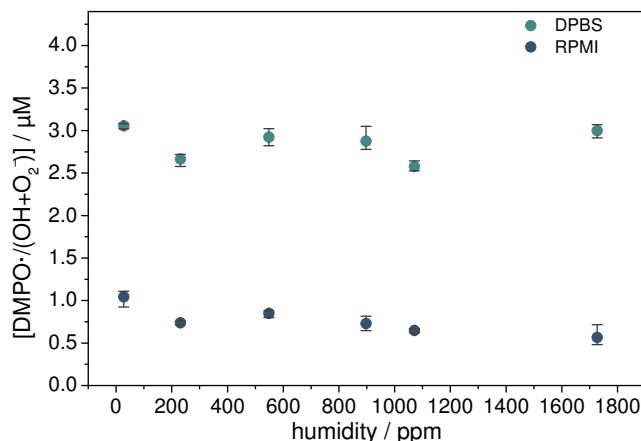


Figure 4.21: Spin trap adduct of DMPO with oxygen radicals as a function of the feed gas humidity. Detected after 40 s plasma treatment in DPBS and RPMI, respectively.

In the case of humidified feed gas no dependence of the formed oxygen radicals in the solution is observed as shown in figure 4.21. There the behavior is shown for the cell culture medium, RPMI 1640, and the phosphate buffered saline, DPBS. The trend for both liquids is similar, only the measured spin trap adduct concentrations differ: in DPBS up to $3\mu\text{M}$ and in RPMI 1640 up to $1\mu\text{M}$ DMPO oxygen radical adducts are formed. This fact is studied in greater detail in the following section (section 4.2.3). The independence of the oxygen radicals of the feed gas humidity can either be caused by the absence of possible highly energetic components in close vicinity of the liquid surface, such as VUV radiation, or metastable species, which can yield the dissociation of aqueous water molecules to form the oxygen radicals directly in solution. Another possible reason is that the generated gaseous oxygen radicals will not be transported into the liquid as radicals due to previous reactions in the gas phase or at the interface with other molecules to new, non-radical products.

In contrast to hydroxyl and superoxide anion radicals, the concentration of hydrogen peroxide correlates strongly with the feed gas humidity as depicted in figure 4.22. With increasing humidity the hydrogen peroxide concentration is also rising. Therefore, the H_2O_2 concentration cannot be caused by the reaction of liquid phase hydroxyl radicals or superoxide anion radicals. The discrepancy could be explained by a dissolving effect of gaseous hydrogen peroxide and its precursors. This assumption will be discussed more in detail in the following section 4.3.1.

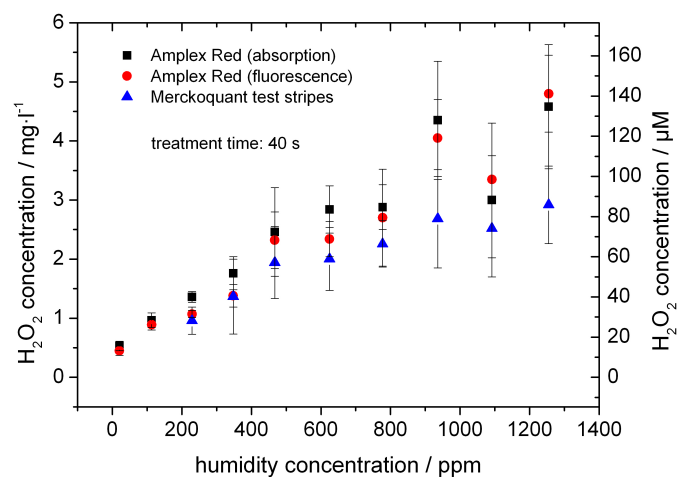


Figure 4.22: Hydrogen peroxide concentration as a function of the feed gas humidity after 40 s plasma treatment of RPMI 1640 ((©2013 IOP Publishing Ltd. Reprinted with permission from [71]).

4.2.3 Impact of liquid ingredients

Besides the gaseous surroundings, the liquid itself has an impact on the species generation [107]. As depicted in figure 4.4 for the presence of a spin trap in the solution, an interaction with components contained in the liquid can take place during plasma treatment (see figure 4.23).

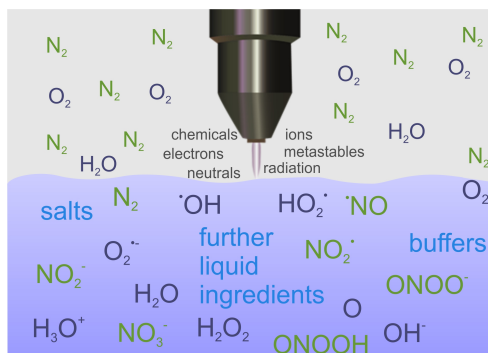


Figure 4.23: Treatment scheme with the focus on the liquid phase and the plasma generated reactive species including further components of more complex liquids.

Starting from the least complex case of biologically relevant solutions, water, the H_2O molecules are possible origins for reactive oxygen species. The interaction of the plasma includes transport processes of the gas phase species generated by plasma as well as direct interaction of active plasma components such as radiation. Therefore, if the required energy of about 5 eV is provided, the water molecules can be dissociated by homolytic fission to hydroxyl radicals, as described in section 2.1.2.1. This energy can reach the H_2O molecules in the form of radiation, for which a wavelength of $\leq 239.8\text{ nm}$ is required [217], or in the form of highly energetic species such as metastable molecular nitrogen, which carries energy of 6.1 eV and can, therefore, deliver sufficient energy for the splitting of the water molecules.

The more complex the liquid becomes, the more potential reaction partners need to be considered. For instance, in sodium chloride solution the chloride could be an origin of hypochlorite or hypochlorous acid as it is suggested in the literature for a radio frequency plasma jet working with argon and admixture of oxygen [65]. In this publication a formation of hypochlorite caused by atomic oxygen is assumed (see equation 4.22). The presence of OCl^- is tested by two commercial colorimetric dyes (aminophenyl fluorescein, APF, and hydroxyphenyl fluorescein, HPF, from invitrogen) which by comparison should give a specific response to hypochlorite. Up to now, no indication of liquid phase OCl^- or HOCl , generated during kinpen09 treatment has been found by the use of this dyes.



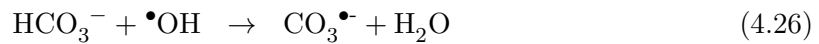
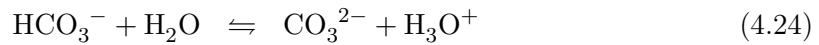
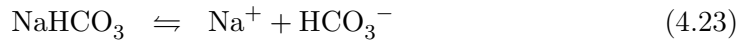
A more biologically relevant solution, Dulbecco's phosphate buffered saline (DPBS) solution contains besides water and sodium chloride also potassium chloride (KCl) and two phosphate containing buffers. These phosphate buffers, namely disodium hydrogen phosphate (Na_2HPO_4) and potassium dihydrogen phosphate (KH_2PO_4) are further sources of reactive oxygen species since the three single P–O bonds could be cleaved by 6.17 eV

4 Results and discussion

Table 4.2: Main ingredients of the investigated liquids (Republished with permission of Begell House Inc., from [33]; permission conveyed through Copyright Clearance Center, Inc.).

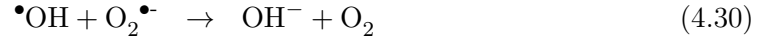
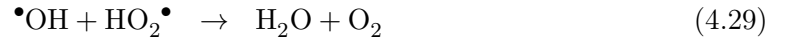
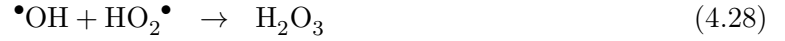
NaCl	DPBS	RPMI
H ₂ O	H ₂ O	H ₂ O
NaCl	NaCl	NaCl
	KCl	KCl
	Na ₂ HPO ₄	Na ₂ HPO ₄ · 7H ₂ O
	KH ₂ PO ₄	NaHCO ₃
		MgSO ₄ · 7H ₂ O
		Ca(NO ₃) ₂ · 4H ₂ O
		glucose
		glutathione
		± phenol red · Na
		amino acids
		vitamins

(corresponding to 201 nm) [217]. In the case of a cell culture medium, here RPMI 1640, beside water, NaCl, KCl and disodium hydrogen phosphate buffer an additional carbonate buffer, sodium bicarbonate (NaHCO₃) is included, as well as further ingredients such as e.g. calcium nitrate, Ca(NO₃)₂ (see table 4.2). In figure 4.24a a decrease in pH related to plasma treatment is shown for sodium chloride solution (marked with open diamonds). The effect is dependent on the curtain gas composition, where the strongest decrease is found in the case of 25% oxygen and 75% nitrogen in the curtain. DPBS (marked with open squares), as mentioned above, does not change in pH, meaning that the buffer capacity is not consumed during treatment. As already mentioned RPMI's pH course (marked with leftwards-oriented open triangles) as a function of the curtain gas composition shows an effect which can be attributed to the bicarbonate buffer. The increase in pH is not caused by the plasma but due to a degassing of this carbonate buffer, also known in the human body as respiratory alkalosis [218]. Furthermore, the reaction of NaHCO₃ with plasma generated hydroxyl radicals contributes to the loss in carbonate buffer according to reactions 4.23 to 4.26. Since the pH is so high that the left side of equation 4.24 dominates, reaction 4.25 plays an almost negligible role in carbonate buffer loss [33].

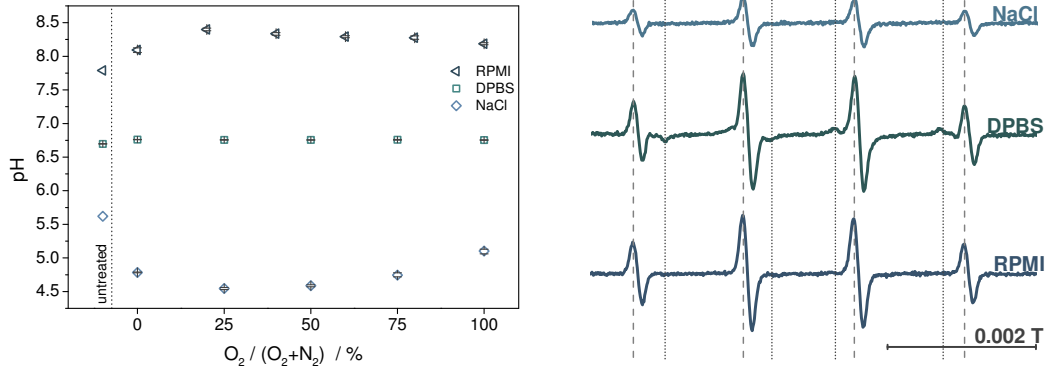


The presence of hydroxyl radical in all three liquids is shown in figure 4.24b for the case of a pure oxygen curtain gas. Furthermore, superoxide anion radicals are observed in DPBS. Since DMPO is not the ideal spin trap for distinguishing between hydroxyl and superoxide anion (see section 4.1.1), the absence of the peaks in the sodium chloride solution and in the cell culture medium does not mean that no O₂^{•-} is generated there.

The so-detected concentration of oxygen radical adducts of DMPO are $1.9 \pm 0.25 \mu M$ for NaCl, $5.6 \pm 0.5 \mu M$ for DPBS, and $3.6 \pm 0.36 \mu M$ for RPMI 1640 [33]. The difference in radical adducts concentrations in the three liquids can be explained by the ingredients of the solutions. Sodium chloride solution only contains NaCl and water. Therefore, water is the only possible origin of plasma generated oxygen radicals within the liquid. DPBS also contains the phosphate buffers; hence, a second potential oxygen radical origin. More important is the stable pH value of DPBS, since the consumption of oxygen radicals by several relevant free radicals are at acid pH diffusion controlled (see equations 4.27 to 4.31[58]). Furthermore, reactions 4.28 and 4.29 occur only for pH values ≤ 4.8 , whereas reaction 4.30 can take place if the pH is ≥ 4.8 .



RPMI 1640 also includes the phosphate buffer system but in addition also the carbonate buffer, which can consume hydroxyl radicals according to equations 4.25 and 4.26 and radical scavengers such as amino acids and vitamins (see table 4.2). Hence, the resulting concentration or RPMI has to be reduced in comparison to DPBS, which is the case as shown by the above values.



(a) The pH value for NaCl, DPBS, and RPMI 1640 as a function of curtain gas composition (Republished with permission of Begell House Inc., from [33]; permission conveyed through Copyright Clearance Center, Inc.).

(b) EPR spectra of DMPO adducts in NaCl, DPBS, and RPMI 1640 after 180 s plasma treatment by the use of a pure oxygen curtain gas. The resulting oxygen radical DMPO adduct concentrations are $1.9 \pm 0.25 \mu M$ for NaCl, $5.6 \pm 0.5 \mu M$ for DPBS, and $3.6 \pm 0.36 \mu M$ for RPMI 1640 (Republished with permission of Begell House Inc., from [33]; permission conveyed through Copyright Clearance Center, Inc.).

Figure 4.24: Differences in resulting chemistry due to variation of the plasma treated liquid, NaCl, DPBS and RPMI 1640 are investigated.

4.3 Origin of selected reactive species in the liquid

For a tailored plasma treatment it is necessary to study the origin of the plasma generated species. Different mechanisms become relevant, if the origin is in the gaseous phase and the species is transported into the liquid, if the generation takes place at the interface, or if the species are produced inside the bulk liquid. To elucidate the reactive species origin, in this work, several studies are performed, on exemplary reactive species, which are hydrogen peroxide (see section 4.3.1), singlet oxygen (see section 4.3.2), and hydroxyl radicals (see section 4.3.3). Specifically, reactive species sources of mass transfer from the plasma or gas phase, a direct formation by plasma generated radiation, as well as by plasma generated energetic species are investigated.

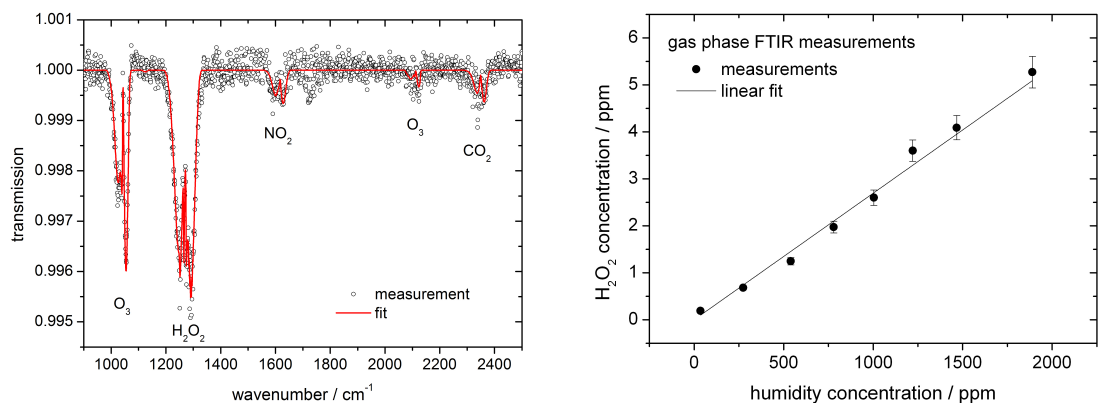
4.3.1 Hydrogen peroxide

The formation of hydrogen peroxide in the liquid phase strongly correlates with the feed gas humidity (see also section 4.2.2). This indicates an origin of an relevant precursor or of hydrogen peroxide itself in the gaseous phase and a carryover to the liquid phase. With this hypothesis, the origin of H_2O_2 detected in solution is investigated from the gas phase to the liquid.

Detection in the gas phase

To study the dependence of the hydrogen peroxide formation in the gas phase, the feed gas of the plasma jet is varied from as dry as possible to humid. This is realized by a partial guidance of the total feed gas flow through a gas washing bottle containing water as described in references [71] and [61]. The plasma is operated in an open atmosphere. These measurements were performed by Dr. J. Winter and S. Schlegel. The investigation of the origin of hydrogen peroxide in the liquid phase includes measurements of the gas phase reactions performed by the use of a Fourier transform infrared absorption spectrometer. In figure 4.25a a measured and fitted Fourier transform infrared radiation (FTIR) spectrum is shown; the measurement and fitting details can be found in the reference [61]. In the spectrum the absorption measured in the multipass cell of the FTIR can be attributed to carbon dioxide, nitrogen dioxide, ozone, and hydrogen peroxide. The fitting of the spectrum is performed by fitting tool software (QMACSoft 1.1.3, neoplas control GmbH, Greifswald, Germany) [219, 220]. From the so-fitted curve the concentration in the multipass cell can be calculated according to the Beer Lambert. The band dominating the spectrum section shown in figure 4.25b is the absorption band of hydrogen peroxide. From this band, the concentration of gaseous H_2O_2 is determined as a function of the feed gas humidity. In the case of dry argon as feed gas a hydrogen peroxide concentration of below 250 *ppb* is measured, whereas for the most humidified case (1800 *ppm*) a concentration of 5.3 *ppm* H_2O_2 can be detected. The formation of hydrogen peroxide in the gas phase is closely linked to the hydroxyl radical formation [5, 118]. The reaction of two $\bullet\text{OH}$ molecules to hydrogen peroxide is the major formation reaction in plasmas, but of course not the only possible one. An alternative generation pathway can take place in the plasma plume region, where ambient oxygen can react with hydrogen radicals to produce hydroperoxyl radicals. The recombination of these can lead to H_2O_2 and molecular oxygen. In the case of simultaneous generation of hydroperoxyl radicals and hydroxyl radicals, a reaction of the two will yield water and molecular oxygen, and hence, the necessary educts for H_2O_2 formation will not be available anymore. According to the literature the formation in the core plasma zone via dissociation of water is 20 times more effective than in the plasma

plume region [201]. Therefore, a dominant role of the H_2O_2 formation by two hydroxyl radicals is assumed to be dominating in contrast to the atmosphere, where hydrogen peroxide is mainly produced via the recombination of two hydroperoxyl radicals [118].



(a) Typical FTIR spectrum when water is present in the feed gas of the kinpen09. Here the humidity of the feed gas is 1220 ppm (©2013 IOP Publishing Ltd. Reprinted with permission from [61]).

(b) Determined gaseous concentration of hydrogen peroxide as a function of feed gas humidity.

Figure 4.25: Influence of the feed gas humidity on hydrogen peroxide in the gas phase (©2013 IOP Publishing Ltd. Reprinted with permission from [61]).

Comparison to liquid concentrations

To study the origin of hydrogen peroxide in the case of humidified feed gas, the concentrations detected in the gaseous phase and the one detected in the liquid phase are compared. In figure 4.26 the hydrogen peroxide net production rates in both phases are depicted as a function of the feed gas humidity. Not only the same trend for the gas and the liquid phase is observed, furthermore, the absolute values for both net production rates are exactly the same. This gives a first indication that in the case of humidified feed gas the formation of hydrogen peroxide can be caused by a dissolving process, i.e. a mass transfer from the gas to the liquid phase.

For a detailed study, the potential precursors in the liquid phases have to be investigated as a function of the water content in the feed gas. In section 4.21, it was already pointed out that the total oxygen radical trend in the liquid shows no dependence on the feed gas humidity in contrast to the aqueous hydrogen peroxide concentration, which shows a drastic dependence on the feed gas humidity as seen in figure 4.26. For a closer look at possible formation pathways the distinction between hydroxyl and superoxide anion radicals is desired as both can be part of in the hydrogen peroxide generation chain in solution. Hence, BMPO is used as spin trap instead of DMPO. Due to handling reasons the measurements are performed in DPBS instead of RPMI 1640. In order to link radical concentrations to the investigations on plasma treatment of skin cells as a function of feed gas humidity as published in the prior study [21], RPMI 1640 is investigated for the hydrogen peroxide measurements. The comparability of the behavior of both solutions is shown in figure 4.21. Figure 4.27 depicts the formed spin trap adducts of BMPO with $\bullet\text{OH}$ (marked with filled dots) and $\text{O}_2^{\bullet-}$ (marked with filled squares), respectively. The trend of both radicals is the same, with increasing humidity in the feed gas the concentrations slightly decrease.

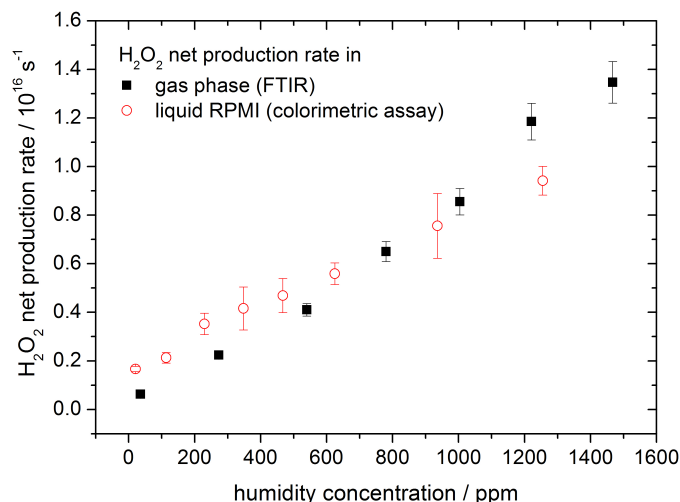


Figure 4.26: Correlation of plasma generated hydrogen peroxide net production rates in the liquid and gaseous phase adapted from ((©2013 IOP Publishing Ltd. Reprinted with permission from [61])).

Comparing these results to the measurements shown in figure 4.21, reveals that neither the total oxygen radical concentration, nor the concentration of either hydroxyl or superoxide anion radicals increases. Hence, it can be stated that the increase of H_2O_2 concentration with increasing feed gas humidity is not explainable by the aqueous oxygen radicals. This acts as a further indication that the plasma treatment with humidified feed gas yields the formation of, at least, the precursors of H_2O_2 in the gas phase.

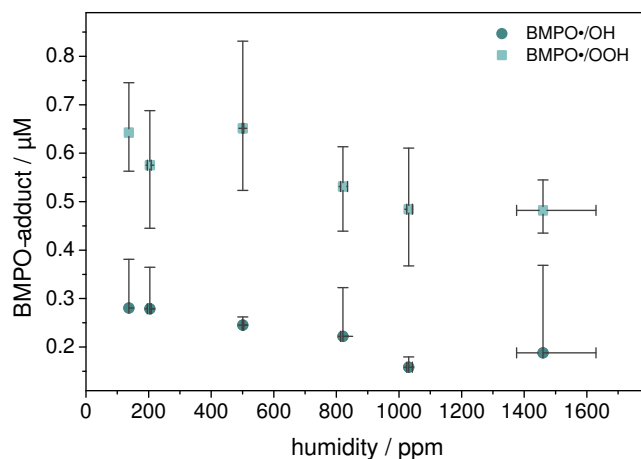


Figure 4.27: Spin trap (BMPO) oxygen radical concentration as a function of the feed gas humidity ((©2013 IOP Publishing Ltd. Reprinted with permission from [61])). Treatment of 5 mL DPBS for 40 s with kinpen09.

As the aqueous oxygen radicals are not the reaction pathway mainly responsible for the formation of hydrogen peroxide, other possibilities need to be taken into account. The prior assumption that a solvation process takes place needs further verification. The solvation of gaseous species in water is described by Henry's law, which is dependent on the temperature [202]. The aqueous concentration (c_{aqueous}) is described by equation 4.32, where $k_H(T)$ is the temperature (T)- dependent Henry coefficient and p_{gas} is the partial

pressure of the gas.

$$c_{aqueous} = k_H(T) \cdot p_{gas} \quad (4.32)$$

The Henry coefficients for room temperature of relevant species can be found in table 4.3. According to equation 4.32, the higher the value the more soluble the molecule is in water. From the listed coefficients given in the table, hydrogen peroxide is highly soluble. Looking only at the Henry's coefficients, it can be assumed that solvation is a reasonable and non-negligible source for the liquid phase H_2O_2 in the presence of a sufficient amount of water in the feed gas.

Table 4.3: Henry coefficients for selected species at standard conditions.

species	Henry coefficient / $M \cdot Pa^{-1}$	References
molecular oxygen (O_2)	$1.2 \cdot 10^{-8}$	[221]
molecular nitrogen (N_2)	$6.5 \cdot 10^{-8}$	[222]
argon (Ar)	$1.4 \cdot 10^{-8}$	[223]
nitric oxide ($\bullet NO$)	$1.9 \cdot 10^{-5}$	[114]
singlet oxygen (1O_2)	$9.8 \cdot 10^{-5}$	[224]
ozone (O_3)	$1.2 \cdot 10^{-4}$	[114]
nitrogen dioxide ($NO_2 \bullet$)	$1.2 \cdot 10^{-4}$	[114]
hydroxyl radicals ($\bullet OH$)	$2.9 \cdot 10^{-4}$	[225, 226]
hydroperoxyl radical ($HO_2 \bullet$)	$4.0 \cdot 10^{-2}$	[226]
hydrogen peroxide (H_2O_2)	$8.3 \cdot 10^{-1}$	[212]
nitric acid (HNO_3)	2.1	[114]

The expected impact of dissolving gaseous molecules is validated for the case of hydrogen peroxide by a comparison of the resulting aqueous H_2O_2 concentration generated either during plasma treatment or by treatment with hydrogen peroxide enriched argon. The enrichment is performed via bubbling argon through a hydrogen peroxide solution whose concentration in the feed gas corresponds to the plasma generated ones for different humidity concentrations. In the latter configuration, only hydrogen peroxide is singled out and investigated detached all other active parts of the plasma treatment.

In figure 4.28 the concentrations gained from the two different configurations are compared as a functions of the gaseous hydrogen peroxide concentration for three different treatment times: 40 s, 60 s, and 80 s. The trend of the liquid phase hydrogen peroxide concentration is the same if H_2O_2 is generated by plasma or by the bubbler setup; the total amount is slightly higher for the case of plasma treatment. This is caused by the additional formation pathways of the other plasma components, which can cause dissociation of water and, therefore, form further hydrogen peroxide in the solution. This observed data supports the assumption that in the case of humidified feed gas the generation process is dominated by a solvation of H_2O_2 produced in the gas phase. A further explanation for the increasing hydrogen peroxide concentration with increasing feed gas humidity is that besides the H_2O_2 itself, also its precursors such as hydroperoxyl and hydroxyl radicals are formed during plasma treatment and they reach the the liquid surface. This interface interaction results in increasing liquid phase hydrogen peroxide concentration as well. Due to the minor reactivity of hydrogen peroxide compared with the oxygen radicals, the loss of gas phase H_2O_2 is assumed to be negligible.

As shown for the case of hydrogen peroxide, reactive species are formed in the liquid

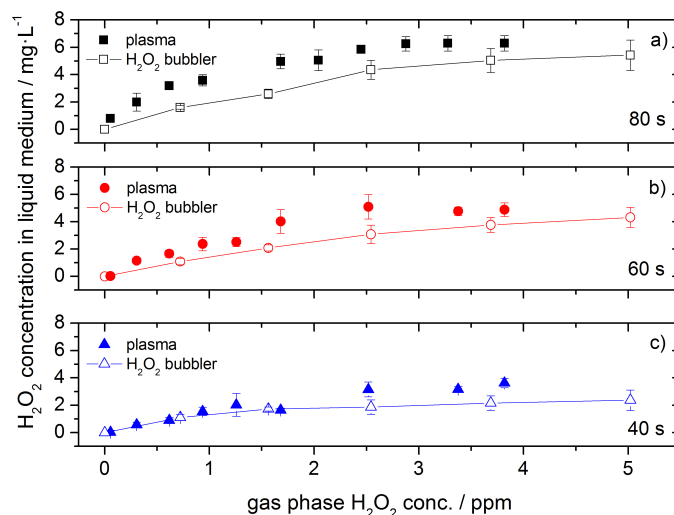


Figure 4.28: Hydrogen peroxide concentration in the liquid as a function of the gas phase hydrogen peroxide concentration for three treatment times measured for two different formation conditions: by plasma treatment by H_2O_2 enriched gas treatment by using a hydrogen peroxide bubbler (©2013 IOP Publishing Ltd. Reprinted with permission from [61]).

by mass transfer in a solvation process. In the following, an investigation on the ozone solvation in plasma treated solution is performed, as ozone is one of the most abundant species present in the gas phase of cold argon oxygen plasmas [7, 181]. For this study, the detection of ozone in the liquid phase is performed by the use of a colorimetric reagent named indigo blue according to the protocol described in section 3.2.3. This assay is well accepted for the detection of dissolved ozone in water although the selectivity of this assay for ozone is doubtful. Nevertheless, this assay has been used several times in the plasma medicine community and, therefore, also is tested in this work. The assay is based on a bleaching of the indigo dye, which can occur not only by reaction with a highly oxidizing species such as ozone but also with hydroxyl radicals. The gained values are evaluated and discussed with caution due to the doubtful selectivity. The investigated treatment times are 60 s, 120 s, 180 s and 300 s, and ultrapure water is used as liquid since the assay is not applicable in chloride-containing liquids. To enhance the gaseous ozone production, the feed gas is enriched with molecular oxygen by admixtures of up to 0.4% according to the literature [181].

In the gas phase the increase of oxygen in the feed gas results an increase of ozone [7]. In solution the resulting trend contradicts the one in the gas phase as shown in figure 4.29. Besides the fact that the error bars are quite large and the determined concentrations are even partially negative, the trend for aqueous ozone shows no increase with higher oxygen concentration in the feed gas. In contrast, the increase of admixed oxygen seems to result in less ozone in the liquid phase. The assay is based on a bleaching effect by oxidizing species. Therefore, in the presence of hydroxyl radicals for example, a reaction cannot be exclusively attributed to ozone. Since the plasma treatment forms aqueous hydroxyl radicals the assay has to be interpreted with caution. In the reference [227], a concentration range of 10 ppb up to approximately 30 ppm is given for the indigo blue assay. The generated ozone concentration in the gas phase is 10 ppm for 0% oxygen in the feed gas; even for 0.1% oxygen the concentration is higher than 40 ppm. A maximum of 80 ppm of ozone is

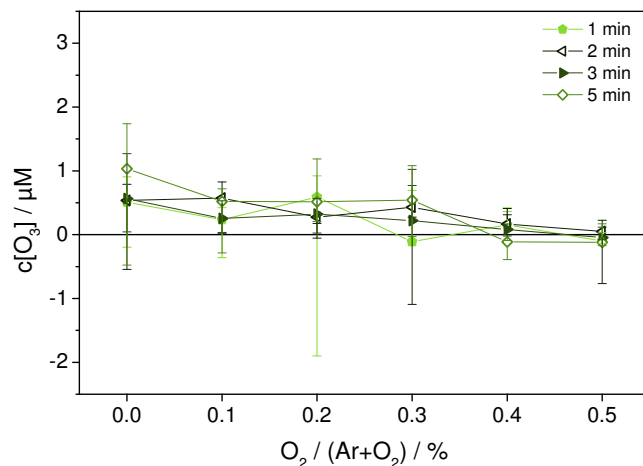
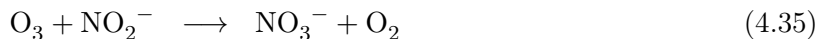


Figure 4.29: Ozone concentration in ultrapure water for different treatment times as a function of the oxygen content in the feed gas.

measured at 0.3% oxygen content in the argon feed gas. According to this range and the gaseous concentration typical for the applied conditions, it is well possible that the assay is unsuitable for determining the liquid ozone concentration for an oxygen admixture to the feed gas, especially due to the present concentration of hydroxyl radicals in the liquid. Additionally, the solubility determined by the Henry coefficient for ozone is approximately six orders of magnitude less than that of hydrogen peroxide. Likewise other species such as water, hydroxide ions, hydrogen peroxide, nitrite and nitric monoxide present in the liquid destroy ozone (see equations 4.33 to 4.36) [17, 228]. The low Henry's constant makes it unlikely that ozone is transferred in large quantities into the liquid and due to the cross reactivity of the available colorimetric probe, the presence of ozone can only be assumed for the here studied conditions. For future investigations and to avoid cross reactivity of the dye with other species besides ozone, the use of scavengers is recommended. A further and quite interesting possibility for the detection of ozone in liquids is the use of ozone specific reactions such as the reaction of phenol to muconic acid [58, 107, 229] or the reaction with Pittsburgh green as recently described in the literature [230].



4.3.2 Singlet oxygen

As a further highly reactive species which is known to be generated in the gaseous phase of atmospheric pressure plasma jets [6, 17] singlet oxygen is investigated with regard to its origin. Singlet oxygen is expected to be present in the gas phase in similar quantities as atomic oxygen or ozone, depending on the parameters and distance from the nozzle. Its presence in the gaseous phase suggests a noteworthy amount in the aqueous phase, and therefore the existence as well as the origin are investigated.

As described in section 2.1.2.2, singlet oxygen is not a radical. However, it can be detected by EPR since it forms with 2,2,6,6-tetramethylpiperidine (TEMP) and TEMP-derivatives such as TEMPD-HCl (2,2,6,6-tetramethyl-4-piperidone hydrochloride) a characteristic EPR active spin trap adduct. In figure 4.30 the distinctive spectrum of the TEMPD-HCl adduct is shown. Due to the poor solubility of the lipophilic TEMP in water, TEMPD-HCl should be used for aqueous solution.

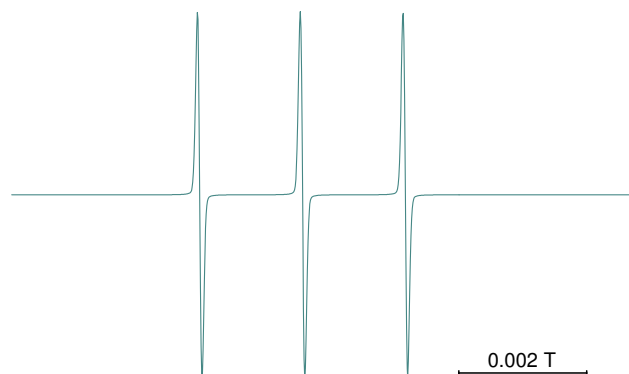


Figure 4.30: Singlet oxygen adduct spectrum of TEMPD-HCl spin trap.

As is known from the modeling in Schmidt-Bleker et al. [17] the ideal parameter of singlet oxygen generation in the gas phase is a pure nitrogen curtain gas and 1% oxygen admixture in the feed gas. Therefore, these parameters are investigated for the plasma treatment of a given solution and the following liquid analysis. In figure 4.31 the resulting spin trap adduct as a function of the treatment time is observed. The adduct shows a linear dependence on the treatment time when 0.1% oxygen is added to the feed gas and the plasma plume is protected by a pure nitrogen curtain gas.

The relation of the oxygen content in the feed gas and the amount of TEMPD-HCl-adduct is investigated by the variation of the oxygen admixed to the argon feed gas. In figure 4.32 this trend is shown for 180 s plasma treatment of DPBS with molecular nitrogen as curtain gas. Here, too, with increasing oxygen content the spin trap adduct concentration rises but the gradient decreases with the higher oxygen amount in the feed gas.

According to the gas phase model described in [17] the presence of oxygen in the closed environment should decrease the singlet oxygen concentration. Therefore, the same experiment is repeated with synthetic air instead of pure nitrogen in the curtain gas. In figure 4.33 the two curves for nitrogen (marked with open squares) and synthetic air (marked with filled squares) as curtain gases are shown. The spin trap adduct of singlet oxygen with TEMPD-HCl has similar trends for both curtain gas compositions but the total amount of

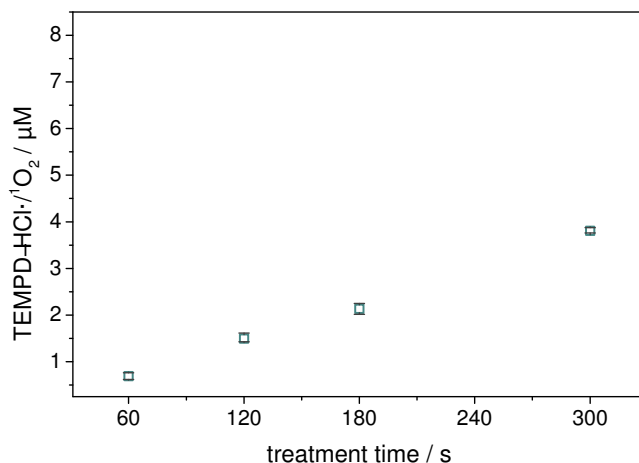


Figure 4.31: Spin adduct of singlet oxygen as a function of the treatment time with 0.1% oxygen in the feed gas with pure nitrogen as curtain gases.

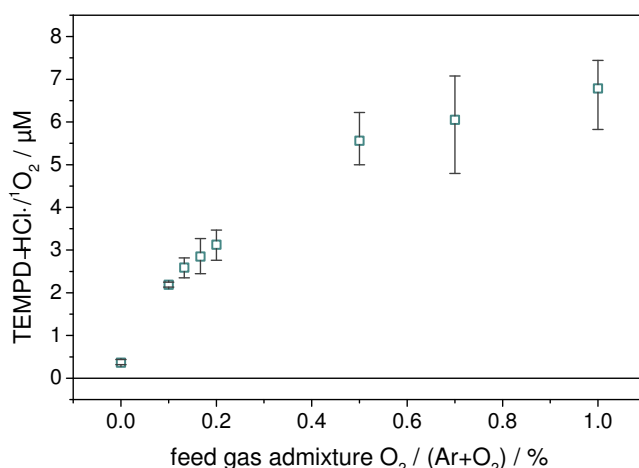


Figure 4.32: Spin adduct of singlet oxygen as a function of the oxygen content in argon with nitrogen as curtain gases.

trapped singlet oxygen measured by EPR is different. In the case of zero percent oxygen in the curtain, the resulting spin trap adduct concentration is slightly higher for synthetic air compared to pure nitrogen curtain. This effect occurs due to the presence of surrounding oxygen as it is the case for synthetic air curtain. The oxygen in the curtain gas can interact with the plasma plume. The pure nitrogen curtain prohibits the diffusion of ambient oxygen into the plasma plume as described in references [21, 170]. Hence, the formed singlet oxygen in the gaseous phase in the case of nitrogen environment can only be explained by impurities in the used gases. The presence of oxygen for the case of synthetic air in the curtain gas results in a slightly higher trapped singlet oxygen concentration in the case of no feed gas admixtures. For oxygen concentrations in the feed gas higher than only the impurity level, this effect becomes negligible. Moreover, the presence of oxygen in synthetic air inhibits or even destroys singlet oxygen for example by the formation of ozone. The synthetic air curtain yields an amount of aqueous singlet oxygen which seems to reach saturation around $2\text{ }\mu\text{M}$ of singlet oxygen trapped by TEMPD-HCl, whereas for the case of a nitrogen curtain gas the singlet oxygen concentration increase is only slowed down.

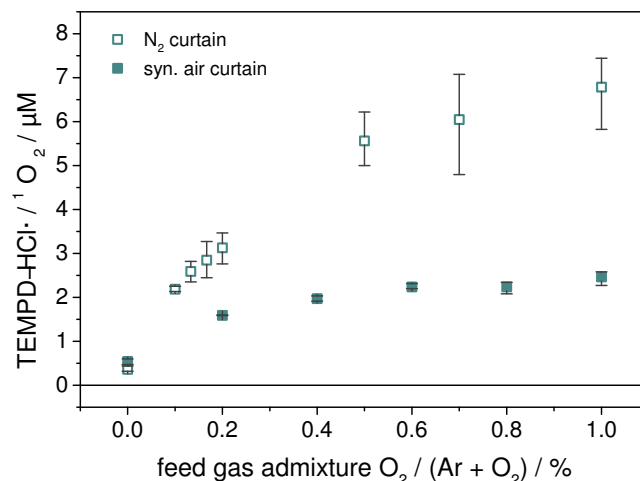


Figure 4.33: Spin adduct of singlet oxygen as a function of the molecular oxygen content in argon with different curtain gases.

To check a correlation of the oxygen feed gas admixture with other reactive oxygen species, the concentration of hydrogen peroxide (see figure 4.34) and of oxygen radicals (see figure 4.35) as a function of oxygen in argon is investigated for curtain gas with and without molecular oxygen. Both curtain gas compositions do not affect the formation of these reactive oxygen species. In figure 4.34, it is shown that for nitrogen and for synthetic air curtain gas as well, the gained radical concentrations do not differ. Furthermore, the measured concentrations decrease by increasing oxygen content in the feed gas and, therefore, show an opposite behavior from that of singlet oxygen. The trend for the oxygen radicals and hydrogen peroxide is similar so that a strong link between these species is further verified for the present conditions of increasing oxygen concentration in the feed gas. Here, the hydrogen peroxide formation seems to be hindered due to the presence of O₂ in the feed gas, as shown above in section 4.3.1 the generation of H₂O₂ depends much stronger on the feed gas humidity. Additionally, the development of the oxygen radical spin trap adduct concentration in the case of oxygen admixture into the feed gas shows the same behavior as hydrogen peroxide: besides the first points - up to 0.2% O₂ admixture - the increase of oxygen concentration in the feed gas does not affect the resulting reactive oxygen concentration. The highest concentrations are observed for both species for the pure argon feed gas. Since the molecular oxygen in the feed gas quenches the VUV radiation, which is assumed to contribute to the formation of the oxygen radicals, a presence of oxygen up to 0.2% in the feed gas still enables the VUV caused production, whereas higher amounts hinder this oxygen radical generation pathway. As the oxygen radicals are the precursors of hydrogen peroxide, if not dissolved from the gas phase, its generation is also partially blocked due to the molecular oxygen in the feed gas. Therefore, aqueous hydroxyl and superoxide anion radicals are assumed to be almost independent of the feed gas manipulation (see section 4.3.1 figure 4.27).

For singlet oxygen, a formation directly in the liquid phase is also possible. The generation mechanisms mostly require superoxide anion radicals (equations 4.37 to 4.41) or reactions with hypochlorite (equations 4.42 to 4.45). The simplest production of singlet oxygen is from superoxide anion radical releasing an electron (eq. 4.37 [231]). The reactions of superoxide anion radicals with hydroxyl radicals (eq. 4.38 [232]) or hydrogen peroxide (eq. 4.39 [233]) will also generate singlet oxygen. In the case of reaction 4.40 both super-

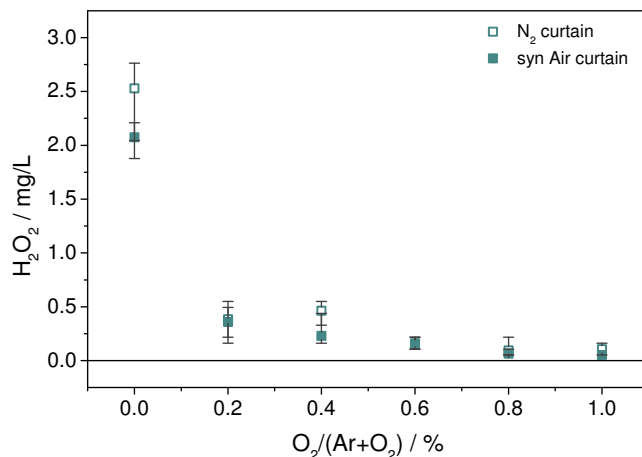


Figure 4.34: Hydrogen peroxide as a function of oxygen admixture into the feed gas and two different curtain gases.

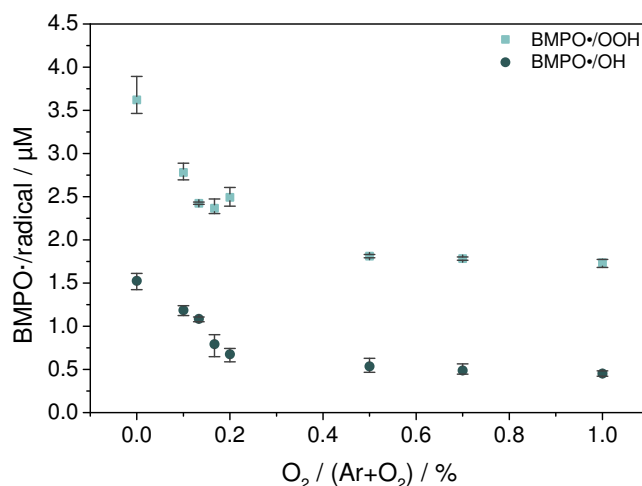


Figure 4.35: BMPO adducts of hydroxyl and superoxide anion radicals as a function of the oxygen content in the feed gas. The used curtain gas is molecular nitrogen.

oxide anion radicals and hydroperoxyl radicals need to be present. This situation occurs if the pH is close to their pK_a value of 4.8. This so-called spontaneous dismutation reaction of superoxide anion has a reaction rate of $9.7 \cdot 10^7 M^{-1}s^{-1}$ at pH 4.8; for pH 6.8 this rate slows down to only 10^{-4} part of it [233]. Since the pH in the study presented here is independent of the oxygen admixture in the feed gas for treatment of DPBS (see figure 4.36) and with 7.5 much higher than the pK_a almost no hydroperoxyl radicals should exist in the solution and, therefore, reactions 4.40 and 4.41 cannot occur. Reactions 4.37 to 4.39 are possible but only in the context of the trapped radical concentrations and trends as well as the hydrogen peroxide concentration. They seem to play only a subordinated role in the aqueous singlet oxygen origination.

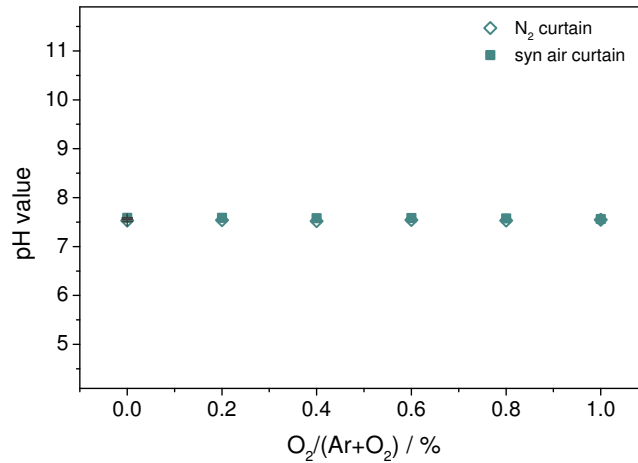
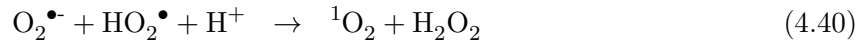
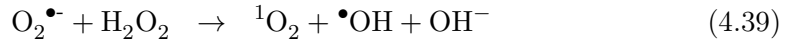
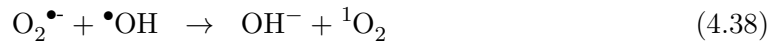
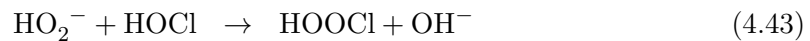


Figure 4.36: The pH value as a function of the oxygen content in the feed gas for a pure nitrogen and a synthetic air curtain gas. A volume of 5 mL DPBS is treated for 180 s.

The other possibility of singlet oxygen formed only in the liquid is by reaction of hypochlorite with hydrogen peroxide (eq. 4.42); it will form hypochlorous acid and subsequently singlet oxygen (equations 4.43 to 4.45). Since no indication of hypochlorite was previously found in the plasma treated DPBS by kinpen09, this formation pathway is assumed to be negligible.



Hence, the origin of aqueous singlet oxygen is assumed to be dominated by a solvation process. For verification, in future, gas phase measurements of singlet oxygen need to be performed and compared to the measured liquid concentration.

4.3.3 Plasma jet VUV radiation

Although vacuum ultraviolet radiation is quenched by oxygen in an air environment, due to the argon feed gas the VUV radiation can reach and interact with the liquid surface. With respect to therapeutic usage of the plasma jet the investigations regarding VUV radiation gains in relevance since VUV is highly energetic and may also transport this energy onto the treated area. As most of the areas such as wounds are normally covered with a thin film of liquid, the study is designed to elucidate whether VUV generates reactive species during plasma treatment and in which amounts it does so. Furthermore, it is studied, whether the so formed reactive species in the aqueous phase will affect the biological tissue beneath the liquid layer as the sketch in figure 4.37 shows.

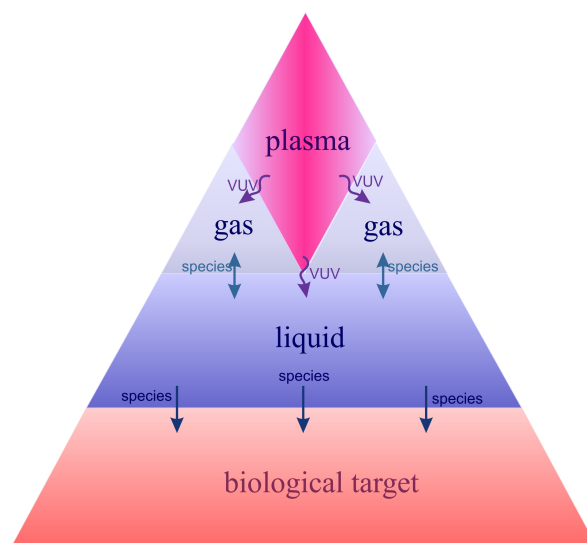


Figure 4.37: Sketch of the plasma jet VUV radiation and its possible impact on a biological target.

4.3.3.1 Gas phase

In figure 4.38 on axis optical emission spectra of the investigated kinpen09 are depicted. The large graph shows the spectrum between 105 to 219 nm, the VUV range, and the inset shows the ultraviolet to near infrared range from 200 up to 850 nm. In the inset, emitted peaks in the UV range are determined, namely the hydroxyl radicals, around 308 nm and the second positive system of molecular nitrogen between 337 and 380 nm. The visible range is mostly free of emission lines whereas the near infrared region of the spectrum is dominated by argon peak. Furthermore, small atomic lines at 777 nm and 844 nm of oxygen are also observed.

The VUV spectrum, shown in the large graph in figure 4.38, is dominated by the second argon excimer continuum around 126 nm. In this continuum lines of atomic oxygen and ozone can also be found [8]. Additionally, atomic hydrogen lines are observed in the VUV spectral range. In figure 4.39 the same spectral range is shown but with different curtain gas compositions, measured at 9 mm distance to the nozzle, which is the working distance for the liquid treatments. The curtain composition's impact on the spectra results in a decrease of the intensities. In the case of 20% oxygen and 80% nitrogen in the curtain gas

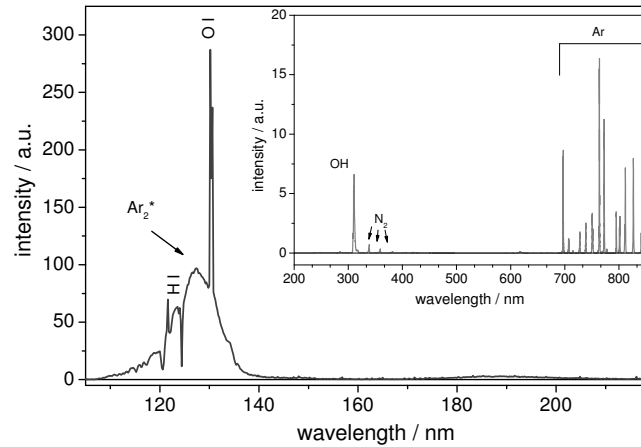


Figure 4.38: On axis VUV spectrum and UV/VIS (inset figure) of the kinpen09 (Reprinted with permission from [63]. ©2015, AIP Publishing LLC.).

the spectrum looks quite similar to the one without curtain, shown in figure 4.38. The pure nitrogen yields a broader continuum without affecting the atomic oxygen peak. For all higher oxygen contents in the curtain the intensity decreases up to the minimum detected for the pure oxygen case. This is expected since oxygen quenches the VUV radiation.

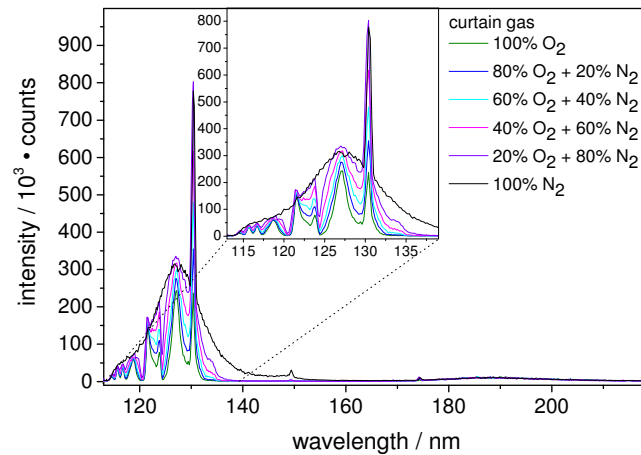


Figure 4.39: The VUV spectrum, measured with an Acton VM 502 monochromator with a slit width of $100\ \mu\text{m}$ and with an integration time of $5\ \text{ms}$, of the kinpen09 with curtain gas variation at the working distance of $9\ \text{mm}$.

From these measurements it can be stated that the VUV radiation of the kinpen09 needs to be considered for plasma-liquid interactions and as a source for reactive species in the liquid phase. Therefore, the absorption of a $400\ \mu\text{m}$ thick water layer and the VUV spectrum of the kinpen09 is compared as depicted in figure 4.40. In this graph the detected VUV radiation and the absorption dependent on the wavelength of the water layer is shown. The cutoff wavelength, which is defined here as the wavelength where the absorption is decreased to 50% of the VUV absorption by water, is slightly above $180\ \text{nm}$. Below $180\ \text{nm}$

the VUV radiation is almost completely absorbed by water. Since the emitted radiation of the kinpen09 in the VUV is within a range between 105 to 145 nm, it is clearly below this wavelength, hence, this radiation will be completely absorbed. The gas phase spectral measurements were performed by Dr. R. Bussiahn, Dr. H. Lange, P. Holtz and A. Monden.

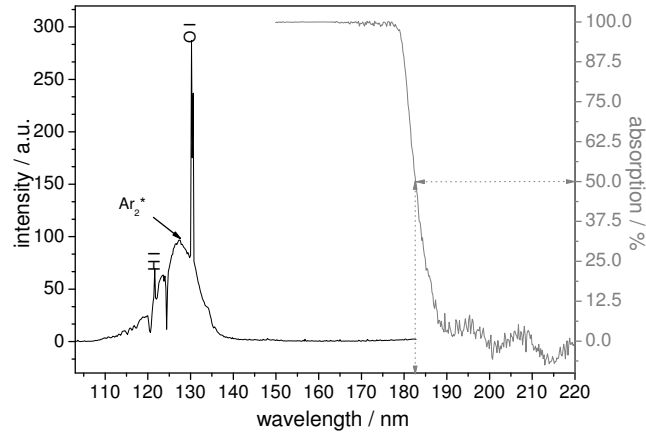


Figure 4.40: VUV spectrum of kinpen09 compared with the VUV absorption of a 400 μm thick water film (Reprinted with permission from [63]. ©2015, AIP Publishing LLC.).

4.3.3.2 Liquid phase

As it was shown in section 4.2.3, the liquid itself is not negligible in the formation or inhibition of reactive species generation. Hence, in the case of plasma jet generated VUV radiation, the impact has also been studied in different biologically relevant liquids. For simplification purposes, water is used as a least complex relevant liquid but simple buffered solutions up to the complex cell culture media are also investigated.

Table 4.4: Ingredients of the investigated liquids for VUV radiation's impact sorted by complexity (Reprinted with permission from [63]. ©2015, AIP Publishing LLC.).

liquid	in-organic salts	buffer	glucose	amino acids	vitamins	HEPES	Fe, Cu, ...	glutathione
water	-	-	-	-	-	-	-	-
SPB	+	+	-	-	-	-	-	-
DPBS	+	+	-	-	-	-	-	-
HBSS	+	+	-	-	-	-	-	-
IMDM	+	+	+	+	+	+	-	-
Epilife	+	+	+	+	+	+	+	-
RPMI	+	+	+	+	+	-	+	+

Absorption behavior of liquids

Starting with the absorption behavior of the different liquids, in figure 4.41a absorption trends of the solutions are plotted. All investigated liquids follow similar trends with differences in the slope and in the cutoff wavelength. A more detailed view and better comparability of the cutoff wavelength for the liquids is given by figure 4.41b for different film thicknesses of $100\ \mu\text{m}$, $200\ \mu\text{m}$, and $400\ \mu\text{m}$. Water, as the least complex solution (see table 4.4), has the lowest cutoff wavelength; the slightly more complex buffered solutions - Sørensen's phosphate buffer (SPB) and Hank's balanced salt solution (HBSS) - also have a cutoff wavelength below $200\ \text{nm}$. Only the three cell culture media absorb 50% and more for a wavelength higher than $200\ \text{nm}$. Hence, all investigated solutions will completely absorb the VUV radiation emitted by the kinpen09. Accordingly, the possibility that the kinpen09-caused VUV radiation will reach a biological cell is vanishingly low.

VUV-caused reactive oxygen formation in liquids

Although the VUV radiation is not expected to reach the cells directly, there is still the possibility of an impact mediated through the liquid. Therefore, the concentration of aqueous reactive oxygen species in water, HBSS and RPMI 1640, is investigated. These measurements are always comparative studies between the complete plasma jet, including all its active components and its VUV radiation separately.

In figure 4.42 the hydrogen peroxide concentration multiplied by the treated volume resulting from either treatment of the complete plasma jet with all its active components, or treatment by only its VUV radiation is shown. The multiplication by the volume enables comparability since the complete plasma jet treatment takes place in a Petri dish ($60\ \text{mm}$ in diameter) with $5\ \text{mL}$ liquid volume, whereas the VUV treatment takes place in the micro chamber with $80\ \mu\text{L}$ liquid volume. Due to handling reasons the use of

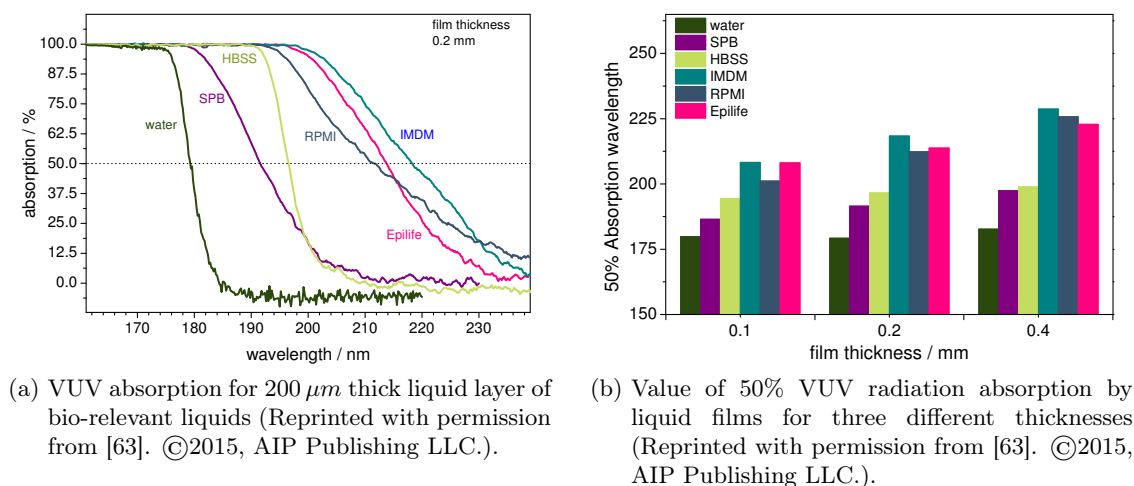


Figure 4.41: Absorption behavior of different biologically relevant solutions.

this micro chamber is necessary for the VUV treatment. The measured data is corrected by the window transmission for the wavelength of 127 nm , which is 57%. The quantum efficiency of photo dissociation of water is assumed to be one. The trend for both graphs is similar but the VUV generated one (marked with light gray squares) reaches a kind of plateau, whereas the complete jet treatment (marked with dark gray dots) leads to an increase in concentration by increasing treatment time. The amount formed due to the complete plasma jet treatment is remarkably higher than the amount due to the VUV radiation treatment only. This behavior is expected since the complete plasma treatment also includes additional plasma components like electrons or metastables [234] or gas phase formation pathways such as solvation of gaseous hydrogen peroxide due to Henry's law [61, 71] (see section 4.3.1).

The formation of the plateau in the case of the VUV treated ultrapure water is caused by a consumption of the precursors of hydrogen peroxide which can only be formed in the water. Therefore, the most likely precursors are hydroxyl radicals and superoxide anion radicals or hydroperoxyl radicals, respectively. From figure 4.42 one can learn that VUV radiation reaches the liquid and also generates reactive oxygen species in the solution, but compared to the complete jet treatment this amount is negligible, no matter if the treatment time is as short as 20 s or moderately long with 360 s.

As mentioned previously, the hydrogen peroxide in the solution formed due to VUV radiation treatment of the plasma jet originated from the oxygen radicals. Therefore, by the use of electron paramagnetic resonance spectroscopy enhanced by spin trapping technique, these two radicals are measured again either for a complete plasma jet treatment or for VUV treatment only. A further plasma jet component, the UV radiation, is implemented in the test to verify that the dissociation of water is caused by the VUV radiation ($100 - 280\text{ nm}$) and not by the UV radiation ($280 - 380\text{ nm}$). This is implemented by replacing the MgF_2 window by a quartz glass, which is transparent only for the UV radiation whereas the magnesium fluoride window transmits both. The energy of ultraviolet radiation is not high enough to cleave the bonds in a water molecule, therefore, UV is not expected to contribute to an oxygen radical generation in the liquids. In table 4.5 the bond dissociation energies of some biologically relevant molecules are listed. According to this data, the UV radiation

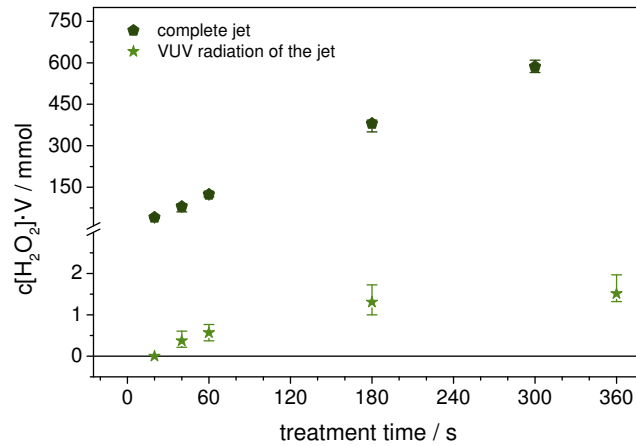


Figure 4.42: Hydrogen peroxide concentration formed by treatment with the complete plasma jet or only by its VUV radiation in ultrapure water as a function of the treatment time (Reprinted with permission from [63]. ©2015, AIP Publishing LLC.). Used volumes are 5 mL for complete plasma jet, and 80 μ L for VUV radiation of the jet, respectively.

is able to break the hydrogen peroxide molecule into hydroperoxyl and hydrogen, but is not able to split water into hydroxyl radicals and hydrogen.

Table 4.5: Bond dissociation energies of biological relevant molecules with the corresponding wavelength (Reprinted with permission from [63]. ©2015, AIP Publishing LLC.).

	bond dissociation energy		wavelength
	$kJ \cdot mol^{-1}$	eV	nm
$HO_2 \rightarrow H + O_2$	197.0 [217]	2.04	607.8
$NH \rightarrow N + H$	356.0 [217]	3.69	336.0
$H_2O_2 \rightarrow HO_2 + H$	374.5 [217]	3.88	319.5
$OH \rightarrow O + H$	428.0 [217]	4.44	279.2
$H_2 \rightarrow 2H$	435.9 [217]	4.52	274.3
$O_2 \rightarrow 2O$	498.3 [217]	5.16	240.3
$H_2O \rightarrow OH + H$	498.7 [217]	5.17	239.8
$CO_2 \rightarrow CO + O$	532.2 [217]	5.52	224.6
$NO \rightarrow N + O$	631.6 [235]	6.55	189.3
$N_2 \rightarrow 2N$	945.4 [217]	9.80	126.5
$CO \rightarrow C + O$	1076.5 [217]	11.16	111.1

In figure 4.43 the concentration of the DMPO trapped oxygen radicals multiplied by the treated volume is depicted for all three investigated plasma jet parts as a function of the treatment time. The DMPO•/OH+OOH adducts trends for complete plasma jet (marked with dark green pentagons) and VUV radiation treatment (marked with green stars) have a similar behavior as observed for hydrogen peroxide. As described for hydrogen peroxide also for the radical adducts the values are corrected by the transmission of the magnesium fluoride window. The complete plasma jet leads to the formation of clearly higher amounts

than the VUV radiation separately. In the case of VUV radiation again a saturation effect is formed for longer treatment times so that the resulting amount for 180 s treatment is not different from that of 300 s. This is an indication that the origins of these oxygen radicals are not available anymore so that all water molecules which could be dissociated by the plasma jet VUV radiation are consumed. Due to the experimental setup no gas flux caused vortexing of the liquid occurs. Hence, all water molecules on the surface will be dissociated after a certain time and only the formed hydrogen peroxides can be cleaved into hydroxyl radicals, which will then almost immediately recombine again to H_2O_2 . Although a diffusion due to the difference in the concentration will take place, the dominating role for this missing increase in concentration from 180 s to 300 s is expected to be the consumption of the dissociable water molecules. Consequently, a saturation of the concentration can be observed. The VUV radiation contributes in the formation of oxygen radicals in ultrapure water by complete plasma treatment in a considerable but not dominating manner.

The UV radiation treatment alone (marked with light green triangles) is realized by replacing the MgF_2 window by a quartz glass window. There, as expected, no radical formation can be detected, meaning that UV radiation is not involved in plasma caused hydroxyl and superoxide anion radical generation. With a spectral range of 280 to 380 nm the available energy of UV radiation is in the range of 4.42 eV to 3.26 eV. An H–O–H molecule can be cleaved into O–H and H by energies of $498.7 \text{ kJ} \cdot \text{mol}^{-1}$ (equal to 5.17 eV or 239.8 nm, respectively) or higher. A further dissociation of the O–H bond into O and H will need additional 4.44 eV. Therefore, UV cannot provide the required energy for splitting the bonds into water molecules. The detected Ar_2^* in the VUV spectrum of the kinpen09 instead provides with 126 nm (corresponds to 9.84 eV) more than the necessary energy for a cleavage of two O–H bonds.

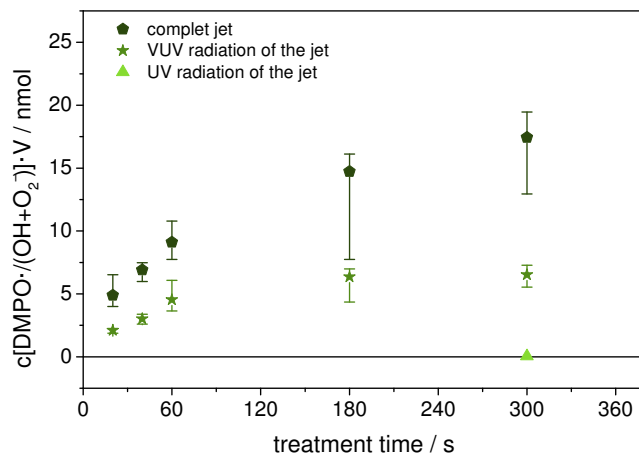


Figure 4.43: Spin trap radical adduct generated either by the complete plasma jet, by its VUV and UV radiation, or by its UV radiation (Reprinted with permission from [63]. ©2015, AIP Publishing LLC.). UPW, containing 100 mM DMPO, is treated for different times in volumes of 5 mL, complete plasma jet, or 80 μL , radiation of the jet, respectively.

By comparison of the values measured for hydrogen peroxide (figure 4.42) and the determined radical adduct amounts (figure 4.43) after VUV treatment of the kinpen09 a clear disagreement is observed. Since the H_2O_2 formation by VUV radiation should be more or

4 Results and discussion

less only caused by the recombination of hydroxyl radicals or by the reaction of superoxide anion radicals, the expected ratio between oxygen radicals, especially $\bullet\text{OH}$, and hydrogen peroxide, is a factor of two because of the reaction 4.10. The discrepancy of the hydrogen peroxide amount and trapped oxygen radicals is contrary in the case of 180 s treatment, approximately $1.5 \text{ mmol H}_2\text{O}_2$ are formed under the same condition where only about 7 nmol oxygen radicals are trapped.

A possible explanation for the difference, which is not only explainable by the efficacy of the hydroxyl radical trapping by DMPO, is the presence of other non-radical oxygen species - not detectable species by EPR spectroscopy - formed by VUV treatment with the plasma jet. The dissociation of water into molecular hydrogen and oxygen (see equation 4.46) can be possible reaction. This reaction in combination with reaction 4.47 is known to be the main pathway for the commercial generation of hydrogen peroxide. It is called anthraquinone process since 2-alkyl-anthraquinone is the catalyst used in the commercial production [123].



As in the reaction 4.46 the cleavage of two water molecules is required; the energy for this part of the reaction chain 5.01 eV is needed [236]. The second part, reaction 4.47, consumes additional 3.76 eV . Hence, the provided energy of the VUV radiation is sufficient for the reaction. Although from an energetic point of view, the reaction could be possible, the branching ratio of possible photo dissociation pathways are unfavorable: cross sections for photo dissociation of water into molecular hydrogen and molecular oxygen are more than one order of magnitude lower than that of water dissociation into $\bullet\text{OH}$ and H [237]. Therefore, the photo dissociation reaction resulting in radical generation can be assumed to be much higher. A further more likely explanation between the measurements of the photo-generated radicals versus the photo-generated hydrogen peroxide is that VUV radiation has a limited penetration depth, which in water is extremely low. By applying the Beer-Lambert law and the absorption coefficient of Ar_2^* emission (126 nm) in water, 10^4 cm^{-1} , the intensity of the radiation is drastically decreased to 1% after $4.6 \mu\text{m}$ depth in water for further $4.6 \mu\text{m}$, so after $9.2 \mu\text{m}$ only 0.01% intensity remains. For $30 \mu\text{m}$ depth the intensity is only 10^{-11} part of the original one. This implies that most hydroxyl radicals will be produced directly at the liquid surface. If, in addition, the fact that the solution is not stirred during VUV radiation treatment - in contrast to complete jet treatment where the gas flow is mixing the solution, and the treatment takes place only spot-like - is considered, a reduced volume element for the treatment can be assumed. So in the case of a volume element radius r of 1 mm , which corresponds approximately with the radius of the visible plasma plume of the kinpen09, and a height h of 2 mm - according to the penetration depth - is presumed, with $[\pi \cdot r^2 \cdot h] = V$ that the effectively treated volume V is only $7.8 \cdot 10^{-8}$ part of the original $80 \mu\text{L}$. This affects both the oxygen radical as well as the hydrogen peroxide formation therefore the measured values need to be corrected by this factor to give the value of the formed amount in the volume element. According to the formation of hydrogen peroxide by the recombination of two hydroxyl radicals, the necessary $\bullet\text{OH}$ concentration can be determined by the multiplication of the hydrogen peroxide amount by the factor of two. Hence, the estimated amount of particles is 1.56 mol , locally generated in this volume element. The applied concentration of the spin trap in the element is with the used concentration of 100 mM DMPO 0.6 pmol . Consequently, this is much too low to trap

all generated hydroxyl radicals, especially before they recombine with each other since their recombination reaction rate is almost diffusion controlled [210]. Only the relative trend results are gained from the measurements where both hydrogen peroxide measurements and oxygen radical measurements are in accordance.

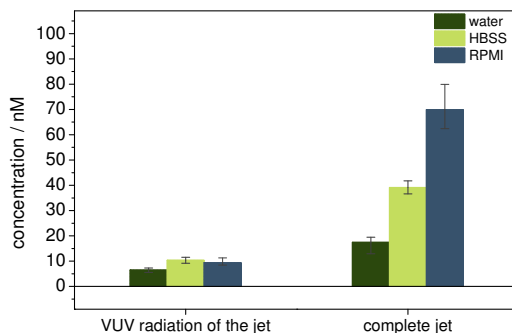


Figure 4.44: Spin trap radical adduct in three different relevant solutions produced by only the plasma jet VUV radiation or by the complete plasma jet (Reprinted with permission from [63]. ©2015, AIP Publishing LLC.). The solutions, containing 100 mM DMPO, are treated for 180 s in volumes of 5 mL, complete plasma jet, or 80 μ L, VUV radiation of the jet, respectively.

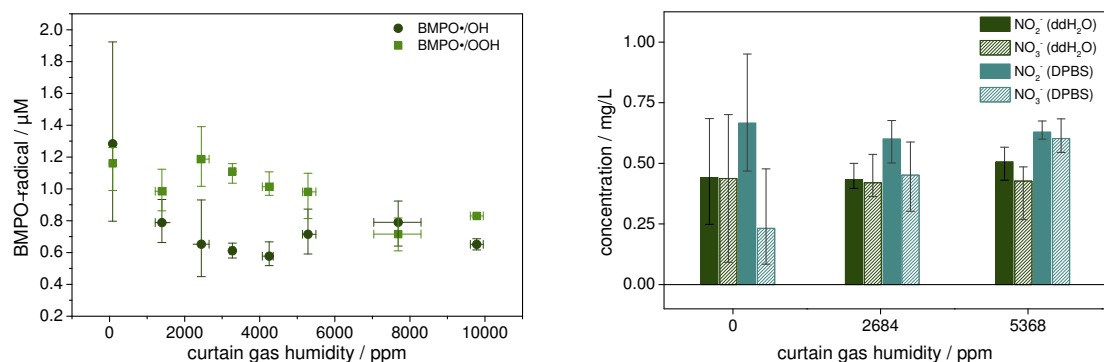
Since it was found that the liquid ingredients play a non negligible role for the resulting reactive species after plasma treatment, different solutions are also investigated regarding the impact of the VUV radiation onto the formation on reactive oxygen species. Ultrapure water, Hank's balanced salt solution and RPMI 1640 are treated for 180 s by the complete plasma jet or just by its VUV radiation. Afterwards the produced amount of DMPO radical adducts with hydroxyl and superoxide anion radicals is observed by EPR spectroscopy as depicted in figure 4.44.

The concentrations caused by only VUV radiation are quite similar in all three solutions despite their different complexities (see table 4.4). Therefore, it can be deduced that the ingredients do not influence the oxygen radical formation only by VUV radiation. This leads to the assumption that the oxygen radicals mainly originate from the photo dissociation of water for all cases. In the case of complete plasma jet treatment, the situation is different as mentioned in section 4.2.3. This recombination reaction by far dominates the spin trap adduct formation in the volume element. According to the literature [238] a DMPO concentration of at least 10 mM is needed to inhibit hydrogen peroxide production to 43% of the case without spin trap. As mentioned above the hydroxyl radical reacts with DMPO but also with each other in a diffusion controlled manner (see section 4.1.2). Theoretically, the concentration of the spin trap has to be increased. Unfortunately, this can not be realized in praxis since the solubility of DMPO in water is too low. Although the determined absolute numbers of the plasma jet VUV radiation formed oxygen radicals are lower than indeed present in the liquid, however the trends of the radicals and hydrogen peroxide are similar. The requirement of further investigations is obvious. In the case of verification of the second assumption, the experimental setup needs to be improved by, for instance, a more homogeneous treatment or an increase in the spin trap concentration or a change in spin trap with an enhance reaction rate, which can overcome the competition with the recombination reaction.

4.3.4 Ion transport from the gas phase

The possibility of a transport of reactive species, especially ions, from the gas phase into the liquid can be connected to plasma generated water clusters. Water clusters are molecular complexes consisting of water molecules. These clusters can surround a reactive ions formed in the gaseous phase and, therefore, enhance its lifetime. With increasing humidity the density of ions is then expected to increase as well. To investigate this, the gas in the curtain device is humidified in order to increase the formation of water clusters. In the gas phase, first indications of the presence of these water clusters were found as described in reference [239]. In the liquid, the concentration of oxygen radicals (see figure 4.45a) and the formed amounts of nitrate and nitrite are determined (figure 4.45b).

In figure 4.45a the resulting BMPO adducts of hydroxyl (marked with filled dots) and superoxide anion radicals (marked with filled squares) are depicted. The radicals have a completely opposite trend from the expected one if water clusters are a relevant source of oxygen radicals in solution. Therefore, it can be stated that, at least for hydroxyl and superoxide anion radicals, water clusters do not contribute remarkably to their plasma-caused liquid concentration.



(a) Spin trap adduct of BMPO with oxygen radicals as a function of the curtain gas humidity. Detected after 180 s plasma treatment in ultrapure water.

(b) Nitrate and nitrite concentrations as a function of the curtain gas humidity in ultrapure water and DPBS.

Figure 4.45: Reactive species formed as a function of the curtain gas humidity.

For nitrate and nitrite in ultrapure water there is no dependence on the clearly observable curtain gas humidity concentration (see 4.45b). The only species investigated which concentration seems to be increasing by humidification of the curtain gas is nitrate in DPBS (shaded cyan colored bars). This could be an indication of a reactive species transport by water clusters from the gas phase into the liquid phase. Although the increase of nitrate with increasing curtain humidity can be caused by an increase in hydrogen peroxide in the presence of nitrite, and therefore, the peroxynitrite reaction chain could be triggered yielding higher concentrations of nitrate [58]. However, in the study in reference [240] water clusters are addressed as dominating species only for the case of about 1% water content in the boundary region of the plasma-liquid interaction, which is the region directly above the liquid interface. In the case of higher water content they assumed the plasma to behave like, in their case, helium water plasma. The present results give first indications on the potential impact of ions and water clusters for the reactive species formation and transport in plasma-liquid-systems.

4.4 Impact on biological targets

It is shown that plasma treatment generates highly reactive species in biologically relevant solutions. The effect of these species on biological targets as well as their formation pathways are of relevance for the therapeutic applications of plasma jets in medicine. Therefore, investigations and estimations of this impact are performed in this work.

4.4.1 Curtain gas impact - eukaryotes versus prokaryotes

In figure 4.46 the interaction of the plasma with the gas phase and with the liquid phase as well as the follow-up interaction of the resulting species with the biological target beneath the liquid is sketched. As the prior results have shown, the gaseous phase determines the liquid reaction, and therefore, also affects the follow-up reactions with the biological target as, for instance wound tissue. In the following, biological responses to the changes in the curtain gas composition are investigated.

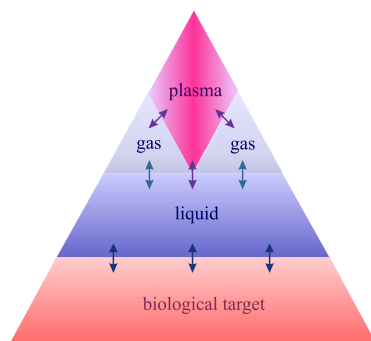


Figure 4.46: Scheme of the plasma-liquid interaction in the presence of a biological target.

In the presented work the biological impact of the atmosphere surrounding the plasma plume is evaluated in two studies, the first study is focused on the effect of reactive species generated by plasma treatment for different curtain gas compositions on human skin cells. This study is published in reference [21] where besides the gas and the liquid phase analysis a viability test on eukaryotes (human keratinocytes, HaCaT cell line) is presented. These cell experiments have been performed by Dr. K. Wende. In a second publication [22] prokaryotic response in the form of bacteria inactivation is correlated with the generated liquid chemistry as a function of the curtain gas composition. For the microbial tests *Escherichia coli* (*E.coli* K12 NCTC 10538) in sodium chloride solution is investigated. The bacteria test have been performed by M. Rostalski (née Hänsch).

In the skin cell experiments a pure oxygen gas curtain results in the lowest viability of the treated cells. This means it is the conditions which are blamed the most for harming the keratinocytes, whereas the closest to regular air composition of 20% oxygen and 80% nitrogen influences the viability least (see figure 4.47a). Looking on the inactivation curves of the bacteria tests in comparison for the different gas ratios in the curtain, the behavior of these two conditions is inverse (see figure 4.47b). The air-like composition leads to the strongest bacteria inactivation of the tested compositions, whereas the pure gas cases, no matter if 100% oxygen or 100% nitrogen, do not influence the bacterial cells in any way. Comparing both biological tests it can be stated that the same curtain gas composition leads to an opposite behavior of eukaryotic and prokaryotic cells. This means that one parameter set is able to inactivate bacteria on the one hand whereas it does not harm the

4 Results and discussion

human skin cells.

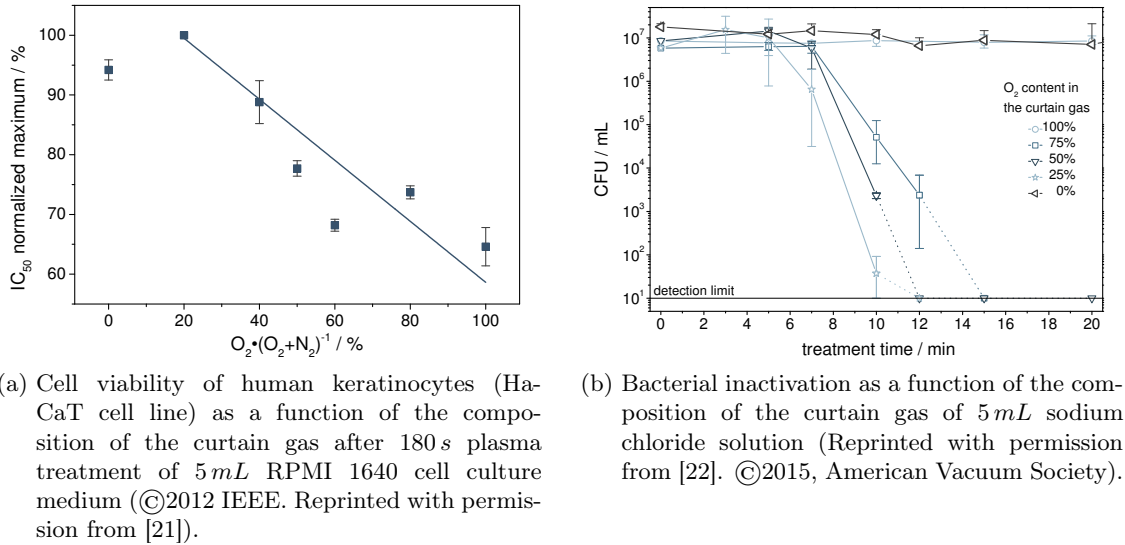


Figure 4.47: Biological experiments on the impact of curtain gas composition on eukaryotic and prokaryotic cell viability.

Upon consideration of the nitrite concentrations (see figure 4.48) formed in both investigated liquids for the investigated treatment times it became obvious that the trend is the same for both NaCl (marked with light blue colored bars) and RPMI 1640 (marked with dark blue colored bars) - only the absolute concentration differs due to the different treatment times used for the respective treatments. As already found for DPBS in section 4.2.1.2 (see figure 4.16) and also for RPMI 1640 and NaCl the lowest concentrations are also determined for the pure oxygen gas curtain and the highest value is observed in the case close-to air, 25% oxygen and 75% nitrogen in the curtain gas. For the eukaryotes the nitrogen species seem not to be harmful, the viability of the HaCaTs is maximum for these conditions, whereas prokaryotic cells are the fastest inactivated in this case. As known from references [32, 51], for a dielectric barrier discharge nitrate and nitrite, as representative nitrogen oxide species are, therefore, considered to be important for the acidification due to plasma treatment. This lowering in pH is essential for the strong antimicrobial activity.

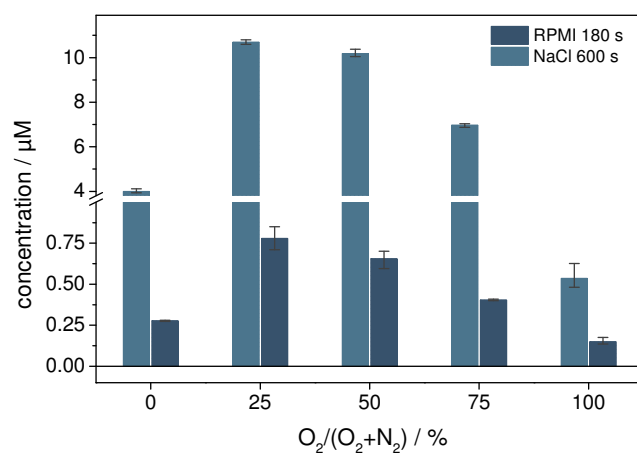


Figure 4.48: Nitrite concentration as a function of the curtain gas composition after plasma treatment of 5 mL solution (adapted from [21] and [22]).

4.4.2 Impact of plasma jet VUV radiation on cell suspension

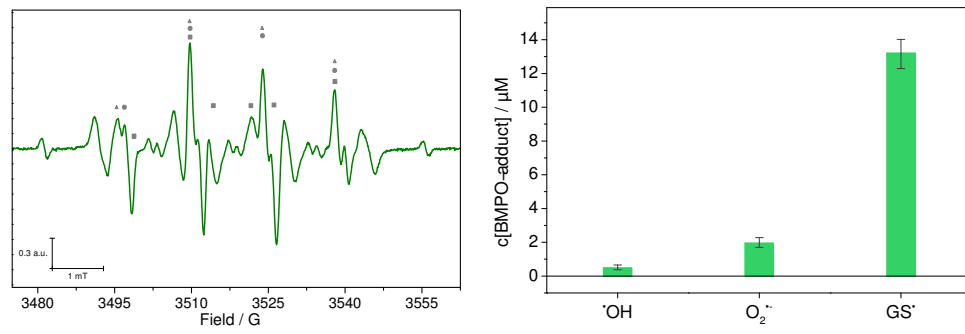
Atmospheric plasma jet applications in medicine requires the study of possible side effects. One of the plasma components which could be responsible for these undesirable effects is the (vacuum) ultraviolet ((V)UV) radiation. As shown in section 4.3.3.2, the VUV radiation can reach the target when the plasma jet operates with noble gases such as argon. The expected absorption in ambient air is suppressed as the radiation is guided through the feed gas largely devoid of air. As mentioned in section 4.3.3.2, the liquid layer thickness drastically influences the penetration depth of the VUV radiation. A thicker layer leads to an extremely fast decrease of the remaining VUV radiation according to the Beer-Lambert law. Most wounds are inherently covered with a thin liquid film (ichor or blood) and therefore the direct interaction of VUV radiation with the cells is highly improbable. A liquid layer at least $25\ \mu\text{m}$ thick is sufficient to protect the cells from the VUV radiation of the plasma jet. Additionally, a risk estimation of plasma jet generated VUV radiation certified as a medical product, the kinpen09 MED, leads to merely 1/30 of the maximum acceptable daily dose [241]. By the combination of the results of the plasma jet VUV radiation study the risk of the produced VUV radiation of this plasma jet regarding its therapeutic application in plasma medicine is almost negligible.

For the investigation of the VUV impact on biological cells a solution of $5 \cdot 10^6$ immune cells in $1\ \text{mL}$ cell culture medium is treated in the specially constructed micro chamber for the plasma jet VUV radiation treatment. The used cell line is a human monocyte cell line, namely the THP-1 cell line. These cells are immune cells involved in the immune response of the human body in case of wounds. These cells require a cell culture medium with the addition of 10% fetal calf serum (FCS) and in total 1% penicillin and streptomycin (PenStrep). In the present study DMEM as well as RPMI 1640 are used as cell culture media. These additional ingredients are also added for the experiments without cells to enable the comparison between solution and cell suspension. For all these measurements BMPO is used as spin trap with a final concentration of $100\ \text{mM}$ in $80\ \mu\text{L}$ solution.

If the THP-1 cell suspension in DMEM is treated by plasma jet's VUV radiation for $180\ \text{s}$ the measured EPR spectrum shows signals from at least three radicals which are identified by comparison with the literature [194]. These three radicals are the oxygen radicals hydroxyl and superoxide anion and the sulfur centered glutathione thiyl ($\bullet\text{SG}$) radical.

In figure 4.49a the related peaks are marked with dots for hydroxyl radicals, with squares for superoxide anion radicals and with triangles for glutathione thiyl radicals, respectively. More peaks appeared in the spectrum which can be simulated with a good agreement but for which an identification by the databases and literature is not possible, as only limited publications are available which analysis spectra of BMPO regarding radicals other than superoxide anion and hydroxyl radicals. In table 4.6 the determined parameters from the spectrum in figure 4.49a, like Landé-factor (g-factor) and hyperfine coupling of the detected radicals after plasma jet VUV radiation treatment are listed. The calculated concentrations for the identified radicals, $\bullet\text{OH}$, $\text{O}_2\bullet^-$ and $\bullet\text{SG}$ are shown in figure 4.49b. In the present study, indirect radical sources are investigated potentially originating from the cells. In order to clarify whether the radicals are formed in the liquid or secreted by the cells, cell culture media with the addition of serum and antibiotics are also treated with plasma jet VUV radiation without cells.

The measurement of only the cell culture medium and additives is compared with the one derived from the treated cell suspension. Figure 4.50a shows an overlay of both spectra in order to highlight the difference of DMEM with and without cells. In the measurements



(a) EPR spectrum after 180 s treatment with VUV radiation of DMEM by an argon atmospheric pressure plasma jet. The detected radicals are the hydroxyl radical, marked in the spectrum with dots, the superoxide anion radical, marked with squares, and the glutathione thiyl radical, marked with a triangles.

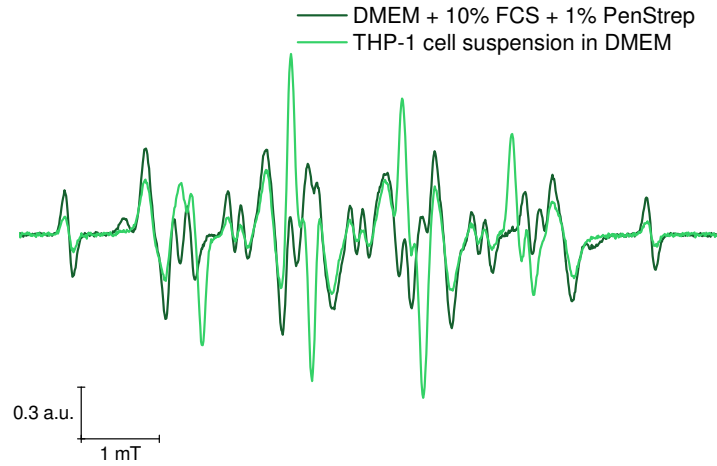
(b) Resulting concentrations of free radicals in VUV treated DMEM-THP-1 cell suspension.

Figure 4.49: Resulting radical adducts of plasma treated cell suspension.

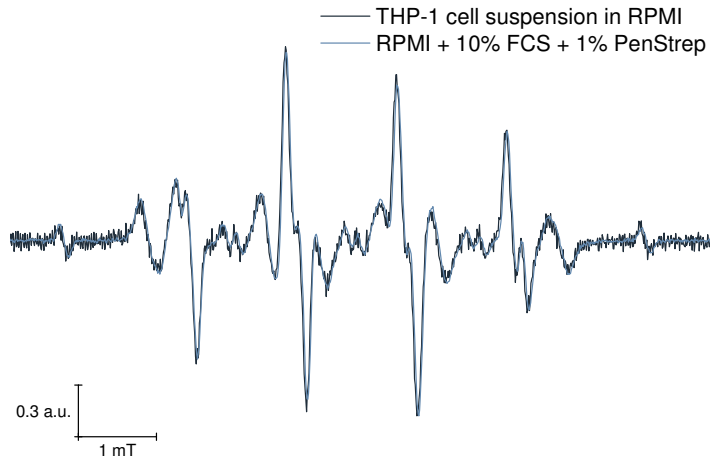
Table 4.6: Radical parameters determined by evaluation of measured EPR spectrum of VUV treated DMEM (see figure 4.49a).

	hydroxyl radical	superoxide anion radical	glutathione thiyl radical
g-factor	2.00577	2.0058	2.00577
a_N/mT	1.176	1.318	1.435
a_{H_1}/mT	1.622	1.425	1.428
a_{H_2}/mT			0.134

of only the cell culture medium with the additives, but without cells, only the peaks of the oxygen centered radicals and the unidentified peaks are observable. In the treated medium with the THP-1 cells shows an additional four peak pattern, which is related to the glutathione thiyl radical. In the spectrum of just cell culture medium all the other peaks also appeared so it can be concluded that the glutathione thiyl radical is a response of the cells to the plasma jet VUV radiation treatment. Usually, RPMI 1640 is used as cell culture medium for this cell line. Therefore, the experiments are also performed in RPMI 1640. This is shown in figure 4.50b, where the similarity of both spectra, with and without cells became obvious. The reason for this is that the glutathione thiyl radical is formed by glutathione, which is also an ingredient of the cell culture medium RPMI 1640 as well as the cells contain it. It is known from the literature that the secretion of $\bullet SG$ radicals can be understood as a response reaction of the cell to oxidative stress caused by oxygen radicals [242]. As shown above in section 4.3.3 the penetration depth of the VUV radiation for an aqueous liquid is limited, so that an direct interaction of the cells in suspension is improbable and the interaction is mediated by the liquid. These above investigations have shown that the reactive species produced at the surface of the liquid, e.g. due to VUV radiation of the plasma source, can reach biological targets below a liquid layer, either due to transport through the liquid or by secondary or tertiary reactions. Hence, the liquid layer is protecting the biological target against e.g. VUV radiation whereas the so generated reactive molecules can interact with the sensitive cells or tissue.



(a) EPR spectra of THP-1 cell suspension in DMEM (light green curve) and only DMEM cell culture medium (dark green curve) after 180 s treatment with VUV radiation of an argon atmospheric pressure plasma jet.



(b) EPR spectra of THP-1 cell suspension in RPMI 1640 (dark blue curve) and only RPMI cell culture medium (light blue curve) after 180 s treatment with VUV radiation of an argon atmospheric pressure plasma jet.

Figure 4.50: EPR spectra of THP-1 cell suspension in two different cell culture media.

5 Summary

The therapeutic application of atmospheric pressure plasmas almost always involves a liquid layer. This layer, which covers the biological tissue, interacts with the plasma. Therefore, these interactions are of drastic relevance for plasma application in medicine. Due to the interaction, chemical reactions are induced not only in the liquid but also in all connected phases which have an effect on the liquid chemistry. This already rather complex system will also have an impact on the mammalian cells or the biological target below. However, fundamental research on the impact of the physical plasma interacting with biologically relevant liquids in the field of plasma medicine have been highly required as only few investigations on the liquid chemistry in such complex systems existed prior to this work. In order to gain insight into the plasma-liquid interaction itself and also the chemical pathways from the plasma to the target, in this study, the focus was set on the highly reactive, short-lived species known to be important in biological systems. For the first time a widespread study on the influence of treatment conditions such as the gaseous surroundings and working gas impurities on liquid chemistry has been performed. Results verify the large and remarkable impact of plasma treatment situations on the ongoing chemistry. The gained knowledge from this work can be summarized as follows in relation to the defined goals:

- Impact of the atmospheric-pressure argon plasma jet on biologically relevant solutions was investigated by:
 - ▷ adaption and development of an experimental procedure for the application of EPR spectroscopy enhanced by spin trapping technique
 - ▷ evaluation of appropriate spin traps for the targeted species in plasma treated liquids
 - ▷ detection of oxygen free radicals in complex biologically relevant solutions
- Influence of surrounding conditions on the formation of liquid-phase reactive species and their tailoring for a desired liquid compositions was identified
 - ▷ tailoring the reactive species output due to controlled conditions was possible by:
 - the use of a curtain gas device, allowing to adjust the reactive species composition in liquids from an ROS to an RNS dominating composition; the following processes have been identified:
 - H_2O_2 concentration is only slightly reduced by addition of O_2 into the curtain gas, a further increase is not possible
 - species other than hydrogen peroxide can be increased in their concentration by a tailoring of the surroundings of the plasma plume
 - curtain gas variation around the plasma plume causes an upwards trend of the oxygen radicals

5 Summary

- a treatment condition was found that allows to inactivated bacteria and at the same time does not harm human skin cells
- molecular admixtures yield a controllable increase in stable species such as H_2O_2 , and highly reactive species, namely $^1\text{O}_2$, $\bullet\text{OH}$ and $\text{O}_2\bullet$:
 - in combination with the controlled surrounding atmosphere this tailoring can be made highly specific
 - feed gas admixture of either N_2 or O_2 results in an increased concentration of liquid phase oxygen radicals, whereas a mixture of both together yield a lower amount
- the liquid ingredients impact on the type and amount of reactive species generated by plasma treatment was evaluated
 - additional ingredients besides water in complex liquids have multiple impact on the plasma-generated reactive species (with the exception of plasma jet VUV treatment, see below)
 - containing molecular groups are potentially cleaved by plasma treatment yielding an additional source for ROS & RNS
 - others molecular ingredients such as vitamins scavenge the produced ROS & RNS
- Underlying mechanisms and origins of the plasma-caused chemical changes in the solutions were identified:
 - ▷ liquid phase hydrogen peroxide is a solvation process from the gaseous H_2O_2 in the specific case of humidified feed gas
 - ▷ solvation is the most likely origin of liquid phase singlet oxygen
 - ▷ impact of VUV radiation on the formation of reactive oxygen species in biologically relevant solution is:
 - argon excimer emission of the plasma jet causes dissociation of water molecules
 - concentration of VUV generated ROS in the liquid is more than about two orders of magnitude lower than the concentration in solution due to the treatment with the complete plasma jet
 - plasma jet VUV treatment of different liquids results in the same type and concentration of ROS, therefore, it can be assumed that the resulting ROS concentration caused by dissociation of water in contrast to complete plasma treatment
 - plasma jet VUV treatment of human immune cell suspension yields the formation of glutathione thiyl radicals, known among others as a cellular response to oxidative stress

The knowledge gained about the liquid species and liquid chemistry is highly relevant to the therapeutic application of the plasma jet in medicine. For instance, the impact of vacuum ultraviolet radiation on liquids and the risk estimation of possible side effects during wound treatment is essential for a safe and health-enhancing treatment. The presented work clearly shows that a direct interaction of VUV radiation during treatment of a liquid covered tissue is already very unlikely if the liquid layer has a minimum thickness of

25 μm . Furthermore, this study shows how the plasma can be controlled and the resulting reactive species can be tuned so that a designed treatment according to the requirements can be adjusted, which will be of great benefit for the application of plasmas in medicine. In the future, the fundamental knowledge of plasma-liquid interaction should be extended by investigation of the underlying mechanisms for the generation and transport of further species in the liquid: a focus need to be set on nitrogen reactive species, especially the nitrogen radicals such as nitric monoxide and nitrogen dioxide radicals. Furthermore, the interfacial chemistry during plasma treatment is highly important for a more detailed understanding and tailoring of plasma treatment in medicine. This thesis has set the fundament for these studies.

List of Figures

1.1	Plasma effect mediated by the liquid to the biological target (translated and reprinted with permission from [1]. ©2014, John Wiley and Sons).	1
2.1	Term scheme of molecular oxygen.	15
2.2	Intensity decrease of electromagnetic radiation due to absorption by a sample of the thickness L	20
2.3	Scheme of an X-band EPR spectroscope setup (adapted from [149]).	28
2.4	Sketch of the modulation of the absorption peak with a modulation frequency. The modulation yields the first derivative of the absorption peak.	30
2.5	Peak pattern of the hydroxyl radical adduct with the common spin trap DMPO.	31
2.6	Reaction of a free radical with a nitroso spin trap forming fairly stable nitroxide radicals.	32
2.7	Reaction of a free radical with a nitron spin trap forming a fairly stable nitroxide radical.	33
3.1	Schematic drawing of the kinpen09.	35
3.2	Kinpen09 treatment setups for different studies.	36
3.3	Reaction of nitrite with sulfanilamide (Griess reagent 1) to diazonium salt.	37
3.4	Reaction of diazonium salt with Griess reagent 2 (N-(1-naphthyl)-ethylenediamine) to the detectable deep purple azo compound.	38
3.5	Reaction of Amplex [®] Red via horseradish peroxidase with hydrogen peroxide to resorufin.	40
3.6	Indigo trisulfonate reaction with ozone to potassium isatin sulfonate.	42
3.7	Schematic drawing of a common pH electrode.	47
3.8	Borosilicate sample tube (a) placed in the ER 4119HS EPR resonator (b) [29].	48
4.1	Interaction of the plasma with the gaseous and aqueous phase.	51
4.2	Liquid treatment situation in open atmosphere for the kinpen09.	52
4.3	Treatment scheme with the focus on the liquid phase and the plasma generated reactive species.	53
4.4	Treatment scheme with the focus on the liquid phase and the plasma generated reactive species including the spin trap. The depicted species amount represents the concentrations neither of the reactive species nor of the spin trap.	54
4.5	DMPO of three different suppliers treated exactly in the same manner shows different spectra (©2013 IOP Publishing Ltd. Reprinted with permission from [29]).	55

4.6	Typical DMPO spectrum of DMPO●/OH (dark dots) and DMPO●/OOH (light squares) measured after 180 s plasma treatment of DPBS and simulated by the EPR software (©2013 IOP Publishing Ltd. Reprinted with permission from [29]).	56
4.7	Decay of spin trap adduct observed over 74 hours (©2013 IOP Publishing Ltd. Reprinted with permission from [29]).	57
4.8	DMPO●/OOH adduct decays into DMPO●/OH (©2013 IOP Publishing Ltd. Reprinted with permission from [29]).	58
4.9	Reaction of BMPO with superoxide anion radical to form a stable adduct BMPO●/OOH.	58
4.10	BMPO spectra of BMPO●/OH and BMPO●/OOH measured after 180 s plasma treatment of DPBS and simulated by Xenon software and Xenon Spin Counting module (Bruker BioSpin, Rheinstetten, Germany) (©2013 IOP Publishing Ltd. Reprinted with permission from [29])	59
4.11	Adducts of spin label for peroxynitrite and superoxide anion, CPH and PPH.	61
4.12	Carboxy-PTIO spectrum measured after 180 s plasma treatment of DPBS, with 100% nitrogen in the curtain gas device, 100% humidified feed gas (Ar + 0.8% N ₂ + 0.2% O ₂) added.	62
4.13	The curtain gas situated around the plasma jet's plume to exclude the ambient influences, such as humidity and diffusion of molecular air species into the plume.	63
4.14	Gas phase measurements of the curtain gas impact.	64
4.15	The change in pH depending on the curtain gas composition in 5 mL DPBS after 180 s plasma treatment (Republished with permission of Begell House Inc., from [33]; permission conveyed through Copyright Clearance Center, Inc.).	65
4.16	Nitrite and nitrate generated in DPBS due to 180 s plasma treatment as a function of the variation of the curtain gas composition. The error bars show minimum and maximum deviations of the mean value of at least three independent measurements (Republished with permission of Begell House Inc., from [33]; permission conveyed through Copyright Clearance Center, Inc.).	67
4.17	The resulting concentration of hydrogen peroxide as a function of the variation of the curtain gas composition for 180 s plasma treatment. The error bars show the minimum and maximum deviations of the mean value of at least three independent measurements (Republished with permission of Begell House Inc., from [33]; permission conveyed through Copyright Clearance Center, Inc.).	69
4.18	Net production rate of DMPO●/OH+OOH adduct after 180 s plasma treatment of DPBS as a function of the curtain gas composition (©2013 IOP Publishing Ltd. Reprinted with permission from [29]). The error bars show the minimum and maximum deviations of the mean value of at least three independent measurements.	70
4.19	Net production rate of BMPO●/OH and BMPO●/OOH adduct after 180 s plasma treatment of DPBS as a function of the curtain gas composition. The error bars show the minimum and maximum deviations of the mean value of at least three independent measurements.	71

4.20	Oxygen radical BMPO adduct in DPBS as a function of oxygen and nitrogen feed gas admixture, formed during 180 s kinpen09 treatment with synthetic air as curtain gas.	73
4.21	Spin trap adduct of DMPO with oxygen radicals as a function of the feed gas humidity. Detected after 40 s plasma treatment in DPBS and RPMI, respectively.	75
4.22	Hydrogen peroxide concentration as a function of the feed gas humidity after 40 s plasma treatment of RPMI 1640 (©2013 IOP Publishing Ltd. Reprinted with permission from [71]).	76
4.23	Treatment scheme with the focus on the liquid phase and the plasma generated reactive species including further components of more complex liquids.	77
4.24	Differences in resulting chemistry due to variation of the plasma treated liquid, NaCl, DPBS and RPMI 1640 are investigated.	79
4.25	Influence of the feed gas humidity on hydrogen peroxide in the gas phase (©2013 IOP Publishing Ltd. Reprinted with permission from [61]).	81
4.26	Correlation of plasma generated hydrogen peroxide net production rates in the liquid and gaseous phase adapted from (©2013 IOP Publishing Ltd. Reprinted with permission from [61]).	82
4.27	Spin trap (BMPO) oxygen radical concentration as a function of the feed gas humidity (©2013 IOP Publishing Ltd. Reprinted with permission from [61]). Treatment of 5 mL DPBS for 40 s with kinpen09.	82
4.28	Hydrogen peroxide concentration in the liquid as a function of the gas phase hydrogen peroxide concentration for three treatment times measured for two different formation conditions: by plasma treatment by H ₂ O ₂ enriched gas treatment by using a hydrogen peroxide bubbler (©2013 IOP Publishing Ltd. Reprinted with permission from [61]).	84
4.29	Ozone concentration in ultrapure water for different treatment times as a function of the oxygen content in the feed gas.	85
4.30	Singlet oxygen adduct spectrum of TEMPD-HCl spin trap.	86
4.31	Spin adduct of singlet oxygen as a function of the treatment time with 0.1% oxygen in the feed gas with pure nitrogen as curtain gases.	87
4.32	Spin adduct of singlet oxygen as a function of the oxygen content in argon with nitrogen as curtain gases.	87
4.33	Spin adduct of singlet oxygen as a function of the molecular oxygen content in argon with different curtain gases.	88
4.34	Hydrogen peroxide as a function of oxygen admixture into the feed gas and two different curtain gases.	89
4.35	BMPO adducts of hydroxyl and superoxide anion radicals as a function of the oxygen content in the feed gas. The used curtain gas is molecular nitrogen.	89
4.36	The pH value as a function of the oxygen content in the feed gas for a pure nitrogen and a synthetic air curtain gas. A volume of 5 mL DPBS is treated for 180 s.	90
4.37	Sketch of the plasma jet VUV radiation and its possible impact on a biological target.	91
4.38	On axis VUV spectrum and UV/VIS (inset figure) of the kinpen09 (Reprinted with permission from [63]. ©2015, AIP Publishing LLC.).	92

4.39	The VUV spectrum, measured with an Acton VM 502 monochromator with a slit width of $100\ \mu\text{m}$ and with an integration time of $5\ \text{ms}$, of the kinpen09 with curtain gas variation at the working distance of $9\ \text{mm}$	92
4.40	VUV spectrum of kinpen09 compared with the VUV absorption of a $400\ \mu\text{m}$ thick water film (Reprinted with permission from [63]. ©2015, AIP Publishing LLC.).	93
4.41	Absorption behavior of different biologically relevant solutions.	95
4.42	Hydrogen peroxide concentration formed by treatment with the complete plasma jet or only by its VUV radiation in ultrapure water as a function of the treatment time (Reprinted with permission from [63]. ©2015, AIP Publishing LLC.). Used volumes are $5\ \text{mL}$ for complete plasma jet, and $80\ \mu\text{L}$ for VUV radiation of the jet, respectively.	96
4.43	Spin trap radical adduct generated either by the complete plasma jet, by its VUV and UV radiation, or by its UV radiation (Reprinted with permission from [63]. ©2015, AIP Publishing LLC.). UPW, containing $100\ \text{mM}$ DMPO, is treated for different times in volumes of $5\ \text{mL}$, complete plasma jet, or $80\ \mu\text{L}$, radiation of the jet, respectively.	97
4.44	Spin trap radical adduct in three different relevant solutions produced by only the plasma jet VUV radiation or by the complete plasma jet (Reprinted with permission from [63]. ©2015, AIP Publishing LLC.). The solutions, containing $100\ \text{mM}$ DMPO, are treated for $180\ \text{s}$ in volumes of $5\ \text{mL}$, complete plasma jet, or $80\ \mu\text{L}$, VUV radiation of the jet, respectively.	99
4.45	Reactive species formed as a function of the curtain gas humidity.	100
4.46	Scheme of the plasma-liquid interaction in the presence of a biological target.	101
4.47	Biological experiments on the impact of curtain gas composition on eukaryotic and prokaryotic cell viability.	102
4.48	Nitrite concentration as a function of the curtain gas composition after plasma treatment of $5\ \text{mL}$ solution (adapted from [21] and [22]).	103
4.49	Resulting radical adducts of plasma treated cell suspension.	105
4.50	EPR spectra of THP-1 cell suspension in two different cell culture media.	106
5.1	Spectrum of EMPO after $180\ \text{s}$ plasma treatment of DPBS.	140
5.2	Spectrum of DEPMPO after $180\ \text{s}$ plasma treatment of DPBS, DEPMPO●/OOH (marked with open blue squares) and DEPMPO●/OH (marked with black dots).	140
5.3	Spectrum of DIPPMPO after $180\ \text{s}$ plasma treatment of DPBS.	141
5.4	Spectrum of CYPMPO●/OH (marked with black dots) after $300\ \text{s}$ plasma treatment of DPBS.	141

List of Tables

1.1	Overview of the plasma-liquid interaction literature of the past five years for helium, argon or air as working gas (adapted from reference [24], reprinted from Clinical Plasma Medicine, Vol 3, Jablonowski, H. & von Woedtke, Th. Research on plasma medicine-relevant plasma-liquid interaction: What happened in the past five years?, pp 42-52, © 2015, with permission from Elsevier).	5
3.1	Used devices and software.	43
3.2	Chemicals used in the study-part 1.	44
3.3	Chemicals used in the study-part 2.	45
3.4	Investigated spin trapping agents.	46
4.1	Spin traps for superoxide anion detection and the lifetime of their spin trap adduct.	60
4.2	Main ingredients of the investigated liquids (Republished with permission of Begell House Inc., from [33]; permission conveyed through Copyright Clearance Center, Inc.).	78
4.3	Henry coefficients for selected species at standard conditions.	83
4.4	Ingredients of the investigated liquids for VUV radiation's impact sorted by complexity (Reprinted with permission from [63]. ©2015, AIP Publishing LLC).	94
4.5	Bond dissociation energies of biological relevant molecules with the corresponding wavelength (Reprinted with permission from [63]. ©2015, AIP Publishing LLC).	96
4.6	Radical parameters determined by evaluation of measured EPR spectrum of VUV treated DMEM (see figure 4.49a).	105
5.1	Pascal's triangle for ratio of relative peak intensities of the split lines according to interactions.	139
5.2	Listed parameters of the EPR spectra-part 1.	142
5.3	Listed parameters of the EPR spectra-part 2.	143
5.4	Listed parameters of the EPR spectra-part 3.	144
5.5	Listed parameters of the EPR spectra-part 4.	145

Bibliography

- [1] S. Reuter, K. Masur, Th. von Woedtke, and K. D. Weltmann. Kalte plasmen in der medizin. *Vakuum in Forschung und Praxis*, 26(5):28–34, 2014.
- [2] V. Schulz von der Gathen, V. Buck, T. Gans, N. Knake, K. Niemi, S. Reuter, L. Schaper, and J. Winter. Optical diagnostics of micro discharge jets. *Contributions to Plasma Physics*, 47(7):510–519, 2007.
- [3] S. Reuter, K. Niemi, V. Schulz-Von Der Gathen, and H. F. Doebele. Generation of atomic oxygen in the effluent of an atmospheric pressure plasma jet. *Plasma Sources Science and Technology*, 18(1):015006, 2009.
- [4] J. Schaefer, R. Foest, A. Ohl, and K.-D. Weltmann. Miniaturized non-thermal atmospheric pressure plasma jet - characterization of self-organized regimes. *Plasma Physics and Controlled Fusion*, 51(12):124045, 2009.
- [5] P. Bruggeman and D. C. Schram. On oh production in water containing atmospheric pressure plasmas. *Plasma sources science & technology*, 19(4), 2010.
- [6] J. S. Sousa, K. Niemi, L. J. Cox, Q. Th. Algwari, T. Gans, and D. O’Connell. Cold atmospheric pressure plasma jets as sources of singlet delta oxygen for biomedical applications. *Journal of Applied Physics*, 109(12):123302, 2011.
- [7] S. Reuter, J. Winter, S. Iseni, S. Peters, A. Schmidt-Bleker, M. Duennbier, J. Schaefer, R. Foest, and K. D. Weltmann. Detection of ozone in a mhz argon plasma bullet jet. *Plasma Sources Science and Technology*, 21(3):034015, 2012.
- [8] S. Reuter, J. Winter, A. Schmidt-Bleker, D. Schroeder, H. Lange, N. Knake, V. Schulz Von Der Gathen, and K. D. Weltmann. Atomic oxygen in a cold argon plasma jet: Talif spectroscopy in ambient air with modelling and measurements of ambient species diffusion. *Plasma Sources Science and Technology*, 21(2):024005, 2012.
- [9] M. Duennbier, A. Schmidt-Bleker, J. Winter, M. Wolfram, R. Hippler, K.-D. Weltmann, and S. Reuter. Ambient air particle transport into the effluent of a cold atmospheric-pressure argon plasma jet investigated by molecular beam mass spectrometry. *Journal of Physics D: Applied Physics*, 46(43):435203, 2013.
- [10] S. Iseni, S. Reuter, and K. D. Weltmann. No2 dynamics of an ar/air plasma jet investigated by in situ quantum cascade laser spectroscopy at atmospheric pressure. *Journal of Physics D: Applied Physics*, 47(7):075203, 2014.
- [11] P. J. Bruggeman, N. Sadeghi, D. C. Schram, and V. Linss. Gas temperature determination from rotational lines in non-equilibrium plasmas: a review. *Plasma Sources Science and Technology*, 23(2):023001, 2014.

- [12] S. Iseni, S. Zhang, A. F. H. van Gessel, S. Hofmann, B. J. T. van Ham, S. Reuter, K. D. Weltmann, and P. J. Bruggeman. Nitric oxide density distributions in the effluent of an rf argon appj: effect of gas flow rate and substrate. *New Journal of Physics*, 16(12):123011, 2014.
- [13] S. Schneider, M. Duennbier, S. Huebner, S. Reuter, and J.ise Benedikt. Atomic nitrogen: a parameter study of a micro-scale atmospheric pressure plasma jet by means of molecular beam mass spectrometry. *Journal of Physics D: Applied Physics*, 47(50):505203, 2014.
- [14] D. Dobrynin and A. Y. Fridman, A. and Starikovskiy. Reactive oxygen and nitrogen species production and delivery into liquid media by microsecond thermal spark-discharge plasma jet. *Plasma Science, IEEE Transactions on*, 40(9):2163–2171, 2012.
- [15] A. Fridman, A. Chirokov, and A. Gutsol. Non-thermal atmospheric pressure discharges. *Journal of Physics D: Applied Physics*, 38(2):R1, 2005.
- [16] A. F. H. Van Gessel, B. Hrycak, M. Jasinski, J. Mizeraczyk, J. J. A. M. Van der Mullen, and P. J. Bruggeman. Temperature and no density measurements by lif and oes on an atmospheric pressure plasma jet. *Journal of Physics D: Applied Physics*, 46(9):095201, 2013.
- [17] A. Schmidt-Bleker, J. Winter, A. Boesel, S. Reuter, and K. D. Weltmann. On the plasma chemistry of a cold atmospheric argon plasma jet with shielding gas device. *Plasma Sources Science and Technology*, 25(1):015005, 2015.
- [18] J. Roepcke, P. B. Davies, N. Lang, A. Rousseau, and S. Welzel. Applications of quantum cascade lasers in plasma diagnostics: a review. *Journal of Physics D: Applied Physics*, 45(42):423001, 2012.
- [19] D. O’Connell, L. J. Cox, W. B. Hyland, S. J. McMahon, S. Reuter, W. G. Graham, T. Gans, and F. J. Currell. Cold atmospheric pressure plasma jet interactions with plasmid dna. *Applied Physics Letters*, 98(4):043701, 2011.
- [20] L. Bundscherer, S. Bekeschus, H. Tresp, S. Hasse, S. Reuter, K. D. Weltmann, U. Lindequist, and K. Masur. Viability of human blood leukocytes compared with their respective cell lines after plasma treatment. *Plasma Medicine*, 3(1-2), 2013.
- [21] S. Reuter, H. Tresp, K. Wende, M. U. Hammer, J. Winter, K. Masur, A. Schmidt-Bleker, and K. D. Weltmann. From rons to ros: tailoring plasma jet treatment of skin cells. *Plasma Science, IEEE Transactions on*, 40(11):2986–2993, 2012.
- [22] H. Jablonowski, M. A. Ch. Haensch, M. Duennbier, K. Wende, M. U. Hammer, K. D. Weltmann, S. Reuter, and Th. von Woedtke. Plasma jet’s shielding gas impact on bacterial inactivation. *Biointerphases*, 10(2):029506, 2015.
- [23] L. Bundscherer, S. Nagel, S. Hasse, H. Tresp, K. Wende, R. Walther, S. Reuter, K. D. Weltmann, K. Masur, and U. Lindequist. Non-thermal plasma treatment induces mapk signaling in human monocytes. *Open Chemistry*, 13(1), 2015.
- [24] Helena Jablonowski and Thomas von Woedtke. Research on plasma medicine-relevant plasma-liquid interaction: What happened in the past five years? *Clinical Plasma Medicine*, 2015.

- [25] B. Halliwell and J. M. C. Gutteridge. *Free Radicals in Biology and Medicine*. Oxford University Press, Oxford, 2007.
- [26] D. B. Graves. The emerging role of reactive oxygen and nitrogen species in redox biology and some implications for plasma applications to medicine and biology. *Journal of Physics D: Applied Physics*, 45(26):263001, 2012.
- [27] B. Halliwell and J. M. C. Gutteridge. Oxygen toxicity, oxygen radicals, transition metals and disease. *Biochemical journal*, 219(1):1, 1984.
- [28] O. I. Aruoma. Free radicals, oxidative stress, and antioxidants in human health and disease. *Journal of the American Oil Chemists' Society*, 75(2):199–212, 1998.
- [29] H. Tresp, M. U. Hammer, J. Winter, K. D. Weltmann, and S. Reuter. Quantitative detection of plasma-generated radicals in liquids by electron paramagnetic resonance spectroscopy. *Journal of Physics D: Applied Physics*, 46(43):435401, 2013.
- [30] Q. Zhang, P. Sun, H. Feng, R. Wang, Y. Liang, W. Zhu, K. H. Becker, J. Zhang, and J. Fang. Assessment of the roles of various inactivation agents in an argon-based direct current atmospheric pressure cold plasma jet. *Journal of Applied Physics*, 111(12):123305, 2012.
- [31] S. Ikawa, K. Kitano, and S. Hamaguchi. Effects of pH on bacterial inactivation in aqueous solutions due to low-temperature atmospheric pressure plasma application. *Plasma Processes and Polymers*, 7(1):33–42, 2010.
- [32] K. Oehmigen, J. Winter, M. Haehnel, C. Wilke, R. Brandenburg, K. D. Weltmann, and Th. von Woedtke. Estimation of possible mechanisms of escherichia coli inactivation by plasma treated sodium chloride solution. *Plasma Processes and Polymers*, 8(10):904–913, 2011.
- [33] H. Tresp, M. U. Hammer, K. D. Weltmann, and S. Reuter. Effects of atmosphere composition and liquid type on plasma-generated reactive species in biologically relevant solutions. *Plasma Medicine*, 3(1-2), 2013.
- [34] K. P. Arjunan and A. M. Clyne. Hydroxyl radical and hydrogen peroxide are primarily responsible for dielectric barrier discharge plasma-induced angiogenesis. *Plasma Processes and Polymers*, 8(12):1154–1164, 2011.
- [35] E. Sosnin, E. Stoffels, M. V. Erofeev, I. E. Kieft, S. E. Kunts, et al. The effects of uv irradiation and gas plasma treatment on living mammalian cells and bacteria: a comparative approach. *Plasma Science, IEEE Transactions on*, 32(4):1544–1550, 2004.
- [36] J. Ehlbeck, U. Schnabel, M. Polak, J. Winter, Th. Von Woedtke, R. Brandenburg, T. Von dem Hagen, and K. D. Weltmann. Low temperature atmospheric pressure plasma sources for microbial decontamination. *Journal of Physics D: Applied Physics*, 44(1):013002, 2011.
- [37] H.-S. Kim, K. C. Wright, I.-H. Hwang, D.-H. Lee, A. Rabinovich, A. A. Fridman, and Y. I. Cho. Effects of h₂o₂ and low pH produced by gliding arc discharge on the inactivation of escherichia coli in water. *Plasma Medicine*, 1(3-4), 2011.

- [38] V. Boxhammer, G. E. Morfill, J. R. Jokipii, T. Shimizu, T. Klaempfl, Y. F. Li, J. Koeritzer, J. Schlegel, and J. L. Zimmermann. Bactericidal action of cold atmospheric plasma in solution. *New Journal of Physics*, 14(11):113042, 2012.
- [39] M. Y. Alkawareek, Q. T. Algwari, S. P. Gorman, W. G. Graham, D. O’Connell, and B. F. Gilmore. Application of atmospheric pressure nonthermal plasma for the in vitro eradication of bacterial biofilms. *FEMS Immunology & Medical Microbiology*, 65(2):381–384, 2012.
- [40] I. Koban, M. H. Geisel, B. Holtfreter, L. Jablonowski, N.-O. Huebner, R. Matthes, K. Masur, K. D. Weltmann, A. Kramer, and T. Kocher. Synergistic effects of nonthermal plasma and disinfecting agents against dental biofilms in vitro. *ISRN dentistry*, 2013, 2013.
- [41] K. Y. Baik, Y. H. Kim, Y. H. Ryu, H. S. Kwon, G. Park, H. S. Uhm, and E. H. Choi. Feeding-gas effects of plasma jets on escherichia coli in physiological solutions. *Plasma Processes and Polymers*, 10(3):235–242, 2013.
- [42] B. K. H. L. Boekema, S. Hofmann, B. J. T. van Ham, P. J. Bruggeman, and E. Middelkoop. Antibacterial plasma at safe levels for skin cells. *Journal of Physics D: Applied Physics*, 46(42):422001, 2013.
- [43] M. J. Pavlovich, H.-W. Chang, Y. Sakiyama, D. S. Clark, and D. B. Graves. Ozone correlates with antibacterial effects from indirect air dielectric barrier discharge treatment of water. *Journal of Physics D: Applied Physics*, 46(14):145202, 2013.
- [44] Z. Machala, B. Tarabova, K. Hensel, E. Spetlikova, L. Sikurova, and P. Lukes. Formation of ros and rns in water electro-sprayed through transient spark discharge in air and their bactericidal effects. *Plasma Processes and Polymers*, 10(7):649–659, 2013.
- [45] R. Matthes, C. Bender, R. Schlueter, I. Koban, R. Bussiahn, S. Reuter, J. Lademann, K. D. Weltmann, and A. Kramer. Antimicrobial efficacy of two surface barrier discharges with air plasma against in vitro biofilms. *PloS one*, 8(7), 2013.
- [46] M. J. Pavlovich, T. Ono, C. Galleher, B. Curtis, D. S. Clark, Z. Machala, and D. B. Graves. Air spark-like plasma source for antimicrobial nox generation. *Journal of Physics D: Applied Physics*, 47(50):505202, 2014.
- [47] E. Dolezalova and P. Lukes. Membrane damage and active but nonculturable state in liquid cultures of escherichia coli treated with an atmospheric pressure plasma jet. *Bioelectrochemistry*, 103:7–14, 2015.
- [48] S. G. Joshi, M. Paff, G. Friedman, G. Fridman, A. Fridman, and A. D. Brooks. Control of methicillin-resistant staphylococcus aureus in planktonic form and biofilms: a biocidal efficacy study of nonthermal dielectric-barrier discharge plasma. *American journal of infection control*, 38(4):293–301, 2010.
- [49] T. Maisch, T. Shimizu, Y.-F. Li, J. Heinlin, S. Karrer, G. Morfill, and J. L. Zimmermann. Decolonisation of mrsa, s. aureus and e. coli by cold-atmospheric plasma using a porcine skin model in vitro. *PloS one*, 7(4):e34610, 2012.

- [50] G. Daeschlein, M. Napp, S. von Podewils, S. Lutze, S. Emmert, A. Lange, I. Klare, H. Haase, D. Guembel, Th. von Woedtke, and M. Juenger. In vitro susceptibility of multidrug resistant skin and wound pathogens against low temperature atmospheric pressure plasma jet (appj) and dielectric barrier discharge plasma (dbd). *Plasma Processes and Polymers*, 11(2):175–183, 2014.
- [51] K. Oehmigen, M. Haehnel, R. Brandenburg, C. Wilke, K. D. Weltmann, and Th. Von Woedtke. The role of acidification for antimicrobial activity of atmospheric pressure plasma in liquids. *Plasma Processes and Polymers*, 7(3-4):250–257, 2010.
- [52] C. W. Chen, H.-M. Lee, and M. B. Chang. Inactivation of aquatic microorganisms by low-frequency ac discharges. *Plasma Science, IEEE Transactions on*, 36(1):215–219, 2008.
- [53] K. P. Arjunan, G. Friedman, A. Fridman, and A. M. Clyne. Non-thermal dielectric barrier discharge plasma induces angiogenesis through reactive oxygen species. *Journal of The Royal Society Interface*, page rsif20110220, 2011.
- [54] P. Sun, Y. Sun, H. Wu, W. Zhu, J. L. Lopez, W. Liu, J. Zhang, R. Li, and J. Fang. Atmospheric pressure cold plasma as an antifungal therapy. *Applied Physics Letters*, 98(2):021501, 2011.
- [55] A. Tani, Y. Ono, S. Fukui, S. Ikawa, and K. Kitano. Free radicals induced in aqueous solution by non-contact atmospheric-pressure cold plasma. *Applied Physics Letters*, 100(25):254103, 2012.
- [56] P. Sun, H. Wu, N. Bai, H. Zhou, R. Wang, H. Feng, W. Zhu, J. Zhang, and J. Fang. Inactivation of bacillus subtilis spores in water by a direct-current, cold atmospheric-pressure air plasma microjet. *Plasma Processes and Polymers*, 9(2):157–164, 2012.
- [57] P. Rumbach, M. Witzke, R. M. Sankaran, and D. B. Go. Plasma-liquid interactions: Separating electrolytic reactions from plasma/gas phase reactions. In *Proc. ESA Annual Meeting on Electrostatics*, page 1, 2013.
- [58] P. Lukes, E. Dolezalova, I. Sisrova, and M. Clupek. Aqueous-phase chemistry and bactericidal effects from an air discharge plasma in contact with water: evidence for the formation of peroxynitrite through a pseudo-second-order post-discharge reaction of h₂o₂ and hno₂. *Plasma Sources Science and Technology*, 23(1):015019, 2014.
- [59] S. H. Nam, H. W. Lee, J. W. Hong, H. J. Lee, and G. C. Kim. Enhanced long-term color stability of teeth treated with hydrogen peroxide and non-thermal atmospheric pressure plasma jets. *Plasma Processes and Polymers*, 11(11):1010–1017, 2014.
- [60] Y. Okazaki, Y. Wang, H. Tanaka, M. Mizuno, K. Nakamura, H. Kajiyama, H. Kano, K. Uchida, F. Kikkawa, M. Hori, et al. Direct exposure of non-equilibrium atmospheric pressure plasma confers simultaneous oxidative and ultraviolet modifications in biomolecules. *Journal of clinical biochemistry and nutrition*, 55(3):207, 2014.
- [61] J. Winter, H. Tresp, M. U. Hammer, S. Iseni, S. Kupsch, A. Schmidt-Bleker, K. Wende, M. Duennbier, K. Masur, K. D. Weltmann, and S. Reuter. Tracking plasma generated h₂o₂ from gas into liquid phase and revealing its dominant impact on human skin cells. *Journal of Physics D: Applied Physics*, 47(28):285401, 2014.

- [62] A. Tani, S. Fukui, S. Ikawa, and K. Kitano. Diagnosis of superoxide anion radical induced in liquids by atmospheric-pressure plasma using superoxide dismutase. *Japanese Journal of Applied Physics*, 54(1S):01AF01, 2015.
- [63] H. Jablonowski, R. Bussiahn, M. U. Hammer, K. D. Weltmann, Th. von Woedtke, and S. Reuter. Impact of plasma jet vacuum ultraviolet radiation on reactive oxygen species generation in bio-relevant liquids. *Physics of Plasmas (1994-present)*, 22(12):122008, 2015.
- [64] N. Puac, M. Miletic, M. Mojovic, A. Popovic-Bijelic, D. Vukovic, B. Milicic, D. Maletic, S. Lazovic, G. Malovic, and Z. L. J. Petrovic. Sterilization of bacteria suspensions and identification of radicals deposited during plasma treatment. *Open Chemistry*, 13(1), 2015.
- [65] K. Wende, P. Williams, J. Dalluge, W. Van Gaens, H. Aboubakr, J. Bischof, Th. von Woedtke, S. M. Goyal, K. D. Weltmann, A. Bogaerts, et al. Identification of the biologically active liquid chemistry induced by a nonthermal atmospheric pressure plasma jet. *Biointerphases*, 10(2):029518, 2015.
- [66] S. Kanazawa, T. Furuki, T. Nakaji, S. Akamine, and R. Ichiki. Measurement of oh radicals in aqueous solution produced by atmospheric-pressure lf plasma jet. *Int. J. Plasma Environmental Sci. Tech*, 6(2):166–171, 2012.
- [67] T. Takamatsu, A. Kawate, K. Uehara, T. Oshita, H. Miyahara, D. Dobrynin, G. Fridman, A. A. Fridman, and A. Okino. Bacterial inactivation in liquids using multi-gas plasmas. *Plasma Medicine*, 2(4), 2012.
- [68] N. Bai, P. Sun, H. Zhou, H. Wu, R. Wang, F. Liu, W. Zhu, J. L. Lopez, J. Zhang, and J. Fang. Inactivation of staphylococcus aureus in water by a cold, he/o2 atmospheric pressure plasma microjet. *Plasma Processes and Polymers*, 8(5):424–431, 2011.
- [69] J. Parkey, J. Cross, R. Hayes, C. Parham, D. Staack, and A. C. Sharma. A battery powered, portable, and self-contained non-thermal helium plasma jet device for point-of-injury burn wound treatment. *Plasma Processes and Polymers*, 2015.
- [70] T. Nakajima, H. Yasuda, H. Kurita, K. Takashima, and A. Mizuno. Generation of bactericidal factors in the liquid phase and approach to new gene transfer technology by low temperature plasma jet treatment. *International Journal of Plasma Environmental Science and Technology*, 5:42–49, 2011.
- [71] J. Winter, K. Wende, K. Masur, S. Iseni, M. Duennbier, M. U. Hammer, H. Tresp, K. D. Weltmann, and S. Reuter. Feed gas humidity: a vital parameter affecting a cold atmospheric-pressure plasma jet and plasma-treated human skin cells. *Journal of Physics D: Applied Physics*, 46(29):295401, 2013.
- [72] M. Hoentsch, Th. von Woedtke, K. D. Weltmann, and J. B. Nebe. Time-dependent effects of low-temperature atmospheric-pressure argon plasma on epithelial cell attachment, viability and tight junction formation in vitro. *Journal of Physics D: Applied Physics*, 45(2):025206, 2012.
- [73] S. Bekeschus, J. Kolata, C. Winterbourn, A. Kramer, R. Turner, K. D. Weltmann, B. Broeker, and K. Masur. Hydrogen peroxide: A central player in physical plasma-induced oxidative stress in human blood cells. *Free radical research*, 48(5):542–549, 2014.

- [74] T. Adachi, H. Tanaka, S. Nonomura, H. Hara, S. Kondo, and M. Hori. Plasma-activated medium induces a549 cell injury via a spiral apoptotic cascade involving the mitochondrial–nuclear network. *Free Radical Biology and Medicine*, 79:28–44, 2015.
- [75] R. Burlica, R. G. Grim, K.-Y. Shih, D. Balkwill, and B. R. Locke. Bacteria inactivation using low power pulsed gliding arc discharges with water spray. *Plasma Processes and Polymers*, 7(8):640–649, 2010.
- [76] N. Shainsky, D. Dobrynin, U. Ercan, S. Joshi, H. Ji, A. Brooks, G. Fridman, Y. Cho, A. Fridman, and G. Friedman. Non-equilibrium plasma treatment of liquids, formation of plasma acid. In *ISPC-20: 20th International Symposium on Plasma Chemistry*, 2011.
- [77] T. Shimizu, Y. Iwafuchi, G. E. Morfill, and T. Sato. Transport mechanism of chemical species in a pin-water atmospheric discharge driven by negative voltage. *Journal of Photopolymer Science and Technology*, 24(4):421–427, 2011.
- [78] Th. von Woedtke, K. Oehmigen, R. Brandenburg, T. Hoder, C. Wilke, M. Haehnel, and K. D. Weltmann. Plasma-liquid interactions: chemistry and antimicrobial effects. In *Plasma for Bio-Decontamination, Medicine and Food Security*, pages 67–78. Springer, 2012.
- [79] K. Oehmigen, R. Brandenburg, K. D. Weltmann, and Th. von Woedtke. Comparison of direct dbd treatment and dbd exhaust gas treatment of liquids. In *Plasma Science (ICOPS), 2012 Abstracts IEEE International Conference on*, pages 3P–79. IEEE, 2012.
- [80] M. A. Ch. Haensch, M. Mann, K. D. Weltmann, and Th. von Woedtke. Analysis of antibacterial efficacy of plasma-treated sodium chloride solutions. *Journal of Physics D: Applied Physics*, 48(45):454001, 2015.
- [81] M. A. Ch. Haensch, J. Winter, R. Bussiahn, K. D. Weltmann, and Th. von Woedtke. A systematic characterization of a novel surface dielectric barrier discharge for biomedical experiments. *Plasma Medicine*, 3(1-2), 2013.
- [82] S. G. Joshi, M. Cooper, A. Yost, M. Paff, U. K Ercan, G. Fridman, G. Friedman, A. Fridman, and A. D. Brooks. Nonthermal dielectric-barrier discharge plasma-induced inactivation involves oxidative dna damage and membrane lipid peroxidation in escherichia coli. *Antimicrobial agents and chemotherapy*, 55(3):1053–1062, 2011.
- [83] Z. Machala, B. Tarabova, M. Pelach, K. Hensel, M. Janda, and L. Sikurova. Streamer corona and transient spark in air for bio-decontamination of water and surfaces.
- [84] K. Kitano, S. Ikawa, A. Tani, T. Ohshima, H. Yamaguchi, H. Yamazaki, R. Arakawa, T. Kitamura, and N. Ohnishi. Innovative plasma disinfection of bacteria in water by the reduced ph method combined with free radicals supplied by non-contact atmospheric plasma. In *Proc. 20th Int. Symp. on Plasma Chemistry (ISPC-20)(Philadelphia, PA, 24-29 July 2011)*, page 17, 2011.
- [85] M.-H. Ngo Thi, P.-L. Shao, J.-D. Liao, C.-C. K Lin, and H.-K. Yip. Enhancement of angiogenesis and epithelialization processes in mice with burn wounds through

- ros/rms signals generated by non-thermal n₂/ar micro-plasma. *Plasma Processes and Polymers*, 11(11):1076–1088, 2014.
- [86] F. Liu, P. Sun, N. Bai, Y. Tian, H. Zhou, S. Wei, Y. Zhou, J. Zhang, W. Zhu, K. Becker, and J. Fang. Inactivation of bacteria in an aqueous environment by a direct-current, cold-atmospheric-pressure air plasma microjet. *Plasma Processes and Polymers*, 7(3-4):231–236, 2010.
- [87] M. J. Pavlovich, D. S. Clark, and D. B. Graves. Quantification of air plasma chemistry for surface disinfection. *Plasma Sources Science and Technology*, 23(6):065036, 2014.
- [88] M. Hoentsch, R. Bussiahn, H. Rebl, C. Bergemann, M. Eggert, M. Frank, Th. von Woedtke, and B. Nebe. Persistent effectivity of gas plasma-treated, long time-stored liquid on epithelial cell adhesion capacity and membrane morphology. 2014.
- [89] Z. Xu, J. Shen, Z. Zhang, J. Ma, R. Ma, Y. Zhao, Q. Sun, S. Qian, H. Zhang, L. Ding, et al. Inactivation effects of non-thermal atmospheric-pressure helium plasma jet on staphylococcus aureus biofilms. *Plasma Processes and Polymers*, 2015.
- [90] Th. von Woedtke, S. Blackert, B. Haertel, M. Harms, U. Lindequist, K. Oehmigen, K. Wende, and K. D. Weltmann. The role of liquid environment as modulating medium for plasma-cell interactions. In *Proc. 20th Int. Symp. on Plasma Chemistry (ISPC-20)(Philadelphia, PA, 24-29 July 2011)*, 2011.
- [91] C. Deutsch, J. S. Taylor, and D. F. Wilson. Regulation of intracellular ph by human peripheral blood lymphocytes as measured by 19f nmr. *Proceedings of the National Academy of Sciences*, 79(24):7944–7948, 1982.
- [92] D. M. Pillsbury and G. Rebell. The bacterial flora of the skin. *J Invest Dermatol*, 18:173–186, 1952.
- [93] K. Bagchi and S. Puri. Free radicals and antioxidants in health and disease. *Eastern Mediterranean Health Journal*, 4(2):350–360, 1998.
- [94] C. Rosales. *Molecular mechanisms of phagocytosis*. Springer, 2005.
- [95] A. D. McNaught. *IUPAC Compendium of Chemical Terminology: The Gold Book*. International Union of Pure and Applied Chemistry, 2005.
- [96] G. M. Rosen, B. E. Britigan, H. J. Halpern, and S. Pou. *Free Radicals: Biology and Detection by Spin Trapping*. Oxford University Press, USA, New York, 1999.
- [97] H. Sies. Strategies of antioxidant defense. In *EJB Reviews 1993*, pages 101–107. Springer, 1994.
- [98] H. Sies and W. Stahl. Vitamins e and c, beta-carotene, and other carotenoids as antioxidants. *American Journal of Clinical Nutrition*, 62(6 Suppl):1315S–1321S, 1995. Sies, H Stahl, W Am J Clin Nutr. 1995 Dec;62(6 Suppl):1315S-1321S.
- [99] W. Pryor. *Free radicals in biology*, volume 1. Academic Press Inc., New York, USA, 1976.
- [100] J. S. Beckman and W. H. Koppenol. Nitric oxide, superoxide, and peroxynitrite: the good, the bad, and ugly. *American Journal of Physiology-Cell Physiology*, 271(5):C1424–C1437, 1996.

- [101] E. Wiberg and N. Wiberg. *Inorganic Chemistry*. Academic Press, 2001.
- [102] B. Halliwell, K. Zhao, and M. Whiteman. Nitric oxide and peroxynitrite. the ugly, the uglier and the not so good: a personal view of recent controversies. *Free radical research*, 31(6):651–669, 1999.
- [103] J. S. Beckman. *The physiological and pathological chemistry of nitric oxide*. Academic Press, Inc., San Diego, California, USA, 1996.
- [104] A. Meulemans. Diffusion coefficients and half-lives of nitric oxide and n-nitroso-l-arginine in rat cortex. *Neuroscience letters*, 171(1):89–93, 1994.
- [105] J. Garthwaite and C. L. Boulton. Nitric oxide signaling in the central nervous system. *Annual review of physiology*, 57(1):683–706, 1995.
- [106] R. E. Huie and S. Padmaja. The reaction of no with superoxide. *Free radical research*, 18(4):195–199, 1993.
- [107] P. Lukes, B. R. Locke, and J.-L. Brisset. Aqueous-phase chemistry of electrical discharge plasma in water and in gas–liquid environments. *Plasma Chemistry and Catalysis in Gases and Liquids*, pages 243–308, 2012.
- [108] L. Brunelli, J. P. Crow, and J. S. Beckman. The comparative toxicity of nitric oxide and peroxynitrite to escherichia coli. *Archives of Biochemistry and Biophysics*, 316(1):327–334, 1995.
- [109] F. Wilkinson, W. P. Helman, and A. B. Ross. Rate constants for the decay and reactions of the lowest electronically excited singlet state of molecular oxygen in solution. an expanded and revised compilation. *Journal of Physical and Chemical Reference Data*, 24(2):663–677, 1995.
- [110] P. B. Merkel and D. R. Kearns. Radiationless decay of singlet molecular oxygen in solution. experimental and theoretical study of electronic-to-vibrational energy transfer. *Journal of the American Chemical Society*, 94(21):7244–7253, 1972.
- [111] P. B. Merkel, R. Nilsson, and D. R. Kearns. Deuterium effects on singlet oxygen lifetimes in solutions. new test of singlet oxygen reactions. *Journal of the American Chemical Society*, 94(3):1030–1031, 1972.
- [112] P. Di Mascio, E. J. H. Bechara, M. H. G. Medeiros, K. Briviba, and H. Sies. Singlet molecular oxygen production in the reaction of peroxynitrite with hydrogen peroxide. *FEBS letters*, 355(3):287–289, 1994.
- [113] W. H. Koppenol. The reduction potential of the couple O_3/O_2^- : 3: Consequences for mechanisms of ozone toxicity. *FEBS letters*, 140(2):169–172, 1982.
- [114] R. Sander. Compilation of henry’s law constants (version 4.0) for water as solvent. *Atmospheric Chemistry and Physics*, 15(8):4399–4981, 2015.
- [115] U. Kogelschatz and P. Baessler. Determination of nitrous oxide and dinitrogen pentoxide concentrations in the output of air-fed ozone generators of high power density. 1987.

Bibliography

- [116] C. Sonntag and U. Von Gunten. *Chemistry of ozone in water and wastewater treatment: From basic principles to applications*. IWA publishing, 2012.
- [117] R. A. Graham and H. S. Johnston. Photochemistry of NO_3 and kinetics of NO_2 - O_3 system. *Journal of Physical Chemistry*, 82(3):254–268, 1978. Ek503 Times Cited:215 Cited References Count:60.
- [118] B. R. Locke, P. Lukes, and J.-L. Brisset. Elementary chemical and physical phenomena in electrical discharge plasma in gas–liquid environments and in liquids. *Plasma Chemistry and Catalysis in Gases and Liquids*, pages 185–241, 2012.
- [119] O. Legrini, E. Oliveros, and A. M. Braun. Photochemical processes for water treatment. *Chemical Reviews*, 93(2):671–698, 1993.
- [120] X. Wang and K.R. Genco. Stabilization of alkaline hydrogen peroxide, January 30 2007. US Patent 7,169,237.
- [121] P. E. Willard. Stabilizer system for commercial hydrogen peroxide, December 7 1982. US Patent 4,362,706.
- [122] A. G. Leigh. Stabilization of hydrogen peroxide, December 8 1981. US Patent 4,304,762.
- [123] J. M. Campos-Martin, G. Blanco-Brieva, and J. L. G. Fierro. Hydrogen peroxide synthesis: an outlook beyond the anthraquinone process. *Angewandte Chemie International Edition*, 45(42):6962–6984, 2006.
- [124] E. A. Veal, A. M. Day, and B. A. Morgan. Hydrogen peroxide sensing and signaling. *Molecular cell*, 26(1):1–14, 2007.
- [125] P. Niethammer, C. Grabher, A. T. Look, and T. J. Mitchison. A tissue-scale gradient of hydrogen peroxide mediates rapid wound detection in zebrafish. *Nature*, 459(7249):996–999, 2009.
- [126] C. E. Mortimer and U. Mueller. *Chemie: Das Basiswissen der Chemie*. Thieme, 10 edition, 2010.
- [127] S. G. Bratsch. Standard electrode potentials and temperature coefficients in water at 298.15 K. *Journal of physical and chemical reference data*, 18(1):1–21, 1989.
- [128] A. R. Butler and M. Feelisch. Therapeutic uses of inorganic nitrite and nitrate from the past to the future. *Circulation*, 117(16):2151–2159, 2008.
- [129] M. Kelm. Nitric oxide metabolism and breakdown. *Biochimica et Biophysica Acta (BBA)-Bioenergetics*, 1411(2):273–289, 1999.
- [130] N. S. Bryan, B. O. Fernandez, S. M. Bauer, M. F. Garcia-Saura, A. B. Milsom, T. Rassaf, R. E. Maloney, A. Bharti, J. Rodriguez, and M. Feelisch. Nitrite is a signaling molecule and regulator of gene expression in mammalian tissues. *Nature chemical biology*, 1(5):290–297, 2005.
- [131] N. S. Bryan. Nitrite in nitric oxide biology: Cause or consequence?: A systems-based review. *Free Radical Biology and Medicine*, 41(5):691–701, 2006.

- [132] M. Kelm and K. Yoshida. Metabolic fate of nitric oxide and related n-oxides. *Methods in Nitric Oxide Research (Feelisch M, Stamler JS, eds)*. Chichester, UK: Wiley, pages 47–58, 1996.
- [133] S. R. Tannenbaum, J. P. Witter, S. J. Gatley, and E. Balish. Nitrate and nitrite: origins in humans. *Science*, 1979.
- [134] M. W. Lister. The decomposition of hypochlorous acid. *Canadian Journal of Chemistry*, 30(11):879–889, 1952.
- [135] T. Hasegawa, E. Malle, A. Farhood, and H. Jaeschke. Generation of hypochlorite-modified proteins by neutrophils during ischemia-reperfusion injury in rat liver: attenuation by ischemic preconditioning. *American Journal of Physiology-Gastrointestinal and Liver Physiology*, 289(4):G760–G767, 2005.
- [136] G. Jeschke. Electron paramagnetic resonance spectroscopy. *Ullmann's Encyclopedia of Industrial Chemistry*, 2004.
- [137] P. Zeeman. On the influence of magnetism on the nature of the light emitted by a substance. *The Astrophysical Journal*, 5:332, 1897.
- [138] W. Gerlach and O. Stern. Das magnetische moment des silberatoms. *Zeitschrift fuer Physik A Hadrons and Nuclei*, 9(1):353–355, 1922.
- [139] G. E. Uhlenbeck and S. Goudsmit. Ersetzung der hypothese vom unmechanischen zwang durch eine forderung bezüglich des inneren verhaltens jedes einzelnen elektrons. *Naturwissenschaften*, 13(47):953–954, 1925.
- [140] I. I. Rabi, J. R. Zacharias, S. Millman, and P. Kusch. A new method of measuring nuclear magnetic moment. *Physical Review*, 53(4):318–327, 1938.
- [141] E. Zavoiskii. Spin-magnetic resonance in paramagnetic substances. *Journal of Physica (Moscow)*, 9:245, 1945.
- [142] D. M. S. Bagguley, B. Bleaney, J. H. E. Griffiths, R. P. Penrose, and B. I. Plumptre. Paramagnetic resonance in salts of the iron group-a preliminary survey: I. theoretical discussion. *Proceedings of the Physical Society*, 61(6):542, 1948.
- [143] J. A. Weil, J. R. Bolton, and J. E. Wertz. *Electron Paramagnetic Resonance: Elementary Theory and Practical Applications*. Wiley, 1994.
- [144] H. M. Assenheim. *Introduction to electron spin resonance*. Monographs on Electron Spin Resonance. Boston, MA : Springer, 1966.
- [145] A. Beer. Bestimmung der absorption des rothen lichts in farbigen fluessigkeiten. *Annalen der Physik und Chemie*, 86(2), 1852.
- [146] W. Demtroeder. *Experimentalphysik 3: Atome, Molekuele und Festkoerper*. Experimentalphysik / Wolfgang Demtröder. Springer, 2005.
- [147] H. M. Swartz, J. R. Bolton, and D. C. Borg. *Biological Applications of Electron Spin Resonance*. Wiley-Interscience, 1972.
- [148] J. E. Wertz and J. R. Bolton. *Electron spin resonance: elementary theory and practical applications*. Chapman and Hall, 1986.

Bibliography

- [149] G. R. Eaton, S. S. Eaton, D. P. Barr, and R. T. Weber. *Quantitative EPR*. Springer-WienNewYork, Wien, 2010. Eaton, GR Eaton, SS Barr, DP Weber, RT.
- [150] G. R. Buettner. Spin trapping: ESR parameters of spin adducts 1474 1528v. *Free Radical Biology and Medicine*, 3(4):259–303, 1987.
- [151] E. G. Janzen. Spin trapping. *Accounts of Chemical Research*, 4(1):31–40, 1971.
- [152] E. G. Janzen and B. J. Blackburn. Detection and identification of short-lived free radicals by an electron spin resonance trapping technique. *Journal of the American Chemical Society*, 90(21):5909–5910, 1968.
- [153] S. Forshult, C. Lagercrantz, and K. Torssell. Use of nitroso compounds as scavengers for the study of short-lived free radicals in organic reactions. *Acta Chem. Scand*, 23(2):522–523, 1969.
- [154] G. R. Chalfont, M. J. Perkins, and A. Horsfield. Probe for homolytic reactions in solution. ii. polymerization of styrene. *Journal of the American Chemical Society*, 90(25):7141–7142, 1968.
- [155] I. H. Leaver and G. C. Ramsay. Trapping of radical intermediates in the photoreduction of benzophenone. *Tetrahedron*, 25(23):5669–5675, 1969.
- [156] I. H. Leaver, G. C. Ramsay, and E. Suzuki. ESR of nitroxide radicals. i. photolysis of indoles, phenols, disulphides, and thiols. *Australian Journal of Chemistry*, 22(9):1891–1897, 1969.
- [157] I. H. Leaver and G. C. Ramsay. ESR of nitroxide radicals. ii. photosensitization of indoles, phenols, and thiols by a diphenylpyrazoline. *Australian Journal of Chemistry*, 22(9):1899–1904, 1969.
- [158] S. Terabe and R. Konaka. Electron spin resonance studies on oxidation with nickel peroxide. spin trapping of free-radical intermediates. *Journal of the American Chemical Society*, 91(20):5655–5657, 1969.
- [159] A. Mackor, Th. A. J. W. Wajer, Th. J. De Boer, and J. D. W. van Voorst. C-nitroso compounds. part i. the formation of nitroxides by photolysis of nitroso compounds as studied by electron spin resonance. *Tetrahedron Letters*, 7(19):2115–2123, 1966.
- [160] A. Mackor, Th. A. J. W. Wajer, Th. J. de Boer, and J. D. W. Van Voorst. C-nitroso compounds. part iii. alkoxy-alkyl-nitroxides as intermediates in the reaction of alkoxy-radicals with nitroso compounds. *Tetrahedron Letters*, 8(5):385–390, 1967.
- [161] Th A J Wajer, A Mackor, Th J de Boer, and J D W van Voorst. C-nitroso compounds. part 2. on the photochemical and thermal formation of nitroxides from nitroso compounds, as studied by e. s. r. *Tetrahedron*, 23(10):4021–4026, 1967.
- [162] Th. A. J. W. Wajer, A. Mackor, and Th. J. De Boer. C-nitroso compounds - vii: An esr study of alkyl nitroxides. *Tetrahedron*, 25(1):175–180, 1969.
- [163] Th. A. J. W. Wajer, H. W. Geluk, J. B. F. N. Engberts, and Th. J. De Boer. C-nitroso compounds. part xvi: The reaction of c-nitroso compounds with benzenesulfinic acid. an esr study of alkyl and aryl benzenesulfonyl nitroxides. *Recueil des Travaux Chimiques des Pays-Bas*, 89(7):696–704, 1970.

- [164] C. Lagercrantz. Spin trapping of some short-lived radicals by the nitroxide method. *The Journal of Physical Chemistry*, 75(22):3466–3475, 1971.
- [165] J. A. Wargon and E. Williams. Electron spin resonance studies of radical trapping in the radiolysis of organic liquids. i. evidence for the primary formation of the methoxy radical in methanol. *Journal of the American Chemical Society*, 94(22):7917–7918, 1972.
- [166] B. C. Gilbert, J. Davies, Royal Society of Chemistry (Great Britain), D. M. Murphy, and D. Becker. *Electron Paramagnetic Resonance*. Specialist Periodical Reports. Royal Society of Chemistry, 2006.
- [167] F. A. Villamena and J. L. Zweier. Detection of reactive oxygen and nitrogen species by epr spin trapping. *Antioxidants and Redox Signaling*, 6(3):619–629, 2004.
- [168] K. D. Weltmann, E. Kindel, R. Brandenburg, Ch. Meyer, R. Bussiahn, Ch. Wilke, and Th. Von Woedtke. Atmospheric pressure plasma jet for medical therapy: plasma parameters and risk estimation. *Contributions to Plasma Physics*, 49(9):631–640, 2009.
- [169] A. Schmidt-Bleker, S. Reuter, and K. D. Weltmann. Quantitative schlieren diagnostics for the determination of ambient species density, gas temperature and calorimetric power of cold atmospheric plasma jets. *Journal of Physics D: Applied Physics*, 48(17):175202, 2015.
- [170] S. Reuter, J. Winter, A. Schmidt-Bleker, H. Tresp, M. U. Hammer, and K. D. Weltmann. Controlling the ambient air affected reactive species composition in the effluent of an argon plasma jet. *Plasma Science, IEEE Transactions on*, 40(11):2788–2794, 2012.
- [171] M. Anbar and H. Taube. Interaction of nitrous acid with hydrogen peroxide and with water. *Journal of the American Chemical Society*, 76(24):6243–6247, 1954.
- [172] B. Zhao, F. A. Summers, and R. P. Mason. Photooxidation of amplex red to resorufin: implications of exposing the amplex red assay to light. *Free Radical Biology and Medicine*, 53(5):1080–1087, 2012.
- [173] H. Bader and J. Hoigne. Determination of ozone in water by the indigo method. *Water research*, 15(4):449–456, 1981.
- [174] American Water Works Association Research Foundation. *Ozone in Water Treatment: Application and Engineering*. Cooperative research report. Taylor & Francis, 1991.
- [175] L. J. Bollyky. *Ozone in Water*, volume 1 of *Instrument Engineer’s Handbook: Process Measurement and Analysis*, chapter 8.45, pages 1540–1543. CRC Press, 4 edition, 2003.
- [176] Mettler-Toledo. A guide to ph measurements - the theory and practice of laboratory ph application. online, 10 2007.
- [177] P. A. Bottomley and E. R. Andrew. Rf magnetic field penetration, phase shift and power dissipation in biological tissue: implications for nmr imaging. *Physics in Medicine and biology*, 23(4):630, 1978.

Bibliography

- [178] P. Roeschmann. Radiofrequency penetration and absorption in the human body: Limitations to high-field whole-body nuclear magnetic resonance imaging. *Medical physics*, 14(6):922–931, 1987.
- [179] R. Foest, E. Kindel, H. Lange, A. Ohl, M. Stieber, and K. D. Weltmann. Rf capillary jet - a tool for localized surface treatment. *Contributions to Plasma Physics*, 47(1-2):119–128, 2007.
- [180] R. Bussiahn, E. Kindel, H. Lange, and K. D. Weltmann. Spatially and temporally resolved measurements of argon metastable atoms in the effluent of a cold atmospheric pressure plasma jet. *Journal of Physics D: Applied Physics*, 43(16):165201, 2010.
- [181] J. Winter, M. Duennbier, A. Schmidt-Bleker, A. Meshchanov, S. Reuter, and K. D. Weltmann. Aspects of uv-absorption spectroscopy on ozone in effluents of plasma jets operated in air. *Journal of Physics D: Applied Physics*, 45(38):385201, 2012.
- [182] J.-Y. Han, J.-T. Hong, S.-Y. Nam, and K.-W. Oh. Evaluation of hydroxyl radical reduction activity of red ginseng extract using esr spectroscopy. *Journal of Biomedical Research*, 13(1):83–92, 2012.
- [183] K. Nakamura, T. Kanno, H. Ikai, E. Sato, T. Mokudai, Y. Niwano, T. Ozawa, and M. Kohno. Reevaluation of quantitative esr spin trapping analysis of hydroxyl radical by applying sonolysis of water as a model system. *Bulletin of the Chemical Society of Japan*, 83(9):1037–1046, 2010.
- [184] B. H. J. Bielski, D. E. Cabelli, R. L. Arudi, and A. B. Ross. Reactivity of $h\nu_2/o_2$ radicals in aqueous solution. *Journal of Physical and Chemical Reference Data*, 14(4):1041–1100, 1985.
- [185] J. Kochany and J. R. Bolton. Mechanism of photodegradation of aqueous organic pollutants. 2. measurement of the primary rate constants for reaction of hydroxyl radicals with benzene and some halobenzenes using an epr spin-trapping method following the photolysis of hydrogen peroxide. *Environmental science & technology*, 26(2):262–265, 1992.
- [186] E. Finkelstein, G. M. Rosen, and E. J. Rauckman. Spin trapping. kinetics of the reaction of superoxide and hydroxyl radicals with nitrones. *Journal of the American Chemical Society*, 102(15):4994–4999, 1980.
- [187] G. M. Rosen and M. J. Turner III. Synthesis of spin traps specific for hydroxyl radical. *Journal of medicinal chemistry*, 31(2):428–432, 1988.
- [188] A. Samuni, C. M. Krishna, P. Riesz, E. Finkelstein, and A. Russo. Superoxide reaction with nitroxide spin-adducts. *Free Radical Biology and Medicine*, 6(2):141–148, 1989.
- [189] H. Zhang, J. Joseph, J. Vasquez-Vivar, H. Karoui, C. Nsanzumuhire, P. Martasek, P. Tordo, and B. Kalyanaraman. Detection of superoxide anion using an isotopically labeled nitron spin trap: potential biological applications. *FEBS letters*, 473(1):58–62, 2000.
- [190] P. Tordo. Spin-trapping: recent developments and applications. *Electron paramagnetic resonance*, 16:116–144, 1998.

- [191] F. Chali er and P. Tordo. 5-diisopropoxyphosphoryl-5-methyl-1-pyrroline n-oxide, dipmpo, a crystalline analog of the nitron e depmpo: synthesis and spin trapping properties. *Journal of the Chemical Society, Perkin Transactions 2*, (12):2110–2117, 2002.
- [192] M. Kamibayashi, S. Oowada, H. Kameda, T. Okada, O. Inanami, S. Ohta, T. Ozawa, K. Makino, and Y. Kotake. Synthesis and characterization of a practically better depmpo-type spin trap, 5-(2, 2-dimethyl-1, 3-propoxy cyclophosphoryl)-5-methyl-1-pyrroline n-oxide (cypmpo). *Free radical research*, 40(11):1166–1172, 2006.
- [193] P. Tsai, K. Ichikawa, C. Mailer, S. Pou, H. J. Halpern, B. H. Robinson, R. Nielsen, and G. M. Rosen. Esters of 5-carboxyl-5-methyl-1-pyrroline n-oxide: a family of spin traps for superoxide. *The Journal of organic chemistry*, 68(20):7811–7817, 2003.
- [194] H. Zhao, J. Joseph, H. Zhang, H. Karoui, and B. Kalyanaraman. Synthesis and biochemical applications of a solid cyclic nitron e spin trap: a relatively superior trap for detecting superoxide anions and glutathionyl radicals. *Free Radical Biology and Medicine*, 31(5):599–606, 2001.
- [195] B. Fink, S. Dikalov, and E. Bassenge. A new approach for extracellular spin trapping of nitroglycerin-induced superoxide radicals both in vitro and in vivo. *Free Radical Biology and Medicine*, 28(1):121–128, 2000.
- [196] S. Dikalov, I. Kirilyuk, and I. Grigor’ev. Spin trapping of o-, c-, and s-centered radicals and peroxynitrite by 2h-imidazole-1-oxides. *Biochemical and biophysical research communications*, 218(2):616–622, 1996.
- [197] S. Dikalov, M. Skatchkov, and E. Bassenge. Spin trapping of superoxide radicals and peroxynitrite by 1-hydroxy-3-carboxy-pyrrolidine and 1-hydroxy-2, 2, 6, 6-tetramethyl-4-oxo-piperidine and the stability of corresponding nitroxyl radicals towards biological reductants. *Biochemical and biophysical research communications*, 231(3):701–704, 1997.
- [198] S. Dikalov, M. Skatchkov, and E. Bassenge. Quantification of peroxynitrite, superoxide, and peroxy radicals by a new spin trap hydroxylamine 1-hydroxy-2, 2, 6, 6-tetramethyl-4-oxo-piperidine. *Biochemical and biophysical research communications*, 230(1):54–57, 1997.
- [199] S. Dikalov, I. A. Grigor’ev, M. Voinov, and E. Bassenge. Detection of superoxide radicals and peroxynitrite by 1-hydroxy-4-phosphonooxy-2, 2, 6, 6-tetramethylpiperidine: quantification of extracellular superoxide radicals formation. *Biochemical and biophysical research communications*, 248(2):211–215, 1998.
- [200] N. Hogg. Detection of nitric oxide by electron paramagnetic resonance spectroscopy. *Free Radical Biology and Medicine*, 49(2):122–129, 2010.
- [201] S. Reuter, J. Winter, S. Iseni, A. Schmidt-Bleker, M. Deunbier, K. Masur, K. Wende, and K. D. Weltmann. The influence of feed gas humidity versus ambient humidity on atmospheric pressure plasma jet-effluent chemistry and skin cell viability. 2014.

- [202] W. Henry. Experiments on the quantity of gases absorbed by water, at different temperatures, and under different pressures. *Philosophical Transactions of the Royal Society of London*, pages 29–276, 1803.
- [203] A. Schmidt-Bleker, .J Winter, S. Iseni, M. Duennbier, K.-D. Weltmann, and S. Reuter. Reactive species output of a plasma jet with a shielding gas device - combination of ftir absorption spectroscopy and gas phase modelling. *Journal of Physics D: Applied Physics*, 47(14):145201, 2014.
- [204] R. Friedl and U. Fantz. Spectral intensity of the n2 emission in argon low-pressure arc discharges for lighting purposes. *New Journal of Physics*, 14(4):043016, 2012.
- [205] M. Simek. Determination of n2 (a $3\sigma_u^+$) metastable density produced by nitrogen streamers at atmospheric pressure: 1. design of diagnostic method. *Plasma Sources Science and Technology*, 12(3):421, 2003.
- [206] A. Lofthus and P. H. Krupenie. The spectrum of molecular nitrogen. *Journal of physical and chemical reference Data*, 6(1):113–307, 1977.
- [207] Y.-R. Luo. Bond dissociation energies and the hammett correlation, part 1: Remotely substituted aromatic compounds and vitamin e. *International journal of chemical kinetics*, 34(8):453–466, 2002.
- [208] G. Czapski. Reaction of. oh. *Methods in enzymology*, 105:209–215, 1984.
- [209] G. V. Buxton, C. L. Greenstock, W. P. Helman, and A. B. Ross. Critical review of rate constants for reactions of hydrated electrons, hydrogen atoms and hydroxyl radicals (oh/o) in aqueous solution. *Journal of physical and chemical reference data*, 17(2):513–886, 1988.
- [210] A. J. Elliot. Rate constants and g-values for the simulation of the radiolysis of light water over the range 0-300 deg c. Technical report, Atomic Energy of Canada Ltd., Chalk River, ON (Canada). Chalk River Nuclear Labs, 1994.
- [211] A. J. Elliot. A pulse radiolysis study of the temperature dependence of reactions involving h, oh and e-aq in aqueous solutions. *International Journal of Radiation Applications and Instrumentation. Part C. Radiation Physics and Chemistry*, 34(5):753–758, 1989.
- [212] D. W. O’Sullivan, M. Lee, B. C. Noone, and B. G. Heikes. Henry’s law constant determinations for hydrogen peroxide, methyl hydroperoxide, hydroxymethyl hydroperoxide, ethyl hydroperoxide, and peroxyacetic acid. *The Journal of Physical Chemistry*, 100(8):3241–3247, 1996.
- [213] G. M. Rosen, P. Tsai, J. Weaver, S. Porasuphatana, L. J. Roman, A. A Starkov, G. Fiskum, and S. Pou. The role of tetrahydrobiopterin in the regulation of neuronal nitric-oxide synthase-generated superoxide. *Journal of Biological Chemistry*, 277(43):40275–40280, 2002.
- [214] H. Tong, A. M. Arangio, P. S. J. Lakey, T. Berkemeier, F. Liu, C. J. Kampf, U. Poeschl, and M. Shiraiwa. Hydroxyl radicals from secondary organic aerosol decomposition in water. *Atmospheric Chemistry and Physics Discussions*, 15(21):30017–30042, 2015.

- [215] L. Sun, A. R. Hoy, and J. R. Bolton. Generation efficiency of the hydroxyl radical adduct of the dmpo spin trap in homogeneous and heterogeneous media. *Journal of Advanced Oxidation Technologies*, 1:44–52, 1996.
- [216] J. Staehelin and J. Hoigne. Decomposition of ozone in water: rate of initiation by hydroxide ions and hydrogen peroxide. *Environmental Science & Technology*, 16(10):676–681, 1982.
- [217] M. H. Stans. Bond dissociation energies in simple molecules. *NIST Special Publication*, 1:58, 1970.
- [218] E. S. Barker, R. B. Singer, J. R. Elkinton, and J. K. Clark. The renal response in man to acute experimental respiratory alkalosis and acidosis. *Journal of Clinical Investigation*, 36(4):515, 1957.
- [219] L. S. Rothman, D. Jacquemart, A. Barbe, D. C. Benner, M. Birk, L. R. Brown, M. R. Carleer, C. Chackerian, K. Chance, L. H. et al Coudert, et al. The hitran 2004 molecular spectroscopic database. *Journal of Quantitative Spectroscopy and Radiative Transfer*, 96(2):139–204, 2005.
- [220] H. Zimmermann. Qmacsoft-ht (computer program), 2010.
- [221] J. H. Carpenter. New measurements of oxygen solubility in pure and natural water1. *Limnology and Oceanography*, 11(2):264–277, 1966.
- [222] E. Wilhelm, R. Battino, and R. J. Wilcock. Low-pressure solubility of gases in liquid water. *Chemical reviews*, 77(2):219–262, 1977.
- [223] T. J. Morrison and N. B. Johnstone. Solubilities of the inert gases in water. *J. chem. Soc.*, pages 3441–3446, 1954.
- [224] W.-F. Liu, X.-M. Han, Y.-Q. Jin, and F.-T. Sang. Jet singlet oxygen generator modeling. *High Power Laser and Particle Beams*, 17(10):1497–1504, 2005.
- [225] V. M. Berdnikov and N. M. Bazhin. Redox potentials of some inorganic radicals in aqueous solutions. *Zh Fiz Khim*, 44:712, 1970.
- [226] D. R. Hanson, J. B. Burkholder, C. J. Howard, and A. R. Ravishankara. Measurement of hydroxyl and hydroperoxy radical uptake coefficients on water and sulfuric acid surfaces. *The Journal of Physical Chemistry*, 96(12):4979–4985, 1992.
- [227] J. Majewski. Methods for measuring ozone concentration in ozone-treated water. *Prz Elektrotech (Electr Rev)*, 88:253–255, 2012.
- [228] P. Lukes, M. Clupek, V. Babicky, V. Janda, and P. Sunka. Generation of ozone by pulsed corona discharge over water surface in hybrid gas–liquid electrical discharge reactor. *Journal of Physics D: Applied Physics*, 38(3):409, 2005.
- [229] P. Lukes. *Water Treatment by Pulsed Streamer Corona Discharge*. Thesis, 2001.
- [230] C. C. Beltran, E. A. Palmer, B. R. Buckley, and F. Iza. Virtues and limitations of pittsburgh green for ozone detection. *Chemical Communications*, 51(9):1579–1582, 2015.

Bibliography

- [231] A. U. Khan and M. Kasha. Chemiluminescence arising from simultaneous transitions in pairs of singlet oxygen molecules. *Journal of the American Chemical Society*, 92(11):3293–3300, 1970.
- [232] R. M. Arneson. Substrate-induced chemiluminescence of xanthine oxidase and aldehyde oxidase. *Archives of biochemistry and biophysics*, 136(2):352–360, 1970.
- [233] M. Tarr and D. P. Valenzano. Singlet oxygen: the relevance of extracellular production mechanisms to oxidative stress in vivo. *Photochemical & Photobiological Sciences*, 2(4):355–361, 2003.
- [234] S. Bekeschus, S. Iseni, S. Reuter, K. Masur, and K. D. Weltmann. Nitrogen shielding of an argon plasma jet and its effects on human immune cells. *Plasma Science, IEEE Transactions on*, 43(3):776–781, 2015.
- [235] Y.-R. Luo and J. A. Kerr. Bond dissociation energies. *CRC Handbook of Chemistry and Physics*, 89, 2012.
- [236] L. M. Dorfman and G. E. Adams. Reactivity of the hydroxyl radical in aqueous solutions. Technical report, DTIC Document, 1973.
- [237] W. F. Huebner and C. W. Carpenter. Solar photo rate coefficients. Technical report, Los Alamos Scientific Lab., NM (USA), 1979.
- [238] B. E. Britigan, T. L. Roeder, and G. R. Buettner. Spin traps inhibit formation of hydrogen peroxide via the dismutation of superoxide: implications for spin trapping the hydroxyl free radical. *Biochimica et Biophysica Acta (BBA)-General Subjects*, 1075(3):213–222, 1991.
- [239] M. Duennbier, H. Tresp, A. Schmidt, J. Winter, M. Wolfram, K. Masur, K.-D. Weltmann, and S. Reuter. Ion measurements of a cold atmospheric pressure argon plasma jet with variation of the ambient air humidity. In Ronny Brandenburg, editor, *14th International Symposium on High Pressure Low Temperature Plasma Chemistry (HANKONE XIV)*, 2014.
- [240] C. Chen, D. X. Liu, Z. C. Liu, A. J. Yang, H. L. Chen, G. Shama, and M. G. Kong. A model of plasma-biofilm and plasma-tissue interactions at ambient pressure. *Plasma Chemistry and Plasma Processing*, 34(3):403–441, 2014.
- [241] R. Bussiahn, N. Lembke, R. Gesche, Th. Von Woedtke, and K. D. Weltmann. Plasma sources for biomedical applications. *Hyg Med*, 38:212–216, 2013.
- [242] W. Droege, K. Schulze-Osthoff, S. Mihm, D. Galter, H. Schenk, H. P. Eck, S. Roth, and H. Gmuender. Functions of glutathione and glutathione disulfide in immunology and immunopathology. *The FASEB journal*, 8(14):1131–1138, 1994.
- [243] S. A. Dikanov and A. R. Crofts. *Handbook of Applied Solid State Spectroscopy*, chapter ELECTRON PARAMAGNETIC RESONANCE SPECTROSCOPY, pages 97–149. Springer US, Boston, MA, 2006.
- [244] A. K. Gelasco and J. R. Raymond. Indoxyl sulfate induces complex redox alterations in mesangial cells. *American Journal of Physiology-Renal Physiology*, 290(6):F1551–F1558, 2006.

- [245] M. Culcasi, A. Rockenbauer, A. Mercier, J.-L. Clement, and S. Pietri. The line asymmetry of electron spin resonance spectra as a tool to determine the cis: trans ratio for spin-trapping adducts of chiral pyrrolines n-oxides: The mechanism of formation of hydroxyl radical adducts of empo, depmpo, and dippmpo in the ischemic-reperfused rat liver. *Free Radical Biology and Medicine*, 40(9):1524–1538, 2006.
- [246] S. Oowada, N. Endo, H. Kameya, M. Shimmei, and Y. Kotake. Multiple free-radical scavenging capacity in serum. *Journal of clinical biochemistry and nutrition*, 51(2):117, 2012.

Appendix

Quantum mechanical consideration of fundamentals

Spin operator and hamiltonian

Eigenvalue equation (5.1) represented systems with discrete energy levels, which are defined by the quantum numbers, whereas $\hat{\Lambda}$ is the eigenfunction equation operator, λ_k is the eigenvalue of the state ' k ', and Ψ_k is the eigenfunction of the state ' k ' [143, 148].

$$\hat{\Lambda}\Psi_k = \lambda_k\Psi_k \quad (5.1)$$

The most relevant part in electron paramagnetic resonance spectroscopy deals with the quantization of the spin angular momentum, therefore, the operator is a spin operator \hat{S} per definition, with \hat{S}_z being its component in z-direction of the applied magnetic field. This gives the following equation for the eigenvalues m_s of a system with a total electron spin of $1/2$ and the quantum numbers $M_s = \pm 1/2$.

$$\hat{S}_z\Phi_e(M_s) = m_s\Phi_e(M_s)$$

There, m_s is the eigenvalue of the operator \hat{S}_z and the corresponding eigenfunction is $\Phi_e(M_s)$. With $\alpha(e) = \Phi_e(M_s = +1/2)$ and $\beta(e) = \Phi_e(M_s = -1/2)$ it can be written as:

$$\begin{aligned} \hat{S}_z\alpha(e) &= 1/2\alpha(e) \\ \hat{S}_z\beta(e) &= -1/2\beta(e) \end{aligned}$$

For the nuclear spin the similar formulation can be used:

$$\begin{aligned} \hat{I}_z\alpha(n) &= 1/2\alpha(n) \\ \hat{I}_z\beta(n) &= -1/2\beta(n) \end{aligned}$$

In the following the Dirac notation the equations is used, the four equations above are than expressed as:

$$\begin{aligned} \hat{S}_z|\alpha(e)\rangle &= 1/2|\alpha(e)\rangle \\ \hat{S}_z|\beta(e)\rangle &= -1/2|\beta(e)\rangle \\ \hat{I}_z|\alpha(n)\rangle &= 1/2|\alpha(n)\rangle \\ \hat{I}_z|\beta(n)\rangle &= -1/2|\beta(n)\rangle \end{aligned}$$

The Hamiltonian $\hat{\mathcal{H}}$ of the time independent Schrödinger's equation represents for the total energy and commutes with the spin operators \hat{S} and \hat{I} .

$$\begin{aligned}\hat{\mathcal{H}}_e |\Phi_e\rangle &= E_{ek} |\Phi_e\rangle \\ \hat{\mathcal{H}}_n |\Phi_n\rangle &= E_{nk} |\Phi_n\rangle\end{aligned}$$

with the expressions of α and β this leads to

$$\begin{aligned}\hat{\mathcal{H}}_e |\alpha(e)\rangle &= E_{\alpha(e)} |\alpha(e)\rangle \\ \hat{\mathcal{H}}_e |\beta(e)\rangle &= E_{\beta(e)} |\beta(e)\rangle \\ \hat{\mathcal{H}}_n |\alpha(n)\rangle &= E_{\alpha(n)} |\alpha(n)\rangle \\ \hat{\mathcal{H}}_n |\beta(n)\rangle &= E_{\beta(n)} |\beta(n)\rangle\end{aligned}$$

Also the Zeeman interactions can be expressed by the use of these operators. In the perturbed case where the magnetic field introduced the Hamiltonian will be applicable. For a system with $S = 1/2$ and $I = 1/2$ (hydrogen atom), which is interaction with a strong magnetic field (oriented in z-direction), the equations are given by the following:

$$\begin{aligned}\hat{\mathcal{H}} &= -\hat{\mu}_z \cdot B \\ \hat{\mu}_{ez} &= \gamma_e \cdot \hat{S}_z \cdot h = -g_e \cdot \mu_B \cdot \hat{S}_z \\ \hat{\mu}_{nz} &= \gamma_n \cdot \hat{I}_z \cdot h = g_n \cdot \mu_n \cdot \hat{I}_z \\ \hat{\mathcal{H}}_e &= g_e \cdot \mu_B \cdot \hat{S}_z \\ \hat{\mathcal{H}}_n &= -g_n \cdot \mu_n \cdot \hat{I}_z\end{aligned}$$

Nuclear hyperfine structure

The nuclear hyperfine structure occurs due to the interaction of the magnetic momentum of the unpaired electron with the magnetic nuclei [243]. With the resulting pattern of the hyperfine structure determination of paramagnetic species as well as their spatial structure is possible. The unpaired electrons with the nucleus can interact in two kinds of hyperfine interaction.

The interaction between two dipoles is called 'anisotropic' or 'dipolare' hyperfine interaction. There the electron spin magnetic momentum interact with the nuclear magnetic momentum. This interaction is depended on the averaged distance between the electron and the nucleus, as well as on the shape of the electronic orbitals.

The so called 'Fermi contact' interaction only considers the electrons located in s-orbitals ($l = 0$), since p-, d-, or f-orbitals nodal planes through the nucleus. This interaction is isotropic and depends on an existing finite spin density of the unpaired electron at the location of the nucleus. The orientation of the paramagnetic species in the magnetic field is for this interaction irrelevant [243]. A is the isotropic hyperfine coupling constant, which is related to the unpaired spin density, there $\Psi(0)$ is the electron wave-function at the

nucleus, μ_e and μ_n are the magnetic moments of the electron respectively of the nucleus. If the electron density in the s-orbital is not zero, the Fermi-contact interaction takes place[143, 146].

$$A = -\frac{8}{3} \cdot \pi \langle \mu_n \cdot \mu_e \rangle \cdot |\Psi(0)|^2$$

The Hamiltonian of one unpaired electron can than be written as follows, whereas \mathcal{H}_{EZ} is the electron Zeeman component, \mathcal{H}_{NZ} the nuclear Zeeman component, and \mathcal{H}_{HFS} is the hyperfine interaction, in this case represented by the Fermi-contact interaction term $-h \cdot S \cdot a \cdot I$:

$$\begin{aligned} \mathcal{H} &= \mathcal{H}_{EZ} - \mathcal{H}_{NZ} - \mathcal{H}_{HFS} \\ \hat{\mathcal{H}} &= g_e \cdot \mu_B \cdot B_{ext} - g_N \cdot \mu_N \cdot B \cdot I_z + h \cdot S \cdot a \cdot I \\ \hat{\mathcal{H}}(\mu_B \gg \mu_N) &= g_e \cdot \mu_B \cdot B_{ext} + h \cdot S \cdot a \cdot I \end{aligned}$$

If it is only one electron interacting with one nucleus $2I + 1$ lines occur in the spectra, for one electron interaction with nonequivalent nuclei (N_1, N_2, \dots) the number of occurring lines is given by $\prod_{i=1}^k (2N_i I_i + 1)$, intensities are distributed according to the Pascal's triangle [143]:

Table 5.1: Pascal's triangle for ratio of relative peak intensities of the split lines according to interactions.

number of equivalent nuclei	relative intensities										number of lines		
1					1	:	1				2		
2				1	:	2	:	1			3		
3			1	:	3	:	3	:	1		4		
4			1	:	4	:	6	:	4	:	1	5	
5		1	:	5	:	10	:	10	:	5	:	1	6
⋮	⋮	:	⋮	:	⋮	:	⋮	:	⋮	:	⋮	:	⋮

Alternative spin traps for oxygen radicals

As described the adduct of DMPO with the superoxide anion radical is not stable, therefore, similar spin traps are investigated to study superoxide anion generated by plasma treatment of liquids.

In figure 5.1 the resulting spectrum of 180 s plasma treatment of DPBS containing 2-ethoxycarbonyl-2-methyl-3,4-dihydro-2H-pyrrole-1-oxide, EMPO as spin trapping agent. Chemically, EMPO differs from DMPO in the replacement of one methyl group by a ethoxycarbonyl group (EtO_2C). The peaks in the spectrum represent the $\text{EMPO}\bullet/\text{OH}$

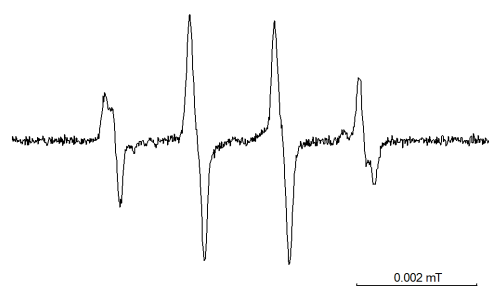


Figure 5.1: Spectrum of EMPO after 180 s plasma treatment of DPBS.

adduct [189, 244]. Since the lifetime of $\text{EMPO}\bullet/\text{OOH}$ is with 10 minutes already longer than the one of DMPO, it is applicable for superoxide anion radical detection.

A phosphorylated derivative of DMPO is 5-diethoxyphosphoryl-5-methyl-1-pyrroline-N-oxide (DEPMPO). The superoxide anion DEPMPO adduct stability is enhanced to 17 minutes lifetime in comparison to DMPO. Just like EMPO and DMPO also DEPMPO can trap beside oxygen radicals also sulfur or carbon centered free radicals.

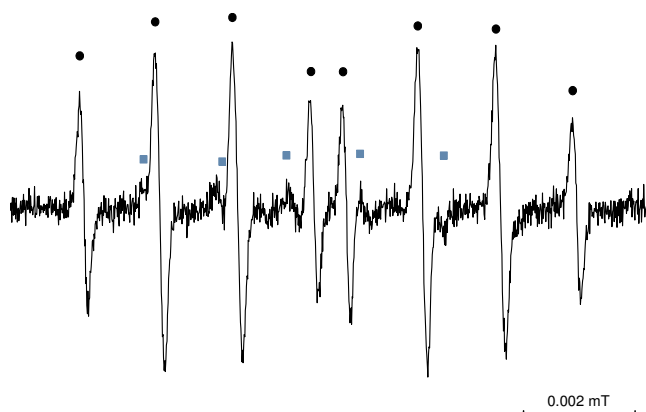


Figure 5.2: Spectrum of DEPMPO after 180 s plasma treatment of DPBS, $\text{DEPMPO}\bullet/\text{OOH}$ (marked with open blue squares) and $\text{DEPMPO}\bullet/\text{OH}$ (marked with black dots).

In figure 5.2 a typical spectrum of $\text{DEPMPO}\bullet/\text{OH}$ adduct is depicted ($\text{DEPMPO}\bullet/\text{OH}$ marked with black dots), the small peaks marked with open blue squares (some peaks of the $\text{DEPMPO}\bullet/\text{OOH}$ spectrum) gives indications to the formation of superoxide anion radicals during treatment.

Some spin traps are more hydrophobic than others and, therefore, are more useful for radical detection in cell membranes such a spin trap is DIPPMPO (5-(diisopropoxyphosphoryl)-5-methyl-1-pyrroline-N-oxide). It is a quite similar spin trap to DEPMPO but more lipophilic. The spectrum of $\text{DIPPMPO}\bullet/\text{OH}$ and $\text{DIPPMPO}\bullet/\text{OOH}$ is resembling the spectrum of $\text{DEPMPO}\bullet/\text{OH}$ and $\text{DEPMPO}\bullet/\text{OOH}$ [245] (see figure 5.3). Due to its

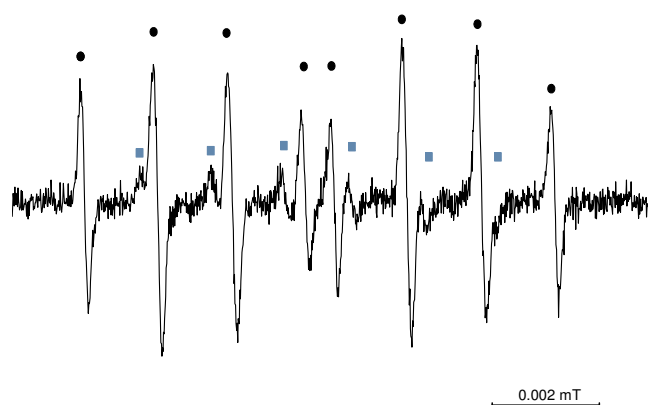


Figure 5.3: Spectrum of DIPPMPPO after 180 *s* plasma treatment of DPBS.

lipophilic property DIPPMPPO is a spin trap well suited for membrane studies as well as for intracellular investigations.

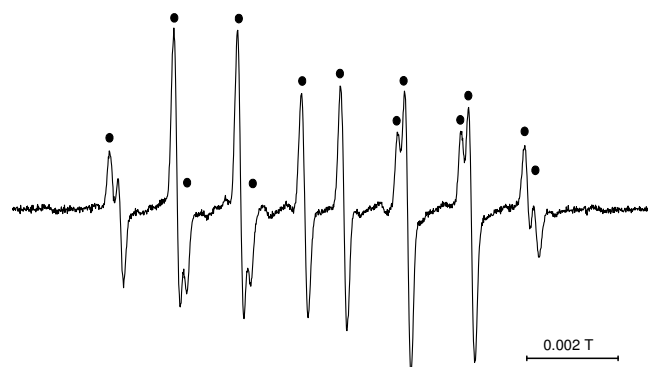


Figure 5.4: Spectrum of CYPMPPO•/OH (marked with black dots) after 300 *s* plasma treatment of DPBS.

A typical spectrum of hydroxyl radical stabilized by CYPMPPO (5-(2,2-dimethyl-1,3-propoxy-5-methyl-1-pyrroline N-oxide) is shown in figure 5.4, also here the peaks related to •OH [246] are marked with black dots. This spin trap has been only marginally researched up to now. The half-life of CYPMPPO•/OOH in a enzyme free system 15 minutes [192].

Parameters of the EPR spectra

Table 5.2: Listed parameters of the EPR spectra-part 1.

Figure	radical	g-value	line width / mT	HFS / mT
4.5 a untreated	$\bullet\text{OH}$	2.00554	0.09	1.47
				1.51
	$\bullet\text{CH}_3$	2.00543	0.15	1.52
				1.43
4.5 a treated	$\bullet\text{OH}$	2.00551	0.12	1.49
				1.47
	$\bullet\text{CH}_3$	2.00546	0.15	1.52
				1.42
4.5 b untreated	$\bullet\text{OH}$	2.00552	0.11	1.50
				1.48
	$\bullet\text{CH}_3$	2.00547	0.15	1.53
				1.44
4.5 b treated	$\bullet\text{OH}$	2.00553	0.12	1.50
				1.48
	$\bullet\text{CH}_3$	2.00547	0.15	1.53
				1.44
4.5 c treated	$\bullet\text{OH}$	2.0055	0.12	1.50
				1.47
4.6	$\bullet\text{OH}$	2.00555	0.12	1.50
				1.47
	$\text{O}_2\bullet^-$	2.00564	0.25	1.43
				1.12
4.7	$\bullet\text{OH} + \text{O}_2\bullet^-$	2.00551	0.12	1.50
				1.50
4.10	$\bullet\text{OH}$	2.0056	0.15	1.54
				1.42
	$\text{O}_2\bullet^-$	2.0056	0.14	1.41
				1.12
4.11 a	$\text{CP}\bullet$	2.00591	0.13	1.62
4.11 b	$\text{PP}\bullet$	2.00593	0.16	1.71
4.12	$\text{C-PTI}\bullet$	2.00665	0.11	0.81
4.18	$\bullet\text{OH}$	2.00555	0.12	1.50
				1.47
	$\text{O}_2\bullet^-$	2.00564	0.25	1.43
				1.12

Table 5.3: Listed parameters of the EPR spectra-part 2.

Figure	radical	g-value	line width / mT	HFS / mT
4.19	$\bullet\text{OH}$	2.00569	0.15	1.42
				1.54
	$\text{O}_2^{\bullet-}$	2.00574	0.13	1.41
				1.27
4.20	$\bullet\text{OH}$	2.00592	0.10	1.42
				1.51
				0.09
	$\text{O}_2^{\bullet-}$	2.00593	0.12	1.41
				1.26
4.21	$\bullet\text{OH} + \text{O}_2^{\bullet-}$	2.00574	0.11	1.49
DPBS				1.46
4.21	$\bullet\text{OH} + \text{O}_2^{\bullet-}$	2.00573	0.12	1.49
RPMI 1640				1.46
4.24 b	$\bullet\text{OH} + \text{O}_2^{\bullet-}$	2.00567	0.12	1.50
NaCl				1.78
4.24 b	$\bullet\text{OH} + \text{O}_2^{\bullet-}$	2.00551	0.12	1.50
DPBS				1.47
4.24 b	$\bullet\text{OH} + \text{O}_2^{\bullet-}$	2.00551	0.12	1.50
RPMI 1640				1.47
4.27	$\bullet\text{OH}$	2.00568	0.15	1.42
				1.29
	$\text{O}_2^{\bullet-}$	2.00572	0.09	1.61
				1.23
4.30	$^1\text{O}_2$	2.00591	0.07	1.61
4.31	$^1\text{O}_2$	2.00596	0.07	1.61
4.32	$^1\text{O}_2$	2.00596	0.07	1.61
4.33	$^1\text{O}_2$	2.00599	0.07	1.61
4.35	$\bullet\text{OH}$	2.00594	0.14	1.42
				1.55
	$\text{O}_2^{\bullet-}$	2.00596	0.13	1.42
				1.27
4.43	$\bullet\text{OH} + \text{O}_2^{\bullet-}$	2.00557	0.12	1.50
VUV				1.78
4.43	$\bullet\text{OH} + \text{O}_2^{\bullet-}$	2.00561	0.12	1.50
UV				1.47
4.43	$\bullet\text{OH} + \text{O}_2^{\bullet-}$	2.00564	0.12	1.50
Jet				1.47

Table 5.4: Listed parameters of the EPR spectra-part 3.

Figure	radical	g-value	line width / mT	HFS / mT
4.44 VUV; dH ₂ O	$\bullet\text{OH} + \text{O}_2^{\bullet-}$	2.00557	0.12	1.50
				1.48
4.44 VUV; HBSS	$\bullet\text{OH} + \text{O}_2^{\bullet-}$	2.00572	0.11	1.50
				1.48
4.44 VUV; RPMI 1640	$\bullet\text{OH} + \text{O}_2^{\bullet-}$	2.00572	0.11	1.50
				1.48
4.44 Jet; dH ₂ O	$\bullet\text{OH} + \text{O}_2^{\bullet-}$	2.00564	0.12	1.50
				1.48
4.44 Jet; HBSS	$\bullet\text{OH} + \text{O}_2^{\bullet-}$	2.00572	0.12	1.50
				1.48
4.44 Jet; RPMI 1640	$\bullet\text{OH} + \text{O}_2^{\bullet-}$	2.00572	0.12	1.50
				1.48
4.45 a	$\bullet\text{OH}$	2.00591	0.10	1.42
				1.50
				0.09
	$\text{O}_2^{\bullet-}$	2.00593	0.12	1.41
				1.24
4.49 a+b	$\bullet\text{OH}$	2.00577	0.08	1.18
				1.62
				1.32
	$\text{O}_2^{\bullet-}$	2.0058	0.11	1.42
				1.43
	$\bullet\text{SG}$	2.00577	0.13	1.43
				1.43
				0.13
4.50 a	$\bullet\text{OH}$	2.0058	0.08	1.41
				1.38
	$\text{O}_2^{\bullet-}$	2.00577	0.15	1.16
				1.65
	$\bullet\text{SG}$	2.00585	0.11	1.42
				1.42
				0.19
4.50 b	$\bullet\text{OH}$	2.00578	0.12	1.21
				1.66
	$\text{O}_2^{\bullet-}$	2.00578	0.08	1.30
				1.41
	$\bullet\text{SG}$	2.00577	0.12	1.43
				1.42
				0.13

Table 5.5: Listed parameters of the EPR spectra-part 4.

Figure	radical	g-value	line width / mT	HFS / mT
5.1	$\bullet\text{OH}$	2.006	0.10	1.42
				1.50
				0.08
	$\text{O}_2\bullet$	2.00603	0.12	1.41
				1.26
5.2	$\bullet\text{OH}$	2.00614	0.12	4.72
				1.40
				1.33
				0.06
	$\text{O}_2\bullet$	2.00623	0.15	1.28
				1.37
5.3	$\bullet\text{OH}$	2.00616	0.12	4.68
				1.40
				1.33
				0.06
	$\text{O}_2\bullet$	2.00623	0.15	1.26
				1.36
5.4	$\bullet\text{OH}$	2.00582	0.14	1.39
				1.41
				5.05
	$\bullet\text{OH}$	2.00579	0.11	1.39
				1.24
				1.89

List of publications and conference contributions

Peer reviewed publications

2012

Fricke, K., Koban, I., Tresp, H., Jablonowski, L., Schröder, K., Kramer, A., ... & Kocher, T. (2012). Atmospheric pressure plasma: a high-performance tool for the efficient removal of biofilms. *PloS one*, 7(8), e42539.

Fricke, K., Tresp, H., Bussiahn, R., Schröder, K., von Woedtke, Th., & Weltmann, K.-D. (2012). On the use of atmospheric pressure plasma for the bio-decontamination of polymers and its impact on their chemical and morphological surface properties. *Plasma Chemistry and Plasma Processing*, 32(4), 801-816.

Reuter, S., Winter, J., Schmidt-Bleker, A., Tresp, H., Hammer, M. U., & Weltmann, K.-D. (2012). Controlling the ambient air affected reactive species composition in the effluent of an argon plasma jet. *Plasma Science, IEEE Transactions on*, 40(11), 2788-2794.

Reuter, S., Tresp, H., Wende, K., Hammer, M. U., Winter, J., Masur, K., ... & Weltmann, K.-D. (2012). From RONS to ROS: tailoring plasma jet treatment of skin cells. *Plasma Science, IEEE Transactions on*, 40(11), 2986-2993.

2013

Winter, J., Wende, K., Masur, K., Iseni, S., Dünnbier, M., Hammer, M. U., Tresp, H., Weltmann, K.-D., Reuter, S. (2013). Feed gas humidity: a vital parameter affecting a cold atmospheric-pressure plasma jet and plasma-treated human skin cells. *Journal of Physics D: Applied Physics*, 46(29), 295401.

Tresp, H., Hammer, M. U., Winter, J., Weltmann, K.-D., & Reuter, S. (2013). Quantitative detection of plasma-generated radicals in liquids by electron paramagnetic resonance spectroscopy. *Journal of Physics D: Applied Physics*, 46(43), 435401.

Tresp, H., Hammer, M. U., Weltmann, K.-D., & Reuter, S. (2013). Effects of atmosphere composition and liquid type on plasma-generated reactive species in biologically relevant solutions. *Plasma Medicine*, 3(1-2).

Bundscherer, L., Bekeschus, S., Tresp, H., Hasse, S., Reuter, S., Weltmann, K.-D., ... & Masur, K. (2013). Viability of human blood leukocytes compared with their respective cell lines after plasma treatment. *Plasma Medicine*, 3(1-2).

2014

Winter, J., Tresp, H., Hammer, M. U., Iseni, S., Kupsch, S., Schmidt-Bleker, A., ... & Reuter, S. (2014). Tracking plasma generated H₂O₂ from gas into liquid phase and revealing its dominant impact on human skin cells. *Journal of Physics D: Applied Physics*, 47(28), 285401.

2015

Bundscherer, L., Nagel, S., Hasse, S., Tresp, H., Wende, K., Walther, R., ... & Lindequist, U. (2015). Non-thermal plasma treatment induces MAPK signaling in human monocytes. *Open Chemistry*, 13(1).

Jablonowski, H., Hänsch, M. A. C., Dünnbier, M., Wende, K., Hammer, M. U., Weltmann, K.-D., ... & von Woedtke, Th. (2015). Plasma jet's shielding gas impact on bacterial inactivation. *Biointerphases*, 10(2), 029506.

Banaschik, R. Lukes, P., Jablonowski, H., Hammer, M. H., Weltmann, K.-D., Kolb, J. F. (2015) Potential of pulsed corona discharges generated in water for the degradation of persistent pharmaceutical residues. *Water Research* 84: 127-135

Jablonowski, H., Bussiahn, R., Hammer, M. U., Weltmann, K.-D., von Woedtke, Th., Reuter, S. (2015) Impact of Plasma Jet Vacuum Ultraviolet Radiation on Reactive Oxygen Species Generation in Bio-Relevant Liquids, *Physics of Plasmas* 22, 122008

Jablonowski, H., & von Woedtke, Th. (2015). Research on plasma medicine-relevant plasma-liquid interaction: What happened in the past five years?. *Clinical Plasma Medicine*, 3(2), 42-52.

2016

Bruggeman, P., Kushner, M., Locke, B., Gardeniers, H., Graham, B., Graves, D., Hofman-Caris, R., Maric, D., Reid, J., Ceriani, E., Fernandez Rivas, D., Foster, J., Garrick, S., Gorbanev, Y., Hamaguchi, S., Iza, F., Jablonowski, H., Klimova, E., Krema, F., Kolb, J., Lukes, P., Machala, Z., Marinov, I., Mariotti, D., Mededovic Thagard, S., Minakata, D., Neyts, E., Pawlat, J., Petrovic, Z., Pflieger, R., Reuter, S., Schram, D., Schroeter, S., Shiraiwa, M., Tarabova, B., Tsai, P., Verlet, J., von Woedtke, Th., Wilson, K., Yasui, K., Zvereva, G. (accepted 2016) Plasma-Liquid Interactions: A Review and Roadmap. *Plasma Sources Science and Technology*. *Plasma Sources Science and Technology*

Conference proceedings

2011

Fricke, K., Tresp, H., Bussiahn, R., Schröder, K., Weltmann, K.-D., & von Woedtke, Th. Modification of the physicochemical surface properties of polymers during the plasma-based decontamination (20th International Symposium on Plasma Chemistry)

2012

Tresp, H., Hammer, M. U., Wende, K., Haensch, M. CA. Ch., Winter, J., Schmidt-Bleker, A., Masur, K., von Woedtke, Th., Weltmann, K.-D., Reuter, S., Plasma-generated reactive species in liquids by a gas shielded atmospheric pressure plasma jet effluent (XXI Europhysics Conference on the Atomic and Molecular Physics of Ionized Gases)

2013

Tresp, H., Hammer, M. U., Weltmann, K.-D., Reuter, S.; Quantitative detection of plasma-generated free radicals in liquids by electron paramagnetic resonance spectroscopy (21st International Symposium on Plasma Chemistry)

2015

Reuter, S., Schmidt-Bleker, A., Jablonowski, H., Winter, J., Bösel, A., Hammer, M., ... & Weltmann, K. D. Fundamental Aspects of Filamentary Jet Discharges Interacting with Biologically Relevant Liquids and with Cells (International Conference on Phenomena in Ionized Gases)

Conference contributions

Oral presentations

2012

Tresp, H., Hammer, M. U., Weltmann, K.-D., Reuter, S.; Untersuchung plasmagenerierter reaktiver Sauerstoffspezies in Flüssigkeiten; Annual Meeting of the German Physical Society (DPG) in Stuttgart, Germany

Tresp, H., Hammer, M. U., Weltmann, K.-D., Reuter, S.; Detection of plasma generated free radicals in liquids; 1st Young Professionals Workshop on Plasma Medicine in Boltenhagen, Germany

2013

Tresp, H., Hammer, M. U., Weltmann, K.-D., Reuter, S.; Respect (Reactive species treatment) by atmospheric pressure plasma jet of liquids; 2nd Young Professionals Workshop on Plasma Medicine in Koelpinsee, Germany

2014

Tresp, H., Hammer, M. U., Weltmann, K.-D., Reuter, S.; Role of Complexity of Liquids – Ingredients are Possible Scavenger and Source of Plasma-Generated Reactive Species; Annual Meeting of COST Action TD 1208 in Lisboa, Portugal

Tresp, H., Bundscherer, L., Monden, A., Hammer, M. U., Masur, K., Bussiahn, R., von Woedtke, Th., Weltmann, K.-D., Reuter, S.; Plasma jet (V) UV-radiation impact on biologically relevant liquids and cell suspension; 5th International Conference on Plasma

List of publications and conference contributions

Medicine (ICPM 5) in Nara, Japan

Tresp, H., Bussiahn, R., Bundscherer, L., Monden, A., Hammer, M. U., Masur, K., von Woedtke, Th., Weltmann, K.-D., Reuter, S.; Plasma jet (V) UV-radiation impact on biologically relevant liquids and cell suspension; 67th Annual Gaseous Electronics Conference (67th GEC) in Raleigh, USA

2015

Jablonowski, H., Schmidt-Bleker, A., Winter, J., Weltmann, K.-D., Reuter, S.; Highly reactive plasma generated species in biorelevant liquids: hydroxyl, superoxide anion, and singlet oxygen; 4th Young Professionals Workshop on Plasma Medicine in Rostock, Germany

Poster presentations

2011

Tresp, H., Hammer, M. U., Reuter, S., Weltmann, K.-D., Electron-Paramagnetic Resonance Spectroscopy – Detecting Radicals in Atmospheric Pressure Plasma Treated Liquids; Plasmamedizin - 10. Anwenderkreis Atmosphärendruckplasma, ak-adp, Workshop in Erfurt, Germany

2012

Tresp, H., Hammer, M. U., Schmidt-Bleker, A., Winter, J., Haensch, M.A. Ch., Wende, K., Schaper, L., Graham, B., Masur, K., von Woedtke, Th., Weltmann, K.-D., Reuter, S., Plasma-Generated Reactive Species in physiological Solutions; 4th International Conference on Plasma Medicine (ICPM 4) in Orleans, France

Tresp, H., Hammer, M. U., Wende, K., Haensch, M. CA. Ch., Winter, J., Schmidt-Bleker, A., Masur, K., von Woedtke, Th., Weltmann, K.-D., Reuter, S., Plasma-generated reactive species in liquids by a gas shielded atmospheric pressure plasma jet effluent; XXI Europhysics Conference on the Atomic and Molecular Physics of Ionized Gases (XXI ES-CAMPIG) in Viana do Castelo, Portugal

Tresp, H., Hammer, M. U., Winter, J., Schmidt-Bleker, A., Duennbier, M., Haensch, M. CA. Ch., Wende, K., Masur, K., von Woedtke, Th., Weltmann, K.-D., Reuter, S., Reactive Species in Liquids after Treatment with a Shielded Atmospheric Pressure Plasma Jet; 12th European Plasma Conference, high-tech plasma processes 12 (http12) in Bologna, Italy

Tresp, H., Hammer, M. U., Wende, K., Winter, J., Schmidt-Bleker, A., Masur, K., von Woedtke, Th., Weltmann, K.-D., Reuter, S., Plasma-Generated Reactive Species in physiological Solutions (65th Gaseous Electronics Conference (65th GEC) in Austin, USA

2013

Tresp, H., Hammer, M. U., Weltmann, K.-D., Reuter, S.; Respect (Reactive species treatment) by atmospheric pressure plasma jet of liquids; COST Action Electrical Discharges with Liquids for Future Applications - WG4 Workshop: Interactions of plasma's reactive species with materials and surfaces in Bratislava, Slovakia

Tresp, H., Hammer, M. U., Weltmann, K.-D., Reuter, S.; Quantitative detection of plasma-generated free radicals in liquids by electron paramagnetic resonance spectroscopy; 21st International Symposium on Plasma Chemistry (ISPC 21) in Cairns, Australia

2014

Tresp, H., Hammer, M. U., Winter, J., Weltmann, K.-D., Reuter, S., Plasma-Liquid-Interactions: Role of Omitted Extrinsic Parameter; XXII Europhysics Conference on the Atomic and Molecular Physics of Ionized Gases (XXII ESCAMPIG) in Greifswald, Germany

Tresp, H., Bundscherer, L., Monden, A., Hammer, M. U., Masur, K., Bussiahn, R., von Woedtke, Th., Weltmann, K.-D., Reuter, S.; Plasma jet (V)UV-radiation impact on biologically relevant liquids and cell suspension; International Workshop on Diagnostics and Modelling for Plasma Medicine (DMPM2014) in Nara, Japan

Tresp, H., Bundscherer, L., Monden, A., Hammer, M. U., Masur, K., Bussiahn, R., von Woedtke, Th., Weltmann, K.-D., Reuter, S.; Plasma jet (V)UV-radiation impact on biologically relevant liquids and cell suspension; Lorentz Meeting - Gas/Plasma-Liquid Interface: Transport, Chemistry and Fundamental Data in Leiden, Netherlands

2015

Jablonowski, H., Schmidt-Bleker, A., Winter, J., Weltmann, K.-D., Reuter, S.; Highly reactive plasma generated species in biorelevant liquids: hydroxyl, superoxide anion, and singlet oxygen; Bioplasmas and Plasmas with Liquids - Joint Conference of COST Actions CMST TD1208 Electrical discharges with liquids for future applications & MPNS MP1101 Biomedical Applications of Atmospheric Pressure Plasma Technology in Bertinoro, Italy

Other scientific achievements

Organization committee member:

- 1st Young Professionals Workshop on Plasma Medicine
- 2nd Young Professionals Workshop on Plasma Medicine
- 3rd Young Professionals Workshop on Plasma Medicine
- 4th Young Professionals Workshop on Plasma Medicine

2nd COST Training School 'All You Need to Know About Plasmas & Liquids and Never Dared to Ask'

Eigenständigkeitserklärung

Hiermit erkläre ich, dass diese Arbeit bisher von mir weder an der Mathematisch-Naturwissenschaftlichen Fakultät der Ernst-Moritz-Arndt-Universität Greifswald noch einer anderen wissenschaftlichen Einrichtung zum Zwecke der Promotion eingereicht wurde.

Ferner erkläre ich, dass ich diese Arbeit selbstständig verfasst und keine anderen als die darin angegebenen Hilfsmittel und Hilfen benutzt und keine Textabschnitte eines Dritten ohne Kennzeichnung übernommen habe.

(Helena Jablonowski)

Greifswald, den 29. Januar 2016